UNIVERSITY OF CALIFORNIA, SAN DIEGO

Investigating the single cell dynamics of *Saccharomyces cerevisiae* using microfluidics

A dissertation submitted in partial satisfaction of the requirements for the degree

Doctor of Philosophy

in

Bioengineering

by

Sujata Nayak

Committee in charge:

Professor Jeff Hasty, Chair
Professor Alexander Hoffmann
Professor Tracy Johnson
Professor Lanping Amy Sung
Professor Shyni Varghese

2013

The dissertation of Sujata Nayak is approved, and it is acceptable in quality and form for publication on microfilm and electronically:

_____

_____

_____

_____

Chair

University of California, San Diego

2013

DEDICATION

For my boys,

Bishnu, Ayush and Aneesh

TABLE OF CONTENTS

LIST OF FIGURES

LIST OF TABLES

ACKNOWLEDGEMENTS

I would like to sincerely thank my adviser, Professor Hasty for welcoming me to his lab and all his guidance, patience, motivation and immense knowledge to help me during my six years of research and stay here at the University of California San Diego. I could not have imagined a better advisor and mentor for my graduate study. I would also like to thank Dr. Tim Elston (UNC), for providing me with guidance and valuable suggestions through out the study. I am indebted to Will Mather for his exceptional talents in dynamic modeling and computational genius and all his assistance for editing and refining the thesis. Thank you for taking intense academic interest in this study as well as providing valuable suggestions that improved the quality of this study. I wish to extend my warmest thanks to everyone at the systems bio-dynamics lab, whose contributions were essential in completing this work. In particular I would like to thank Natalie and Mike for extensive wet-lab knowledge, Scott for his microfluidics expertise, Ivan for his help with the microscope software, Nan Hao and Meng Jin for being excellent collaborators. In addition to the people at school, I am lucky enough to have the support of many good friends. I'll be forever grateful to Jyoti Mohanty and Gati Krushna Singh for all their help during my thesis writing.

Finally, I would like to express special thanks to my husband Bishnu Nayak, without his encouragement, help and understanding it would have been impossible for me to finish this work.

Chapter 2 contains material originally published as Hao, N., Nayak, S., Behar, M., Shanks, R.H., Nagiec, M.J., Errede, B., Hasty, J., Elston, T.C., and Dohlman, H.G. (2008): Regulation of cell signaling dynamics by the protein kinase-scaffold Ste5. Molecular Cell ,Vol. 30, Issue 5, pp. 649-656.

Chapter 3 contains material that is a preprint of, Jin,M., Behar, M., Nayak, S., Mather, W., Hasty,J., Errede, B., Dohlman, H.G., Elston, T.C., (2010): Computational modeling of yeast chemotrophic growth reveals the role of the protease Bar1 in gradient sensing., which is in preparation for submission by April 2010.

Chapter 4 contains material originally published as Bennett, M.*, Pang, W.* Ostroff, N., Baumgartner, B., Nayak, S., Tsimring, L., and Hasty, J., 2008: Metabolic gene regulation in a dynamically changing environment. Nature, 454(7208):1119-22. (*equal contribution).

Chapter 5 contains material that is a preprint of Mather, W*., Nayak, S*., Henrik Dohlman., Beverly Errede., Jeff Hasty., Tim Elston. (2010): Developmental switching in a spatially changing environment, Nature, in preparation. (*equal contribution)., Nature, which is in preparation for submission by March 2010.

VITA

1996	Bachelor of Science in Physics Utkal University, Regional Institute of Education, India.
2005-2008	Teaching Assistant Department of Bioengineering, University of California, San Diego
2003-2004	Research Assistant Department of Bioengineering, University of California, San Diego
2008	Master of Science in Bioengineering University of California, San Diego
2013	Doctor of Philosophy in Bioengineering University of California, San Diego

PUBLICATIONS

Peer Reviewed Journal Articles

Hao, N., Nayak, S., Behar, M., Shanks, R.H., Nagiec, M.J., Errede, B., Hasty, J., Elston, T.C., and Dohlman, H.G: Regulation of cell signaling dynamics by the protein kinase-scaffold Ste5. Molecular Cell - 5 June 2008 (Vol. 30, Issue 5, pp. 649-656).

Bennett, M.*, Pang, W.*, Ostroff, N., Baumgartner, B., Nayak, S., Tsimring, L., and Hasty, J., (2008): Metabolic gene regulation in a dynamically changing environment. Nature, 454 (7208):1119-22. (*equal contribution).

Mather, W*., Nayak, S*., Henrik Dohlman., Beverly Errede., Jeff Hasty., Tim Elston. (2013): Developmental switching in a spatially changing environment, Nature, in preparation. (*equal contribution).

Jin,M., Behar, M., Nayak, S., Mather, W., Hasty,J., Errede, B., Dohlman, H.G., Elston, T.C., (2010): Computational modeling of yeast chemotrophic growth reveals the role of the protease Bar1 in gradient sensing. In preparation.

FIELDS OF STUDY

Major Field: Bioengineering (Microfluidics)

Advisor: Professor Jeff Hasty

ABSTRACT OF THE DISSERTATION

Investigating the single cell dynamics of *Saccharomyces cerevisiae* using microfluidics

by

Sujata Nayak

Doctor of Philosophy in Bioengineering

University of California, San Diego, 2013

Professor Jeff Hasty, Chair

Systems biology has grown immensely in the wake of human genome project. In recent years, there has been a tremendous increase in measurement capabilities (e.g., microarray and proteomic technologies, improved reporter genes). However, future success depends not only on effective measurement techniques but also on the design and implementation of appropriate experimental stimuli. In

this project, we investigate experimental approaches where the long-term dynamics of single cells subjected to a dynamic environment can be observed. We use microfluidic technology to develop a device where cells can be subjected to a stable and precise chemical gradient. We overcome the typical problem with many earlier gradient devices, where the high fluid flow needed to maintain the gradient renders such devices undesirable for the study of yeast cells. We use the gradient device along with fluorescence microscopy and molecular biology techniques to study gradient sensing and cell polarization during mating in the model organism *Saccharomyces cerevisiae*. We generalize the chemical gradient device such that the direction of the gradient can be specified as a function of time. The response of yeast cells to spatiotemporal signals generated by this device reveals aspects of yeast polarization adaptation that are unlikely to be observed in static environments. An integrated computational and experimental analysis of the pheromone response of yeast will provide a detailed understanding of the gradient sensing in yeast. Because MAP kinase signaling cascades and cell polarization machinery are conserved in most eukaryotes, understanding of the pheromone pathway should lead to improved models of cell polarization and gradient sensing in more complex organisms.

Chapter 1.

Introduction

1.1 Systems biology

It is evident that for a complete description of any biological system, integration of computational and experimental methods is imperative. Systems biology is a fast growing field that aims at system-level understanding of biological systems and has made great progress since the human genome project. Examples include the use of high-throughput technology to successfully reconstruct gene regulatory networks in several organisms (Ideker et al., 2001; Ibarra et al., 2002; Gardner et al., 2003), and development of computational models to explain various fundamental cellular processes (Simon et al., 2001; Breeden, 2003; Bartek et al., 2004). But many scientific challenges in this field still remain to be

resolved. These advances have led to the generation of large volumes of data whose specific results cannot always be interpreted. There is a need for development of new methods to gain to insights into the dynamics of motif clusters and biological function. For example sensitive tools to make dynamic measurements and quantify concentrations, and interactions of various types of molecules at high resolution both in space and time are required.

1.2 Why Microfluidics?

Biological systems in their natural environments are exposed to countless stimuli, e.g. changes in nutrients and growth factors. Yet, complex external stimuli are either minimized or eliminated altogether in laboratory conditions. That raises a question: are the biological systems in the laboratory settings a true depiction of their natural behavior? Current high throughput technologies such as flow-cytometry and gene microarrays have found broad spectrum of application in biological systems; however these technologies are not well suited when the investigation of the dynamics of the biological system is desired. In order to describe the dynamics of important cellular processes quantitatively, there is a need for novel experimental techniques that will allow us to generate time-series data for the governing proteins in a large number of individual living cells. Ideally, there is a need for a data acquisition system where a population of cells can be

grown and monitored in a defined environment using high resolution microscopy for an extended period of time. To achieve this, scientists have often employed the use of microfluidic systems. Such microfluidic based fluorescence microscopy enables us investigate the ability to precisely and dynamically manipulate the local environment without sacrificing temporal resolution in reporter readouts. Microf-without sacrificing temporal resolution in reporter readouts. Microfluidics involves designing and manufacturing devices that are basically a network of channels where very small fluid flows, in the range of microliter/nanoliter, can flow.

There are many advantages to using microfluidics: the amount of reagents and analytes used is quite small as the volume of fluids within the channels is very small. This is especially important while using expensive reagents. Low thermal mass, efficient mass transport and large surface-area-to-volume ratios are among the other benefits of using such systems. The fundamental physics that govern fluid flow changes drastically as dimensions are minimized to the micrometer scale. The relationship between volumetric flow and resistance in the micro-channel is analogous to that of Ohm's law for linear electric circuits. Fluid viscosity and not inertia dominates at such scale and hence the Reynolds number is very low rendering all the flows to be laminar as having turbulent flow in a channel containing cells for high resolution imaging will be detrimental for observing cellular behavior under high magnification. Microfluidics has become increasingly popular in recent years and has been used in a variety of applications such as generation of thermal or chemical gradients (Dertinger et al., 2001; Mao et al., 2002; Lin et al., 2004), long duration gene expression (Banerjee et al.,

2004, Cookson et al., 2005, Thompson et al., 2004), population dynamics (Balagadde et al.,2005), cell sorting (Fu et al., 2002; Huh et al., 2005); cell patterning (Chiu et al., 2000).

As mentioned above the microfluidic technology has aided bio medical research immensely, hence, here in the Hasty lab the main focus of my graduate work has been to design, develop and use novel microfluidic platforms to investigate the of single cell organisms. While there has been much success in the design and implementation of microfluidic devices, there are still some major limitations to using microfluidic devices for the creation of spatial and temporal environmental perturbations. Recently, Bennett et al. 2008, used a microfluidic chip that could create user-defined temporal waveforms to examine the transcriptional response of the glucose-galactose switch in *S. cerevisiae*. Drawing inspiration from this, a microfluidic device capable of generating spatiotemporal gradient was built in the Hasty lab. We use this new device to systematically probe yeast's ability to respond to a spatiotemporally changing environment. A detailed description of this device design and the yeasts mating pathway follows.

1.2.1 Microfluidic device fabrication process

Most recently, soft lithography has become the favored method for fabricating microfluidic devices for science. (Whitesides et al., 2001; Sia and Whitesides, 2003). Softlithography utilizes rapid prototyping techniques to produce replica moldings of polydimethylsiloxane (PDMS) against a photolithographically

produced master mold. Softlithographic processes have the advantage of rapid prototyping, ease of fabrication, and increased compatibility to biological surface changes. Microfabrication process is a three-step process comprising concept development, photolithography, and replica molding. (See Figure 1). The first step, involves drafting a device design using in standard vector graphics utilities. Here design of the a device that serves some scientific purpose is laid out and using the principles of fluid dynamics for laminar flow regime, the required flow rates and resistances are calculated. After the design is finalized to meet the desired requirement, it is drawn using a computer aided design program. The device design is separated into multiple layers, where all features of a particular height are positioned on a single layer for photolithographic purposes based on the device in question. Finally these designs are printed on a high resolution transparency that are typically glued to ultra-transmissive borosilicate glass for later use in the photolithographic process as the “photomasks”. The photlithogphy a positive or negative photoresist depending on the use is spin-coated onto a clean silicon wafer at a specified speed to get a particular thickness and then photopatterned by exposure to ultraviolet (UV) light through the photomask. Exposure to UV selectively crosslinks the features in the photomask thus creating a pattern on the wafer. As each layer in the photo mask is of a specific height the process of photolithography is repeated to pattern all the layers. Finally we get a positive relief of photoresist on the silicon wafer, called the “master mold,” whose topology precisely reflects the desired device channel and geometry. This

Master mold can be used repeatedly to generate several batches of microfluidic device.

The last step is the rapid prototyping technique that utilize replica molding of liquid prepolymer (usually PDMS) , master mold. The PDMS is first poured onto the silicon wafer and then baked to cure it. Cured PDMS monolith is then peeled off the master mold revealing the feature topology represented by the master mold in reverse. The chips are individually cut out from the PDMS monolith, punched to allow for connection to fluid reservoirs and then surfaces cleaned. Finally they are permanently bonded to glass cover slip using low-power oxygen plasma.

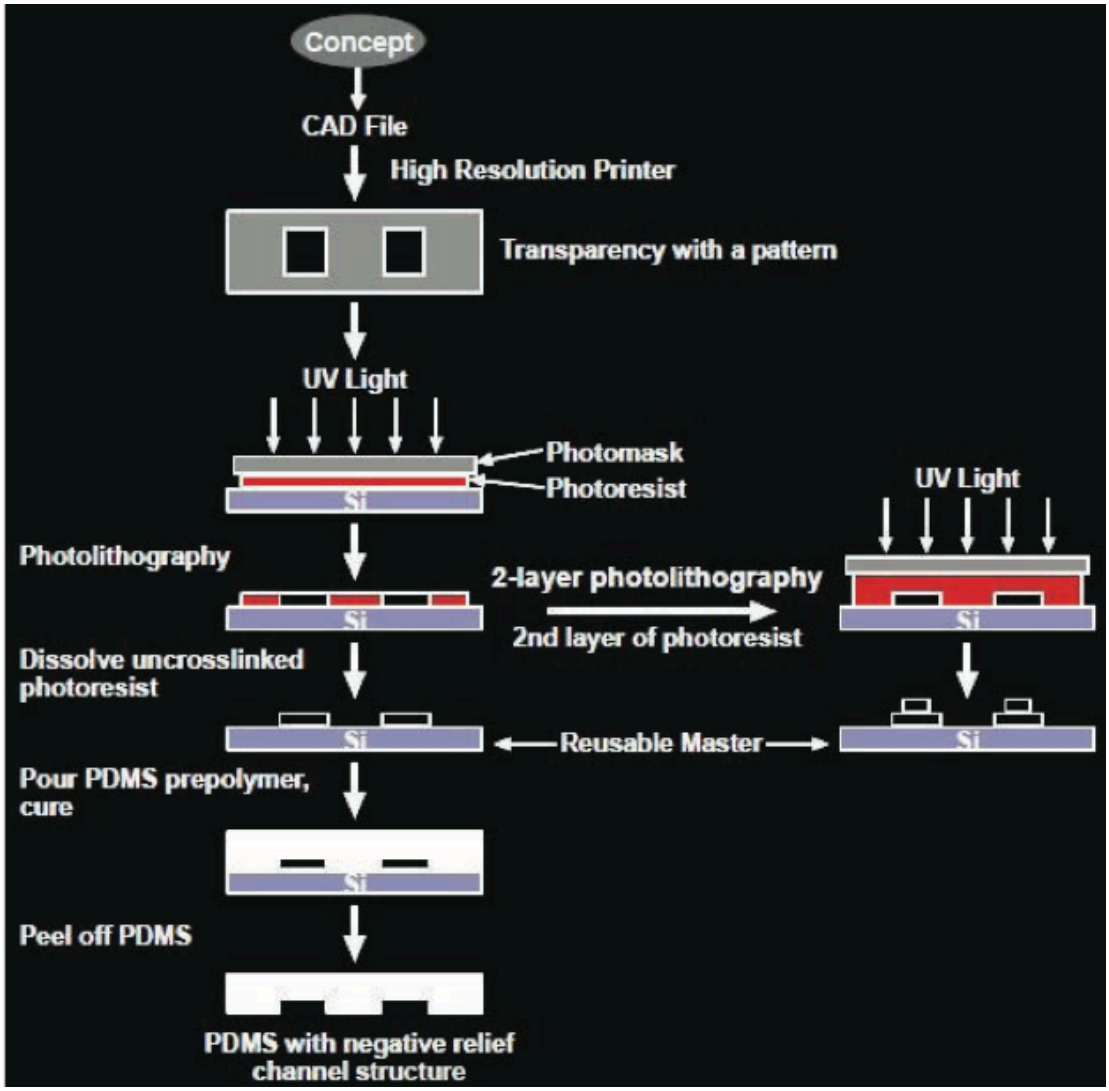

Figure 1.1: Microfluidic device fabrication process

1.3 Model System:

Saccharomyces cerevisiae, baker's yeast, is the model eukaryotic organism of choice, due to its simple genetics and relatively high growth rate. The pheromone response system in *Saccharomyces cerevisiae* is arguably the best-

characterized signaling pathway of any eukaryote, and it has long served as a prototype for hormone, neurotransmitter and sensory responses in humans. Yeast represents a unique and informative model system; these cells are non-motile yet are able to form tube-shaped cells that expand dramatically in the direction of a gradient. Given the extensive structural and functional similarities between yeast and mammalian signaling systems, discoveries made in yeast are often applicable to humans. Moreover, given their small size (5 microns) yeast must detect and respond to an extremely small concentration differential across the length of the cell.

1.4 Overview of the Yeast pheromone response pathway

Haploid yeast cells are of two mating types, MATa and MATα. Two haploid cells of opposite mating type can come together, stop dividing (growth arrest), and develop a polarized growth projection towards their mating partner. Eventually, cells fuse at the tips of these projections, giving rise to a diploid zygote MATa/ MATα. MATα cells secrete a 13 residue peptide (sequence WHWLQLKPGQPMY), called alpha factor, and respond to a-Factor. Similarly, MATa cells secrete a-factor, a covalently modified peptide and respond to α factor. Yeast use the pheromone concentration to sense the direction and proximity of a possible mating partner and orient their shmoo in the direction of the closest mating partner. Pheromone secreted by a cell of one mating type binds to a

seven transmembrane receptor on the surface of a partner of the opposite mating type.

The signaling in yeast mating pathway begins with G protein-coupled receptors at the plasma membrane. G proteins are Guanine nucleotide-binding proteins, which are made up of alpha (α), beta (β) and gamma (γ) subunits and are activated by G-Protein Coupled Receptors (GPCR). The activation of the G protein leads to a series of changes. The signaling mechanism involves the exchange of GDP for GTP as a "switch" to allow or inhibit biochemical reactions. The binding of alpha factor to the receptor activates a cascade of four protein kinases, and culminates with the phosphorylation and activation of nuclear proteins that control cell polarity, transcription, and progression through the cell cycle (Cross et al., 1988; Sprague and Thorner, 1992; Kurjan, 1993; Herskowitz, 1995). Mitogen activated protein (MAP) kinases are serine/ threonine specific protein kinase that respond to the extracellular stimuli (mitogens) and regulate various cellular activities, such as gene expression, mitosis, differentiation and cell survival/ apoptosis. The pheromone, alpha-factor, binds the receptor Ste2 in the "MATa" type yeast cells. The activated Ste2 in turn activates the heterotrimeric G protein. The Gα subunit dissociates from the G protein, and the Gβγ subunit in turn binds to Ste20 and to Ste5 (scaffold protein). These reactions result in the scaffold-dependent MAPK cascade of four protein kinases Ste20 is activated via its interaction with Cdc42. Cdc42 is a Small rho-like G-protein, binds to Ste20, Bem1, and others and is permanently pinned to the plasma membrane by a covalently attached lipid moiety Ste20 is in the vicinity of the MAPK cascade

proteins by virtue of its association with Cdc42 and Bem1 (involved in polarity establishment and binds Ste5, Cdc42, Cdc24 and Ste20). The MAPK cascade: Ste20 phosphorylates, and thereby activates, Ste11 and activates Ste11 (MAPKKK), which phosphorylates and activates Ste7 (MAPKK), and Ste7 in turn phosphorylates and activates Fus3 (MAPK).

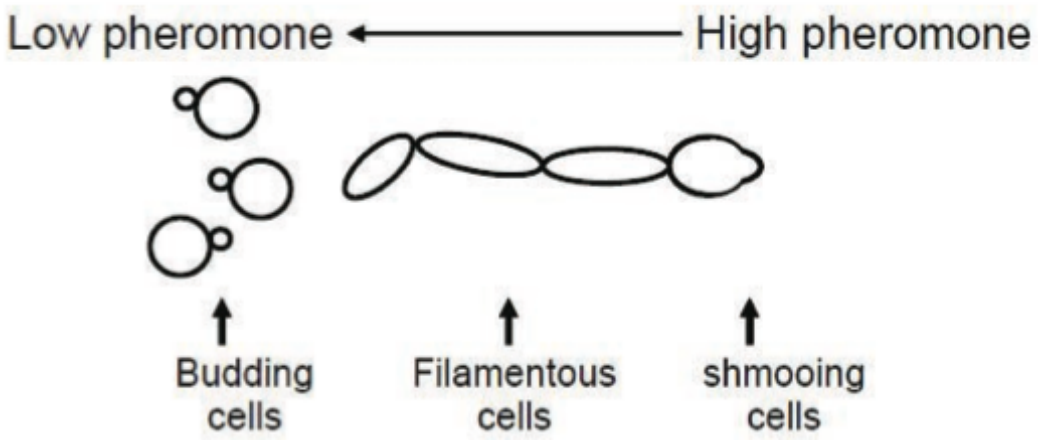

Figure 1.2: Cartoon of the how cells behave in a gradient of pheromone Yeast undergoes a developmental decision based on the concentration of alpha factor. At high pheromone levels, they arrest growth and generate a mating projection ("shmoo" morphology). At intermediate concentrations they elongate in the direction of an increasing pheromone gradient (chemotropic growth). This decision requires that the mating response pathway transmit quantitative information about the external pheromone concentration.

A second MAP kinase called Kss1 does not bind to Ste5, but appears able to transmit the mating signal in the absence of Fus3, since deletion of both MAPK genes is needed to confer sterility (Dohlman et al., 2001). Whereas either Fus3 or Kss1 will sustain the elongated cell morphology, Fus3 alone is required for growth-arrest, shmoo formation (Erdman et al., 2001) as well as chemotropic growth (growth towards a pheromone gradient, Hao et al., 2008). The cascade is

highly dependent on the scaffold protein Ste5 which acts as an adapter that binds to Ste11, Ste7 and Fus3. Fus3 and Ste5 shuttle between the cytosol and nucleus.

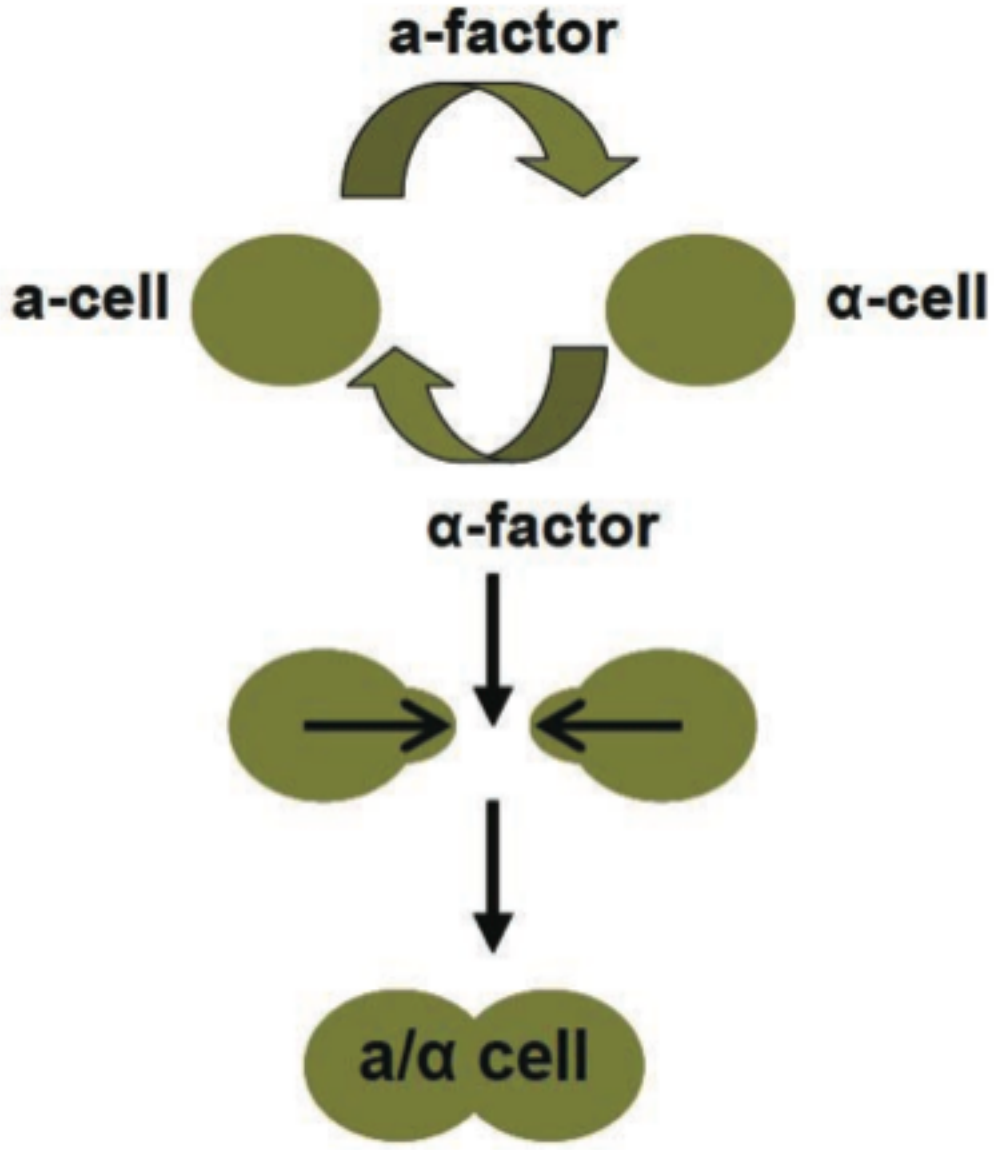

Figure 1.3: Mechanism of Yeast mating. Mating requires exchange of a- and α factor pheromones that stimulate development of a special projection called "shmoo" and eventually leads to cell fusion.

The phosphorylated Fus3 may enter the nucleus to inhibit Dig1/2 and activate the transcription factor Ste12 which promotes the transcription of a set of genes involved in mating-specific functions. The negative regulators of the pathway are the RGS protein Sst2 that accelerates the rate of GTP hydrolysis thereby forming the inactive heterotrimer. Bar1 is an extracellular, pepsin-like protease secreted by MATa cells that degrades alpha-factor (Chasse et al., 2006, Ciejek et al., 1979) BAR1 expression is induced upon pheromone stimulation.

As stated above the yeast system bears strong structural and functional similarity to signaling pathways in mammals. In particular the G-protein and MAPK components share extensive sequence similarity with their human counterparts (Dohlman et al., 2001). Thus the goal of the research is to achieve an integrated (systems level) understanding of the pheromone response pathway in yeast that can be extended to mammals.

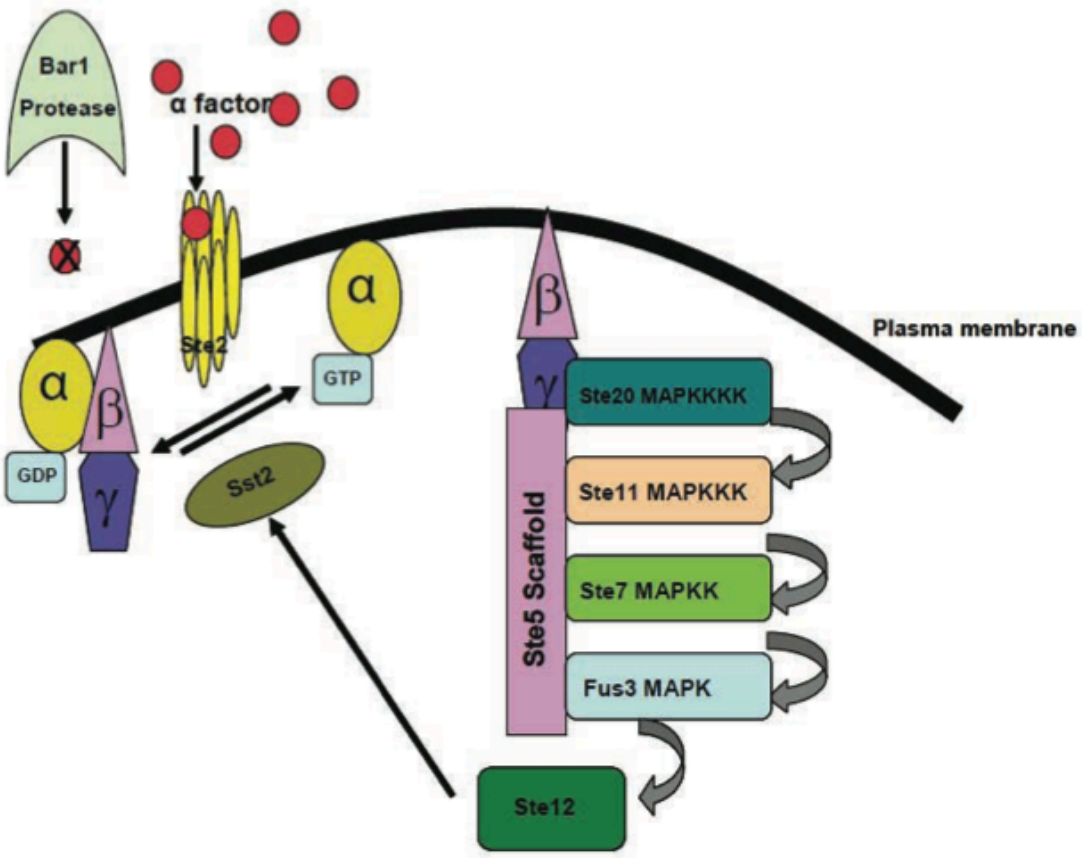

Figure 1.4: Components of the pheromone response pathway.

1.5 Yeast cell polarization

Establishment and the maintenance of cell polarity is an interplay between the asymmetric organization of the mobile cellular components like the regulatory molecules and the orientated organization polar cytoskeletal filaments. Asymmetry can be directed from internal or external cues. Chemical signaling molecules are one of the very common external cues. Eukaryotic cells can sense a gradient of

the chemical, interpret these cues by restructuring its internal apparatus, and then either move towards the signal, a process called chemotaxis, or project towards the source of the signal, commonly called chemotropism. Directed cell movement is critical in proper development, immunity, and cancer metastasis. Examples include the following: Cell orientation is directed by chemoattractant gradients of a variety of signals, such as growth factor hormones and chemokines. Much of the investigation of gradient-sensing has focused on Dictyostelium discoideum (Devreotes et al., 1998) and neutrophils (Servant et al., 2000, Srinivasan et al., 2003, Weineret al., 2002) but has also included analysis of directed movement in fibroblasts during dermal wound healing (Schneider et al., 2005).

How cells break symmetry and establish polarity is a profound question in cell biology which is still not fully understood, and an answer to which is likely to bring fundamental insights into the physical principles that govern cellular organization and morphogenesis. Haploid yeast cells upon exposure to alpha factor initiates the arrest of the cell cycle, expression of mating specific genes, and polarized growth toward the mating partner. Proteins involved in signaling, polarization, cell adhesion, and fusion are localized to the tip of the mating cell (shmoo) where fusion will eventually occur. How the cell targets and retains the proteins involved in the shmoo tip is still not completely understood.

Many of the mechanisms that regulate cell polarity in yeast are conserved in higher eukaryotes (Moseley et al., 2006, Wedlich-Soldner., 2005), Cell polarization in yeast involves choosing the direction of polarity. Internal cue within the cells produce precise patterns of polarization from which bud formation

and cell division follow. Mating cells polarize in the direction of their mating partner that is chosen by gradient sensing. Once the cell has integrated spatial cues from budding landmarks or mating pheromone, this information is fed to the polarity establishment machinery, which is responsible for polarization of the cytoskeleton and cellular components along the chosen axis. Polarity is then reinforced with targeted secretion that leads to the deposition of molecules needed for growth at the chosen site.

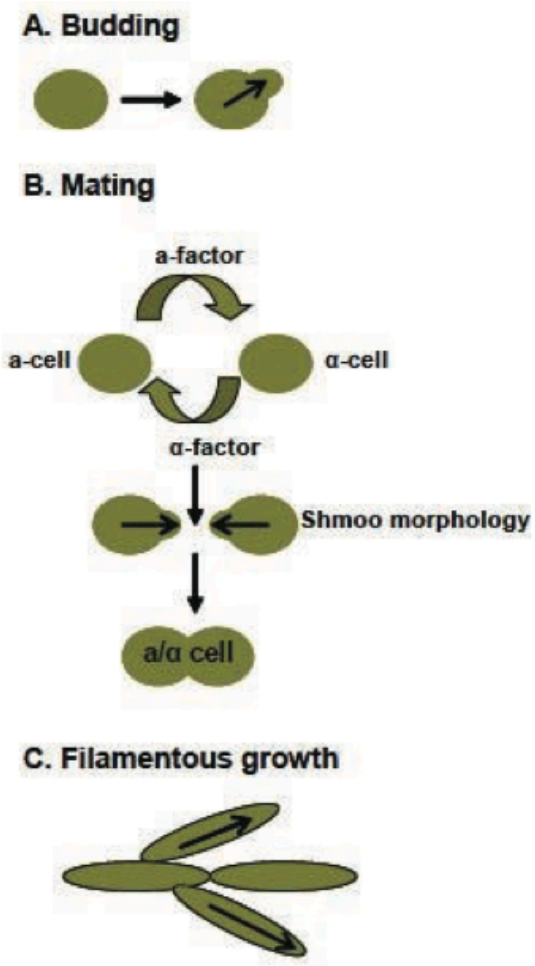

Figure 1.5: Polarized growth in the life cycle of the budding yeast during budding, mating, and nutritional starvation.

Budding yeast exhibits different types of cell polarity. During budding, the location of the bud site depends on the mating locus and pedigree of the cell (Chant et al., 1995, Freifelder et al., 1960, Hicks et al., 1997). Bud emergence initiates during the late G1 stage of the cell cycle and the bud continues to grow, the growth is focused there and restricted to the new bud by a diffusion barrier made of septins that is placed as a collar at the neck between mother and daughter cell (Chant et al., 1999, Faty et al., 2002, Barral et al 2000, Takizawa et al., 2000, Nern et al., 2000).

The second kind of polarized growth occurs during yeast mating response. Pheromone stimulation results in the activation of a mitogen-activated protein kinase signaling cascade and polarized growth toward the mating partner (Jackson et al., 1990). Polarized growth leads to the formation of a mating projection toward the mating partner, eventually bringing the two cells in direct contact (Jackson et al., 1990).

A third form of polarized growth in occurs during limited access to specific nutrients, such as nitrogen deprivation. Under these conditions, diploid yeast cells initiate pseudohyphal growth where the cells elongate, bud mainly from one pole of the cell, and form elongated cells that can invade a solid medium (Gehrung et al., 1990, Kron et al., 1995). A related response occurs in haploids, called invasive growth, under intermediate pheromone concentration (Hao et al., 2008).

In our entire study we focus on haploid yeast cells. Cytoskeletal polarity in yeast is guided by the distribution of Cdc42p on the plasma membrane. Cdc42 is

a small GTPase of the Rho family that stands out as playing a central role in establishing cell polarity in all eukaryotic cells irrespective of the biological context (Etienne-Manneville et al., 2004). Cdc42p activation is both necessary and sufficient to promote spontaneous cell polarization and must be controlled temporally and spatially. Under physiological conditions, proper Cdc42p function requires its ability to hydrolyze GTP. GTP binding requires the guanine-nucleotide-exchange factor (GEF) Cdc24p. The initial polarization of Cdc24p and Cdc42p during mating and bud-site selection is dependent on the protein which co localizes with Cdc24p and Cdc42p to growth sites, in the plasma membrane (Bender et al., 1991). During the mating response, pheromone stimulation leads to the dissociation of the Gß subunit, which recruits the Far1 protein to the plasma membrane (Butty et al., 1998). Far1 is used to recruit Cdc24 to active Gß subunits of the heterotrimeric G-protein (Butty et al., 1998, Shimada et al., 2000, Nern et al., 1999). This interaction allows Cdc24 to convert Cdc42 from its GDP bound state to its active GTP-bound state near active G-protein coupled receptors (Butty et al., 1998, Shimada et al., 2000, Nern et al., 1999). GAP proteins promote the hydrolysis of GTP, converting Cdc42 back to its inactive form. Active Cdc42 can interact with the scaffold protein Bem1, which also interacts with Cdc24. The interaction of Bem1 with Cdc42 and Cdc24 increases Cdc24's ability to act as a GEF, thereby forming a positive feedback loop (Irazoqui et al., 2003, Kozubowski et al., 2008).

The precise mechanism by which Bem1 increases the GEF activity of Cdc24 is unknown, but it has been shown to require the p21 associated kinase

Ste20 (Kozubowski et al., 2008). Polarized Cdc42GTP directs the assembly of actin cables, which change the morphology of the cell (Park et al., 2007, Sohrmann et al., 2003). The polarized cytoskeleton further stabilizes cell polarity by directly transporting Cdc42 to the polarization site via the actin cables (Park et al., 2007, Wedlich-Soldner et al., 2003). Even in the presence of a spatially homogenous pheromone concentration, haploid yeast can establish and maintain a polarized distribution of signaling proteins (Sohrmann et al., 2003, Nern et al., 2000, Wedlich-Soldner et al., 2003). In this case polarization occurs toward the previous bud site. When proteins that mark the bud site, such as Rsr1, are removed polarization occurs in a random direction (Nern et al., 2000). This type of behavior is termed spontaneous symmetry breaking, because cell polarization occurs in the absence of any external or internal cues. In this situation the localized cluster of Cdc42 does not remain fixed, but diffuses around the plasma membrane (Nern et al., 2000). Importantly, spontaneous polarization does not require actin-directed transport of signaling proteins in early phase. (Irazoqui et al., 2003).

Persistent advancement in systems biology relies on the development of experimental technologies that both complement and validate computational models. Many prior studies up until now have utilized static (steady-state) measurements of gene expression. It is evident form the literature that the focus has been on simple dynamic inputs and responses to those inputs, while on the contrary biological systems may ex-perience many complex and dynamic stimuli in their natural habitat. For future success, it is vital that we are able to track single-cells

in a time dependent manner for a long time in response to dynamic perturbation. Microfluidic technology continues to hold great promise in re-creating in vivo-like microenvironments for studying cellular processes. With their capabilities to constrain and dynamically control the cellular growth environment, microfluidic devices support real-time and long-term measurement of single cell dynamics. In the following chapters, we describe various studies that take an integrative approach by using the microfluidic technology along with molecular biology and computational modeling to understand the cellular response to a changing environment by using Yeast as our model organism.

Chapter 2.

Regulation of Cell Signaling Dynamics by the Protein Kinase-Scaffold Ste5

2.1 Introduction

Cell differentiation requires the ability to detect and respond appropriately to a variety of extracellular signals. Here we investigate a differentiation switch induced by changes in the concentration of a single stimulus. Yeast cells exposed to high doses of mating pheromone undergo cell division arrest. Cells at intermediate doses become elongated and divide in the direction of a pheromone gradient (chemotropic growth). Either of the pheromone-responsive MAP kinases, Fus3 and Kss1, these two protein kinases equally promotes cell elongation,

but only Fus3 promotes chemotropic growth. Whereas Kss1 is activated rapidly and with a graded dose-response profile, Fus3 is activated slowly and exhibits a steeper dose-response relationship (ultra-sensitivity). Fus3 activity requires the scaffold protein Ste5; when binding to Ste5 is abrogated, Fus3 behaves like Kss1, and the cells no longer respond to a gradient or mate efficiently with distant partners. We propose that scaffold proteins serve to modulate the temporal and dose-response behavior of the MAP kinase.

Different environmental stimuli often employ the same set of signaling proteins to achieve very different developmental outcomes. A prototypical example occurs in the yeast *Saccharomyces cerevisiae.* Haploid cells exposed to mating pheromones will undergo cell division arrest and polarized cell expansion leading to shmoo formation. These events prepare haploid a- and a-type cells to mate, resulting in the formation of an a/a diploid (Wang and Dohlman, 2004). Alternatively, cells in nutrient-poor media exhibit an altered budding pattern, long branching filaments, and increased adherence and invasion of the substratum. This behavior is variously known as invasive growth, pseudohyphal growth, or filamentous growth (Figure 1A). Despite striking differences in cell morphology and behavior, the pheromone- and nutrient-response pathways employ the same protein kinase cascade comprised of Ste20, Ste11, Ste7, and either of two mitogen-activated protein (MAP) kinases, Kss1 and Fus3 (Liu et al., 1993; Roberts and Fink, 1994). Kss1 is needed for invasive growth, while Fus3 is required for growth arrest (Cook et al., 1997; Madhani and Fink, 1997; Roberts et al., 2000; Roberts and Fink, 1994; Sabbagh et al., 2001) (Figure 1A).

Another lesser-known example of component sharing is the differentiation switch triggered by alterations in pheromone concentration. Whereas yeast cells exposed to a high dose of pheromone undergo cell division arrest and shmoo formation, at lower doses they transiently arrest, become elongated, and then divide, presumably in the direction of a pheromone gradient (Dorer et al., 1995; Erdman and Snyder, 2001; Paliwal et al., 2007; Segall, 1993) (Figure 1A). The growth-arrest and elongated- growth pathways employ the same cell-surface receptor, G protein transducer, and downstream protein kinases (Figure 1A). Whereas either Fus3 or Kss1 will sustain the elongated cell morphology, Fus3 alone is required for growth arrest and shmoo formation (Erdman and Snyder, 2001). It is not known if Fus3 or Kss1 contribute to a chemotropic-growth response.

In the past, stimulus-specific responses have been ascribed to the scaffolded association of specific protein kinases. The term scaffold is commonly used to describe a protein that can assemble multiple distinct binding partners and promote their mutual interactions. In yeast, the scaffold protein Ste5 has binding partners that include Ste11, Ste7, and Fus3. Where as Ste5 is absolutely required for activation of Fus3 (Andersson et al., 2004; Breitkreutz et al., 2001; Flatauer et al., 2005; Kusari et al., 2004; Maleri et al., 2004), Ste5 binds poorly to Kss1 and is not required for the Kss1-mediated invasive-growth response (Choi et al., 1994; Kusari et al., 2004; Printen and Sprague, 1994). Based on these differences, it has been widely assumed that Ste5 insulates Fus3 from other MAP kinases that use

the same upstream components and thus prevents activation by irrelevant signals. While clearly required for Fus3 activity, however, Ste5 nevertheless allows activation of Kss1 by pheromone (Andersson et al., 2004; Breitkreutz et al., 2001; Choi et al., 1994; Flatauer et al., 2005; Maleri et al., 2004; Printen and Sprague, 1994). These observations have prompted a search for additional functions for Ste5.

More recently, Ste5 was reported to undergo a stimulus induced conformational change and to allosterically regulate Fus3 kinase activity (Bhattacharyya et al., 2006; Sette et al., 2000). Ste5 stimulates Fus3 autophosphorylation at Tyr-182, one of two sites normally phosphorylated upon full activation of the kinase (Gartner et al., 1992). This monophosphorylated form of Fus3 is partially active. Moreover, the interaction of Ste5 with Fus3 results in diminished overall signaling at the level of new gene transcription (Bhattacharyya et al., 2006; Sette et al., 2000). Thus, Ste5 is essential for Fus3 signaling but also limits the overall output of the Fus3 signaling pathway.

Here we establish a role for Ste5 in mediating chemotropicgrowth behavior in yeast. We show that Ste5 acts as a dynamic modulator of Fus3, conferring slow kinase activation and a sigmoidal (ultrasensitive) pheromone dose-response profile.

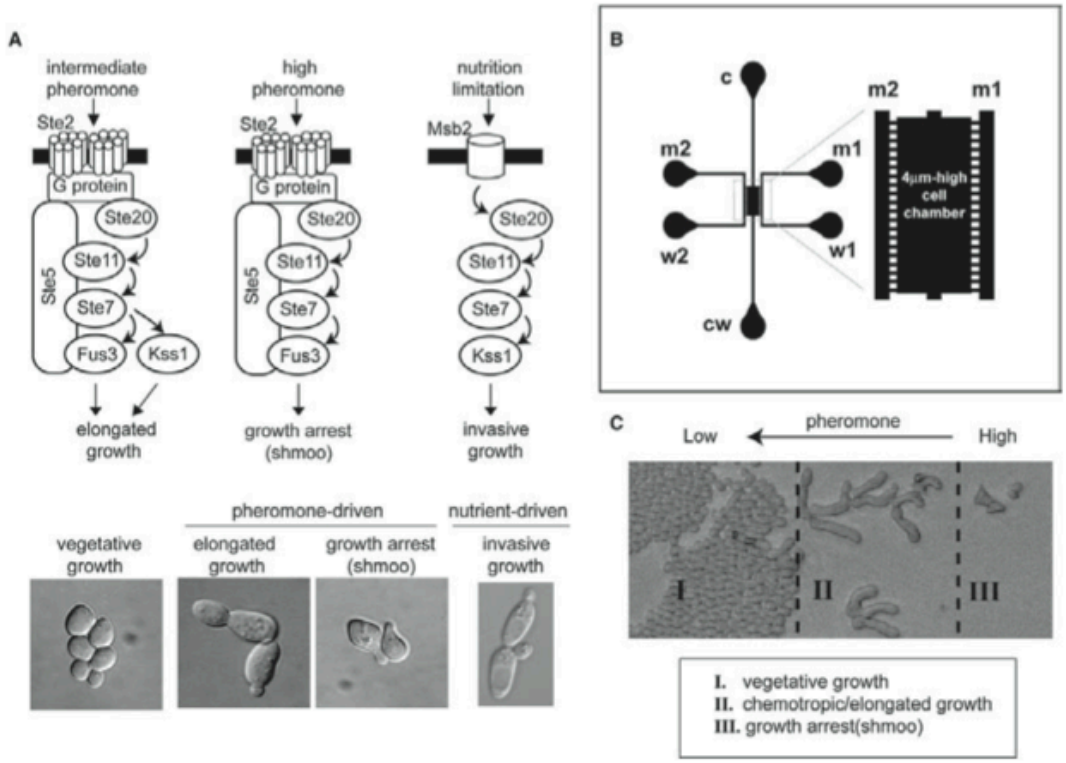

Figure 2.1: Yeast Cell Differentiation Induced by Different Concentrations of Pheromone: (A) Common signaling components are used for nutrient-driven invasive growth, as well as for the pheromone-driven switch from vegetative growth to elongated or chemotropic growth and growth arrest. (B) Schematic of the microfluidic gradient device. Ports c and cw correspond to cell loading and cell waste, respectively. Ports m1 and m2 are for media supply, w1 and w2 are media waste ports. Gradient within the chamber is established by diffusion between m1 and m2 via the microchannels that connect the media channels to the cell chamber. (C) Yeast cells undergo three distinct developmental fates in a pheromone gradient. Cells are loaded evenly and at a very low density, but rapidly dividing cells eventually fill the chamber at the lowest concentrations of pheromone (zone I).

By comparison, Kss1 activation is rapid and exhibits a graded dose-response behavior. We propose that Ste5 allows cells to discriminate between

pheromone doses appropriate for chemotropic growth versus growth arrest and mating and does so by altering the time and dose-dependent behavior of Fus3.

2.2 Results

Yeast cells are well-known to undergo a developmental switch from nutrient-driven invasive growth to pheromone-driven growth arrest and mating. Previous investigations have highlighted the fact that these pathways share many, but not all, component proteins. However, it remains unclear which pathway specific components are required for signal fidelity as opposed to pathway specific behaviors such as altered morphology or invasion. As an alternative approach, we investigated a distinct differentiation switch triggered by a common stimulus (Figure 1A). At high doses of pheromone, cells arrest in G1 and exhibit the characteristic shmoo morphology. At intermediate doses, they grow slowly and appear elongated (Figure 1A). Given that these events require the same receptor and G protein, as well as many of the same effector kinases, this system provides an excellent opportunity to determine the function of pathway-specific components. Here we investigate the role of Ste5.

Initially we investigated dose-dependent responses to pheromone, using a variety of functional assays. Pheromone-induced transcription has been shown to exhibit a graded dose-response profile (Poritz et al., 2001), whereas downstream processes such asG1arrest and mating are switch-like. Switch-like behavior is an

extreme example of ultrasensitivity, defined as any response with a Hill coefficient greater than one (Ferrell and Machleder, 1998; Goldbeter and Koshland, 1981). To determine if other aspects of the pheromone response exhibit ultrasensitivity, we monitored differentiation of cells exposed to a range of pheromone concentrations. Cells were classified into one of three categories: vegetative growth, elongated growth, or shmoo. Vegetative growth occurs in the absence of pheromone. In this case, cells divide rapidly and bud axially (new buds emerge from the daughter cell in the direction of the mother cell). At intermediate doses of pheromone, the cells appear elongated, proliferate slowly, and divide in a bipolar fashion, opposite the mother cell (Dorer et al., 1995; Erdman and Snyder, 2001; Madden and Snyder, 1992). At high doses of pheromone, the cells arrest and form a "shmoo".

Each of these morphologies is illustrated in Figure 1. As shown in Figure 2A, 85% of wild-type cells grow vegetatively at pheromone concentrations of 0.1 mMor less. At concentrations of 0.33 mM, the population transitions from vegetative growth to elongated growth, even in the absence of a pheromone gradient. At 10 mM, nearly all cells undergo growth arrest and shmoo formation. The first transition occurs over a broader range of pheromone concentrations, as compared with the second transition. Thus, the differentiation switch from elongated growth to growth arrest may exhibit ultrasensitivity.

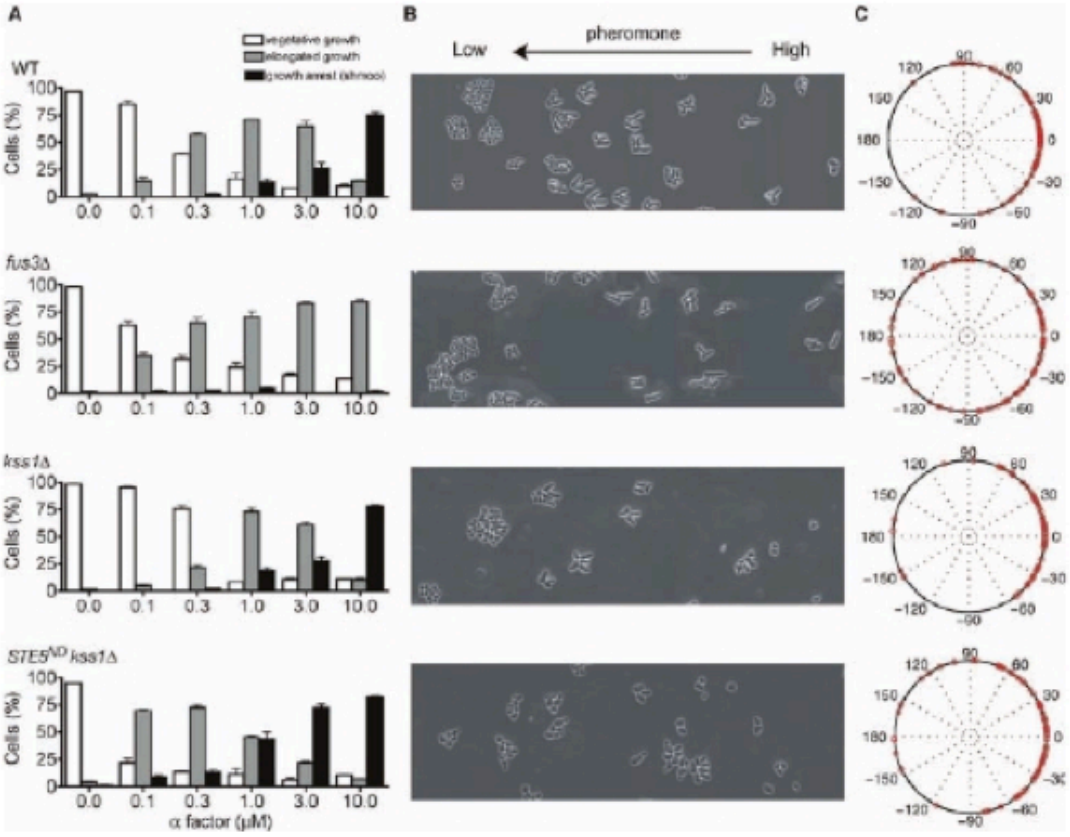

Figure 2.2: Experimental Measurements of Yeast Cell Differentiation: (A) Cell morphologies classified as vegetative growth, elongated growth (length:width R 1.6), or shmoo. Wild-type and mutant cells exposed to a uniform concentration of pheromone exhibit each of the three morphologies. (B) Cells exposed to a linear gradient of pheromone exhibit the three morphologies depending on their position within the chamber. Cell differentiation was recorded at 600 min for three independent experiments. (C) Chemotropic growth quantified as the angle of cell projections and the direction of the gradient, represented with polar plots. Error bars, ± standard error of the mean.

We then investigated how the MAP kinases contribute to the two developmental transitions. It is well-established that mutants lacking Fus3 are unable to shmoo but maintain the ability to transition from vegetative growth to elongated growth (Figure 2A, second row). Conversely, cells lacking Kss1 still undergo both transitions (Figure 2A, third row), but the dose-response profile for

the transition from vegetative growth to elongated growth is significantly steeper than that of cells containing both MAP kinases or Kss1 alone. Signaling exclusively through Fus3 increases the pheromone concentration required for elongated growth, thereby reducing the range of pheromone levels for which this behavior is observed. Kss1 broadens this range, allowing cells to become elongated at lower doses of pheromone as compared with cells that express both MAP kinases. Thus Kss1 and Fus3 confer distinct dose-response characteristics on cell growth: Kss1-mediated responses are graded, while Fus3 responses appear ultrasensitive.

We next examined whether elongated growth corresponds to chemotropic growth, defined here as cell expansion and division in the direction of a stimulus gradient. It has been suggested that chemotropic growth could allow yeast, which are otherwise non-motile, to orient new bud formation in the direction of a weak pheromone stimulus and thus toward a distant mating partner (Dorer et al., 1995; Erdman and Snyder, 2001; Madden and Snyder, 1992). To this end, we constructed a microfluidic chamber capable of exposing cells to a precisely controlled linear concentration gradient. The gradient is achieved by passive diffusion between two parallel microchannels containing either no pheromone or a dose of pheromone sufficient to induce cell division arrest (Figure 1B and see the Supplemental Data available online). There is no active flow within the growth chamber, thereby allowing the non-adherent cells to remain stationary during the course of the experiment. In this method, the cells are at low density and the

pheromone is constantly replenished, resulting in a lower dose-activity profile (see below).

As shown in Figures 1C and 2B, as well as in Figure S1 and the accompanying movies (Supplemental Data), cells within the growth chamber exhibit all three morphologies, depending on the local concentration of pheromone. Cells exposed to minimal doses of pheromone grow vegetatively and divide axially (Dorer et al., 1995; Madden and Snyder, 1992). Cells exposed to high doses of pheromone undergo cell division arrest and form a shmoo. At intermediate doses, the cells appear elongated but continue to divide slowly and in the direction of increasing pheromone concentrations (Figure 2B). This chemotropic-growth response generally entails just one round of elongated growth, after which the daughter cell detaches from the mother cell and forms a shmoo. This is in contrast to invasive growth, in which cells undergo several rounds of polarized budding to form a long filament.

In wild-type cells, the vast majority of new buds and cell projections emerge within ±60 of the gradient, and very few are outside 90 (Figure 2C). Mutants lacking Fus3 or Kss1 retain the ability to undergo the elongated-growth response. Likewise, mutants lacking Kss1 are able to divide in the direction of the gradient, although Kss1 may contribute at very low doses of pheromone or in mutants that are supersensitive to pheromone (Figures 2B and 2C) (Dorer et al., 1995; Erdman and Snyder, 2001; Paliwal et al., 2007; Segall, 1993). In cells lacking Fus3, however, newly formed buds emerge randomly with respect to the gradient, and the cells no longer undergo growth arrest and shmoo formation

(Figures 2B and 2C). Thus Fus3 is specifically required for chemotropic growth but is dispensable for elongated growth. Cellular responses mediated by Fus3 appear to be ultrasensitive, while responses mediated by Kss1 appear graded (Figure 2).

Measurements of cell morphology are somewhat qualitative, however, so we also measured changes that occur at a molecular level. Specifically, we asked if there is ultrasensitivity at the level of protein kinase activity. To this end, we monitored Fus3 and Kss1 activation in cells treated with a range of pheromone concentrations, using antibodies that recognize the dually phosphorylated (fully activated) form of each protein. As shown in Figure 3A and Figure S2, the temporal and dose-response profiles for Fus3 and Kss1 phosphorylation are distinct. At 1 mM pheromone (a dose sufficient to trigger chemotropic growth but not shmoo formation), Fus3 is phosphorylated to 22while Kss1 is phosphorylated to 48% of maximum. At 10 mM pheromone (a dose sufficient to trigger cell division arrest and shmoo formation), both kinases are maximally activated. Remarkably, we found that maximum kinase activity occurs at different times depending on the pheromone concentration; for example, Fus3 activity peaks at 60 min in response to 10 mM pheromone, whereas it peaks at 15 min in 1 mMpheromone (Figure 3A). Thus, two different doses may produce identical kinase activity at a single (early) time point but nevertheless exhibit dramatic differences in the duration and final maximum level of kinase activation. Accordingly, we quantified peak kinase activity (Figure 3D) and area under the curve (Figure 3F) for each dose of pheromone. The latter incorporates the

elements of duration and activity into a single parameter. Both of these methods accurately account for the observed differences in activity and yielded similar results. As shown in Figure 3F, the effective Hill coefficient for activation of Fus3 is substantially higher than for activation of Kss1 (nH = 2.2 and 1.3, respectively). This difference mirrors the dose-response profiles for Fus3 and Kss1-mediated cell differentiation responses, as reported in Figure 2. Note that we measured the MAP kinase activation of a population of cells. The response might be even more switch-like in individual cells. Fus3 and Kss1 are activated by the same upstream protein kinases, most immediately by the MAP kinase kinase Ste7. Nevertheless we have shown above that Fus3 and Kss1 exhibit very different temporal and dose-dependent behaviors. Whereas Kss1 activity peaks quickly, Fus3 activity increases slowly at a constant rate (slope) that is independent of the pheromone level. In both cases, increasing the pheromone level delays the time at which MAP kinase activity begins to decline.

One way to account for this unusual behavior is to assume that the predominant effect of increases in pheromone concentration is to prolong the duration of Ste7 activity (Figure 3B, top panel). To address this possibility, we constructed simple mathematical models of Fus3 and Kss1 activation and investigated each models response to varying durations of Ste7 activation. Both models assume that the phosphorylation and dephosphorylation reactions follow Michaelis-Menten kinetics. Each model further assumes that the Vmax for phosphorylation of the MAP kinase is proportional to the active Ste7 concentration. The difference between the models is that the rate constants

describing phosphorylation and dephosphorylation of Kss1 are larger than those of Fus3 (Supplemental Data). Figure 3B shows the Ste7 activation profile used as the input signal for both MAP kinases (top panel), as well as the activity for Fus3 (middle panel) and Kss1 (bottom panel) predicted by the corresponding models. There is a very good qualitative agreement between these simulations (Figure 3B) and the experimental data (Figure 3A). The models also demonstrate how a purely kinetic mechanism (slow activation) can be used to convert a graded response to one that is more switch-like (see the Discussion). We then considered why Fus3 is activated more slowly than Kss1. This difference could be an inherent property of each kinase.

Alternatively, slow activation of Fus3 could be due to binding of Ste5. Indeed, Ste5 was reported previously to diminish Fus3-mediated transcription responses (Bhattacharyya et al., 2006). To investigate the contribution of Ste5 to Fus3 dynamics, we monitored kinase activation in the absence of Ste5-Fus3 interaction. Deletion of STE5 blocks signaling altogether, so as an alternative we used a mutant form of Ste5 in which Fus3 docking is disrupted (nondocking allele, Ste5ND). This mutant binds poorly to Fus3 (Maeder et al., 2007) yet produces an enhanced transcription-induction response (Bhattacharyya et al., 2006). Thus we investigated how Ste5ND affects dose- and time-dependent signaling events including cell morphogenesis, gradient sensing, and kinase activation.

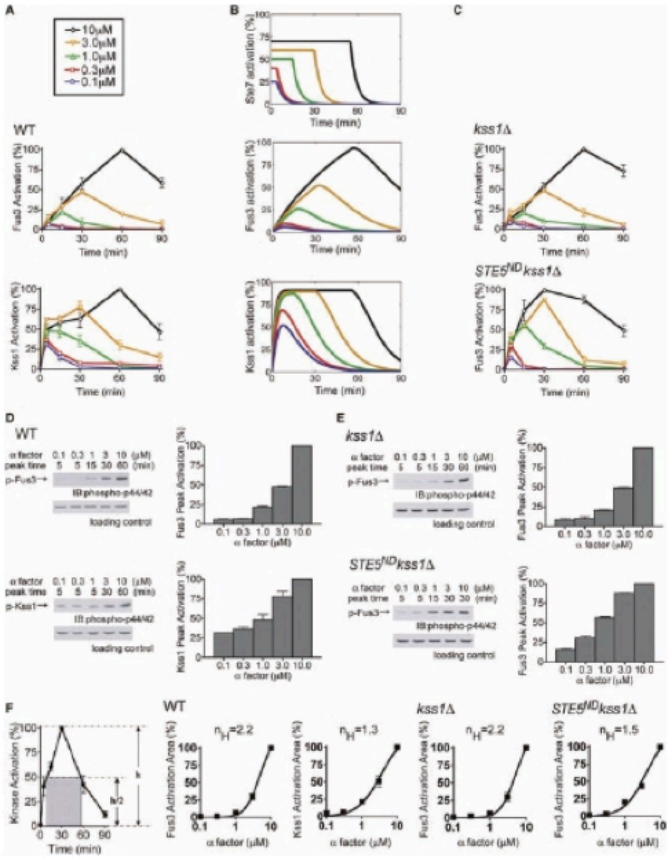

Figure 2.3: Experimental and Computational Analysis of MAP Kinase Activation with or without Ste5: Time course of MAP kinase activation monitored in wild-type (A and D) and mutant (C and E) strains treated with the indicated pheromone concentrations, using phospho-p42/44 antibodies that recognize the dually phosphorylated (fully activated) form of each protein. (B) Simple mathematical models qualitatively reproduce the experimental data for Fus3 and Kss1 activation. Each model assumes that the upstream signal (e.g., Ste7) is saturated at early times and at low pheromone concentrations, and any further increases in pheromone concentration prolong the duration of the upstream signal. (D and E) Kinase activation quantified as the percentage of maximum activation obtained at each dose (Peak Activation). (F) Kinase activation at different concentrations of pheromone quantified as the area of the rectangle fit to half-maximum activity (Activation Area) and fit by the Hill equation (nH, Hill coefficient). Band intensity from three or more experiments was quantified by scanning densitometry presented as percentage of maximum intensity. Error bars, standard error of the mean.

To eliminate any possibility that Kss1 can substitute for Fus3 or otherwise modulate Fus3 activity in the absence of Ste5, these experiments were conducted in a Kss1-deficient strain. As shown in Figure 2A, cells that express Ste5ND are able to undergo the transitions from vegetative growth to elongated growth and then to growth arrest. However, the transitions occur at lower pheromone concentrations and the dose-response profile is more graded than that seen in wild-type cells. Indeed, we observed considerable overlap in the distribution of all three categories of cells within the gradient chamber.

Moreover, cells that express Ste5ND exhibit diminished elongation and orientation toward the source of pheromone (Figures 2B and 2C). Likewise, Fus3 becomes fully activated in the Ste5ND strain, but activation occurs with faster kinetics (Figure 3C). Additionally, the Hill coefficient for activation of Fus3 is reduced from nH = 2.2 in wild-type cells to nH = 1.5 in Ste5ND mutant cells, a value similar to that normally observed for Kss1 (nH = 1.3) (Figure 3F). Thus, under conditions in which it is no longer modulated by Ste5, the dynamic and dose-dependent behavior of Fus3 resembles that of Kss1. We also considered the possibility that Ste5ND might affect the activity of other signaling components upstream of Fus3, such as Ste11 or Ste7. To test this, we examined whether Ste5ND alters the activity of Kss1, which likewise requires Ste11 and Ste7. In accordance with the model, Ste5ND (in the absence of Fus3 expression) had no effect on Kss1 activation (Figure S3). Another upstream mechanism of regulation is pheromone degradation. The pheromone protease Bar1 is upregulated upon prolonged pathway activation, and different degrees of induction by Fus3 and

Kss1 might somehow underlie the differences observed for the two kinases. To address this concern, and as a further test of our computational model, we measured Fus3 and Kss1 activation in a bar1D mutant strain (Figure 4A). As anticipated, differences in the dynamic and dose-dependent behaviors of Fus3 and Kss1 remain unchanged. Strikingly, by altering only the input signal profile, the equations and parameters that govern kinase activation in wild-type cells could also be used to accurately describe kinase activation in the bar1D mutant cells (Figure 4B).

Finally, we examined physiological importance of the elongated and chemotropic growth behaviors in mating. Previous investigations employed the pheromone-confusion assay, which compares overall mating efficiency in the presence or absence of added pheromone. The underlying assumption is that exogenous pheromone will obscure natural pheromone gradients and thereby diminish the ability of cells to detect a potential mating partner (Dorer et al., 1995; Nern and Arkowitz, 1998; Strickfaden and Pryciak, 2007; Valtz et al., 1995). One drawback to this method is that addition of excess exogenous pheromone is also likely to obscure or otherwise interfere with pheromone clearance by Bar1 protease, receptor occupancy, and adaptation/ desensitization responses that further impinge on mating efficiency. As an alternative approach, we measured mating efficiency under conditions in which potential mating partners are rare (10:1 ratio) and spatially segregated (plated on solid growth medium). As shown in Figure 4, the Ste5ND mutants mate substantially better than wild-type cells, presumably because they can better detect and respond to a distant mating

partner. Conversely, Ste5ND mutants mate more poorly under conditions in which potential mating partners are more abundant (1:10 ratio) but still dispersed, presumably because they can no longer orient toward the closest of multiple potential mating partners. This reduction in mating efficiency occurs despite the increase in pheromone sensitivity. From these data, we conclude that Ste5 confers the slow and ultrasensitive responses characteristic of Fus3. If Fus3 cannot bind to Ste5, the cells no longer undergo chemotropic growth and exhibit an altered ability to mate efficiently with partners at a distance.

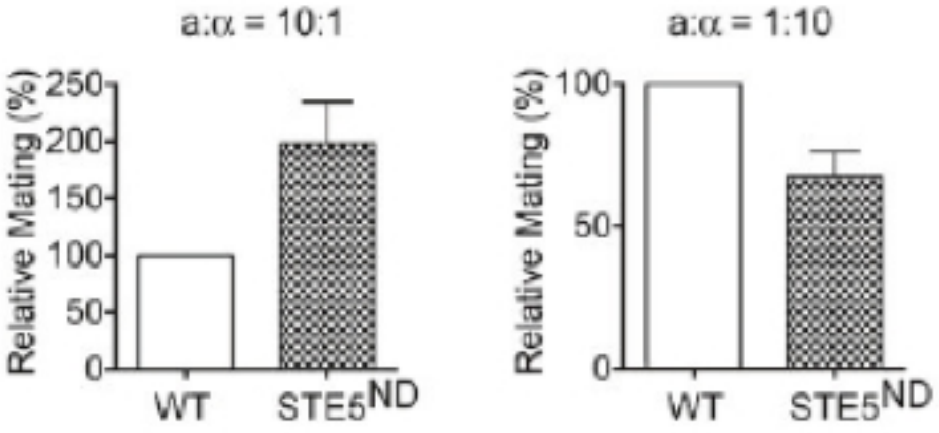

Figure 2.4: Physiological Analysis of the Role of Ste5 in Mating : Wild-type or STE5ND a-type cells and a-type tester cells were spread separately and evenly onto plates containing selective medium. Colonies of a/a diploids were counted after 2 days. Mating efficiencies averaged from three independent experiments are relative to wild-type (WT). Error bars, standard error of the mean.

2.3 Discussion

The pheromone response pathway is perhaps the best-characterized signal transduction system in any eukaryote, and it has long served as a prototype for hormone, neurotransmitter, and sensory-response systems in humans (Wang and Dohlman, 2004). Genetic and biochemical studies revealed that pheromone-induced growth arrest requires a protein kinase cascade comprised of Ste20, Ste11, Ste7, and Fus3. These same signaling components are required for pheromone-induced elongation and gradient-sensing behavior. Thus, an important question is how the same pathway elicits different developmental responses. Here we demonstrate that Ste5 selectively alters the temporal and dose-dependent behavior of Fus3 and thereby allows cells to perceive a stimulus gradient. The cells are subsequently able to undergo chemotropic growth, growth arrest, and effective fusion with a distant mating partner.

Experiments conducted in a variety of other systems have revealed that MAP kinases can produce distinct cellular responses depending on the temporal behavior of the pathway. In one oft-cited example, epidermal growth factor causes transient activation of the ERK MAP kinase leading to cell proliferation, while nerve growth factor causes sustained ERK activation and cell differentiation (Marshall, 1995). Similarly in yeast, temporal differences in MAP kinase activation can dictate whether cells follow a mating or nutrient-driven invasive-growth program. Specifically, when upstream kinases Ste11 or Ste7 are mutated so as to

be permanently active, Kss1 is activated in a sustained manner, in preference to Fus3, and this condition leads to invasive growth but not mating (Andersson et al., 2004; Flatauer et al., 2005; Maleri et al., 2004).

Another way MAP kinases can produce distinct cellular responses is through changes in the dose-dependent behavior of the pathway. MAP kinase signaling pathways have long been known to exhibit ultrasensitivity (Koshland et al., 1982). For example, MAP kinase cascades in Xenopus oocytes use a variety of mechanisms to produce an all-or-none response leading to cell maturation (Ferrell and Machleder, 1998). On the other hand, the pheromone-induced transcription response in yeast exhibits a more graded dose-response profile (Poritz et al., 2001), even when downstream processes such as G1 arrest and mating are switch-like. Our data reveal that the two pheromone-responsive MAP kinases exhibit distinct dose-dependent behaviors. Whereas activation of Kss1 is graded, activation of Fus3 is ultrasensitive. The ultrasensitivity exhibited by Fus3 is not as dramatic as that demonstrated in Xenopus but is comparable to the benchmark example hemoglobin, which exhibits a Hill coefficient of 2.8. Our data show that Ste5 is required for the unique time- and dose-dependent characteristics exhibited by Fus3. Ste5 was originally considered to function as a passive tether for protein kinases. More recently, Ste5 was shown to be required for Fus3 activation but also impedes full activation of the signaling pathway (Bhattacharyya et al., 2006). That loss of signaling was demonstrated using a reporter transcription assay. To determine the contribution of Ste5 to MAP kinase function, we evaluated signaling in the absence of Fus3 binding (Ste5ND). Signaling was monitored by cell

differentiation, gradient sensing, and MAP kinase activation assays. By all of these measures it appears that Ste5 is necessary for the slow and ultrasensitive responses exhibited by Fus3. When Ste5 binding is abrogated, Fus3 behaves like Kss1.

A distinction between our analysis and prior investigations is that we considered the role of pheromone gradient sensing. Most studies of the yeast pheromone response have been done with uniform and saturating concentrations of pheromone. In a physiological setting, however, yeast cells are likely to be exposed to a pheromone gradient emanating from a potential mating partner. When that partner is too distant for mating to occur, the gradient will be weak and some mechanism must exist to bridge the divide. Here we demonstrate that Ste5 promotes cell elongation in the direction of a pheromone gradient, thereby increasing the probability of mating with a distant partner.

Finally, our computational analysis reveals how a kinetic mechanism(specifically, slow activation) can potentially be used to convert a graded response to one that is more switch-like. We postulate that the main effect of increasing pheromone concentration is to increase the time the signal is on. In this scenario, the fast activation kinetics of Kss1 allows it to faithfully track the input signal. Conversely, the slow activation kinetics of Fus3 means that it does not saturate while the incoming signal is present. Because Fus3 activity increases linearly with time, the response increases with time and thus with pheromone concentration.

In summary, the findings presented here reveal one way that scaffolds contribute to protein kinase activity. In this example, Ste5 alters the dynamic

behavior of Fus3, and these changes promote gradient sensing and orientation toward a distant mating partner. Given the prevalence of scaffold proteins in signaling cascades, the mechanisms elucidated here for Ste5 will likely prove applicable to cell differentiation programs in other cellular systems.

2.4 Experimental Procedures

2.4.1 Strains and Plasmids

Standard methods for cell growth and maintenance were used throughout. Strain BY4741 (MATa leu2D met15D his3D ura3D) and BY4741-derived mutants were used unless otherwise indicated. Details of plasmid construction are provided in the Supplemental Data.

2.4.2 Immunoblot Analysis

Cell extracts (20 mg/lane) were resolved by 12% SDS-polyacrylamide gel electrophoresis and immunoblotting as described (Sabbagh et al., 2001). Band intensity was quantified by scanning densitometry using ImageJ (National Institutes of Health).

2.5 Microfluidics Chamber and Quantification of Gradient Sensing

A microfluidic device was constructed similar to one described previously (Paliwal et al., 2007) was constructed. The devices were generated using standard techniques of photolithography and replica molding described earlier by various groups (Duffy et al, 1999; Hansen and Quake, 2003). Briefly, the device design was first drawn using AutoCAD 2005 (Autodesk Inc.) and then a Photomask was printed onto a transparent film at 10,000 DPI (Output City, Poway, CA). For the Master molds, a clean silicon wafer was spin coated with SU-8 2000 (MicroChem Corp., Newton, MA) to appropriate depths using a Headway PWM32 programmable spinner (Headway Research Inc., Garland, TX) and patterned by UV light through the Photomask. Lastly, the silicon/SU-8 master mold was treated with chlorotrimethylsilane vapors (Sigma) for 2 minutes for easy release of the PDMS monolith. Poly-dimethylsiloxane (PDMS, Sylgard 184, Dow Corning, Midland, MI) was mixed 10:1 (resin:crosslinking agent) and poured onto the silicon/SU-8 master mold and left for baking at 80◦CC for 1.5 h in a dry gravity oven (Fisher Scientific). The PDMS mix was degassed in a vacuum desiccator prior to pouring into the master mold. Cured PDMS monolith was then peeled off the master mold and fluidic ports (for media/cell loading) were punched with gauge 20 Luer stub (McMaster-Carr). The punched holes were then flushed with 0.2-mm filtered dH2O to remove debris. Chips were individually cut out from the PDMS monolith and their surface was cleaned using office grade Scotch Tape (Type 810, 3M). These clean individual chips were then plasma bonded to glass cover slips to be used in the experiment.

First, the PDMS chips and the cover slips (24-40 mm, Corning Inc., Corning, NY) were cleaned with acetone, isopropanol, methanol in sequence and air dried using high velocity stream of filtered air, followed by exposure to oxygen plasma for 3 minutes in UVO cleaner. Next, the chip was laid on top of the cover slip to bring the two in contact and baked at 80◦C overnight to develop very strong bonding (Wu et al, 2002).

The fluidic channels (black in Fig. a) were 10 μm high. The cell trapping region was fabricated to a depth of 4 μm. The small diffusion channels (red in Fig. a) were fabricated to be 1 μ tall to restrict the cells in the chamber and allow for diffusion to occur between the two input channels. This device offers a number of significant technical advantages. Fabrication and operation of the device is fairly straightforward, as it requires only a single PDMS layer and has relatively fewer-number of ports. The gradient generation does not require active flow in the cell-trapping region during operation, a critical factor for chemotropism studies in a concentration gradient. Furthermore, cell flocculation is avoided by using a height-constrained cell chamber that allows monolayer growth to achieve long-term single-cell temporal data (Cookson et.al 2005.).

2.5.1 Cell loading and gradient generation cell culture

Yeast cells were grown in synthetic drop-out (SD) medium containing 2% glucose supplemented with all the essential amino acids. Cultures were grown at 30◦CC for 18-24h to a density of 1.0±0.25 at OD600. For loading, cultures were diluted with media to an OD600 of 0.05. In preparation for cell imaging, devices were mounted on to the Microscope stage and primed with 0.2mm filtered dH2O. Each of the ports (m, w, w2, cw, see fig a) were then connected to individual syringe (10 ml) filled with media using microbore Tygon tubing (Cole Parmer, ID 0.02). The media in syringe at port m2 was added with pheromone (Sigma) and a red fluorescent dye (Sulphorhodamine 101, Sigma) for gradient generation and easy visualization of the gradient profile. All the flows in the device were driven by gravity based hydrostatic pressure (inH2O). The syringe heights were set such that media inputs at port m1 and m2 were maintained at same pressure. Similarly the two waste ports (w1 and w2) were also maintained at same pressure but lower than that of the input ports.

The cells were introduced into the chamber using a syringe containing cell suspension. To facilitate cell loading, the cell port was pressurized by raising the height of the syringe containing cell suspension. Once there were enough cells in the chamber syringe height was adjusted to the same height as that of the cell-waste port. During the operation, the heights of the input port pair were set the highest, cell/cell-waste ports set between, and the waste ports were set the lowest. The pressure differences at the various port pairs were such that during the operation there would be no active flow through the cell chamber. The concentration gradient was established solely due to molecular diffusion between

the two input channels through the small diffusion channels. The pheromone concentration ranged from 0 to 300nM in the cell chamber such that all the three developmental stages were in the same field of view.

Image acquisition was done with a Nikon Diaphot TMD epifluorescence or Olympus IX81 inverted microscope. Image processing and analysis was done using Slide Book 4.1 Advanced Imaging Software and ImageJ. Polar plots are presented using MATLAB (Mathworks).

2.5.2 Quantitative Mating Efficiency Assay

DC17 (MATa his1) and BY4741 cells were grown to A600nm 1.0, diluted with water, and spread separately and evenly onto plates containing synthetic growth medium. Diploid colonies were counted after 2 days. Mating was conducted with 5 × 10^4 α cells and 5 × 10^5 a cells (1:10), or 5 × 10^5 α cells and 5×10^4 a cells (10:1).

2.6 Acknowledgements

Chapter 2 contains material originally published as Hao, N., Nayak, S., Behar, M., Shanks, R.H., Nagiec, M.J., Errede, B., Hasty, J., Elston, T.C., and Dohlman, H.G. (2008): Regulation of cell signaling dynamics by the protein kinase-scaffold Ste5. Molecular Cell ,Vol. 30, Issue 5, pp. 649-656.

Chapter 3.

Computational modeling of yeast chemotrophic growth reveals the role of the protease Bar1 in gradient sensing

3.1 Introduction

Following our success in adapting microfluidics to study the MAPK cascade in yeast mating pathway, we used the static gradient device developed in Hao, N., Nayak, S., Behar, M., Shanks, R.H., Nagiec, M.J., Errede, B., Hasty, J., Elston, T.C., and Dohlman, H.G. (2008), to investigate the role of the protease Bar1 in gradient sensing in yeast. *Saccharomyces cerevisiae* undergo chemotrophic growth in which cells elongate in the direction of increasing pheromone concentration. Here we further analyze and provide computational investigation of

the signaling events that regulate chemotrophic growth. Our results elucidate the role of the extracellular protease Bar1 in gradient sensing. In particular, we demonstrate and confirm experimentally that Bar1 allows cells of similar mating type to avoid one another. We also show how Bar1 enables a-cells to act a pheromone sinks, thereby generating significant pheromone gradients in the direction of opposite mating type α-cells.

We then develop a model for the intracellular signaling of gradient sensing based on a Turing mechanism. Mathematical analysis of the model demonstrates the fine-tuned the spatiotemporal dynamics through GTPase-activating proteins. Finally, we combine our models for gradient sensing and Bar1 and generate a full model for chemotrophic growth. An important property of *Saccharomyces cerevisiae* (yeast) is their ability to propagate as haploids. Yeast haploid cells have two cell-types denoted as a and . Haploid a- and α-cells secrete cell-type-specific pheromones (a-factor and α-factor, respectively) that promote cell fusion and the formation of an a/ diploid. Pheromone stimulation leads to a well-defined series of events required for mating, including readily-assayed responses such as MAPK phosphorylation, new gene transcription and morphological changes. In particular, at intermediate levels of α-factor, a-cells undergo chemotrophic growth in which they elongate in the direction of increasing pheromone concentrations. Thus yeast is an ideal model system for studying cell differentiation and gradient sensing.

An interesting property of a-cells is that they secrete the protease Bar1 that degrades α-factor pheromone secreted by α-cells (Hicks and Herskowitz,

1976). It is typically thought that Bar1 serves to "desensitize" the pheromone pathway and restore normal cell division if mating is unsuccessful (Ciejek and Thorner, 1979). However, Jackson and Hartwell showed that bar1 mutant cells were poorly able to find a mating partner when presented with a mixture of pheromone-producing and non-producing α-cells (Jackson and Hartwell, 1990). This finding suggests that Bar1 has an important positive role in mating, despite its role in attenuating the initial stimulus. Using an analogy to electrostatics, Barkai et al. postulated that Bar1 limits the diffusion range of pheromone in the vicinity of α-cells, thereby creating local pheromone gradients that are better aligned with the direction of the nearest potential mating partner (Barkai et al., 1998). We combine computational modeling and experimental investigations to more closely examine the role of Bar1 in chemotrophic growth. Our model takes into account cell growth and the external concentrations of pheromone and Bar1. We use the model to demonstrate how Bar1 dynamically modulates the extracellular environment to sharpen the gradient toward an opposite mating type and allows a-cells to avoid one another. This novel self avoidance mechanism is validated by experiments performed in a microfluidics gradient chamber. Computer simulations demonstrate how both properties of Bar1 improve mating efficiency.

The first step in chemotrophic growth is the establishment of cell polarity in which proteins required for cell growth localize to regions of high pheromone concentration. To investigate the regulatory mechanisms responsible for cell polarization and gradient sensing, we develop a model that describes the spatiotemporal dynamics of the signaling proteins involved in these processes.

Important characteristics of yeast gradient sensing that constrain models of pheromone-induced polarization are the ability of yeast cells to detect a wide range of pheromone gradients and to spontaneously polarize in the presence of a homogenous pheromone concentration (Nern and Arkowitz, 2000; Paliwal et al., 2007; Segall, 1993). To capture these two properties, our model for gradient sensing is based on a Turing instability in which a local increase in pathway activity is amplified (positive feedback), while subsequent fluctuations in distant regions of the cell are repressed (global inhibition) (Gierer and Meinhardt, 1972; Turing, 1952). The results of modeling highlight the roles of Guanine nucleotide dissociation inhibitors (GDI) and G-protein activating proteins (GAP) in polarization and gradient sensing. Finally, we combine the models of cell elongation and gradient sensing to produce a full model of chemotrophic growth.

3.2 Computational Framework for chemotrophic growth

We developed a computational platform for studying yeast chemotrophic growth. The full simulations involve solving reaction-diffusion equations for the external concentrations of pheromone and Bar1 and the internal concentrations of the polarity proteins, and updating geometry changes during growth. This platform is built on COMSOL with MATLAB. Below, we describe the process for simulating chemotrophic growth. The computational domain that contains the cells is taken to be a square. Initially, cells are assumed to have a circular geometry.

Biochemical species, reactions, boundary conditions and initial conditions are defined in the relevant domains (see below).

1. We assume that cell growth occurs on a longer timescale than the chemical reactions and thermal diffusion. Therefore, all chemical species reach their steady state before cell growth occurs. This simplification allows us to separate solving the reaction diffusion equations from growing the cells. Solving the reaction-diffusion equations for all the chemical species in each domain produces the spatial profiles for the extracellular pheromone and Bar1 concentrations and the intracellular polarity proteins. 2. For cases in which the internal gradient sensing model is not included in the simulations, the location of the maximum pheromone concentration (Pmax) around each cell is found. The concentration diametrically opposite from Pmax is defined as Pback. The relative gradient is then computed as: 2 (Pmax-Pback)/ (Pmax+Pback). If the relative gradient is above threshold, a narrow rectangular segment (S1) is inserted between the half circle defined with Pmax as its midpoint and the half circle defined with Pback as its midpoint (Fig. 1B). Otherwise the cell is elongated in a random or pre-specified direction. The half circle, which contains Pmax and is moved to accommodate S1, is defined as the leading edge. The other half circle is taken to be the back of cell and remains fixed throughout the simulation. When an internal mechanism for polarization is included, the cell is elongated in the direction of the maximum active Cdc42 concentration (Fig. 1B). 3. Following cell elongation, the program recomputes the steady-state profiles of the reaction-diffusion equations. The initial condition for each species is the final solution from the previous step.

4. In later growth steps, only the pheromone concentration across the leading segment is considered, because this is where growth occurs. For this case the relative gradient is computed as 2(P max − P min)/(P max + P min), where Pmin is the minimum pheromone concentration over the leading segment. If the relative gradient is above threshold, the new segment (S2, S3,... Sn) is inserted between the front arc and the previous segment and rotated by angle formed by the previous direction of growth and Pmax (Fig. 1B). Otherwise the new segment is inserted in the same direction as the previous one. For simulations with internal polarization mechanism, the position of the maximum Cdc42GTP concentration (Cmax) on the front arc is calculated instead of the relative gradient. The growth direction and turning angle is determined from the previous direction of growth and the Cmax. Steps 4 and 5 are repeated until all cells grow to the desired length.

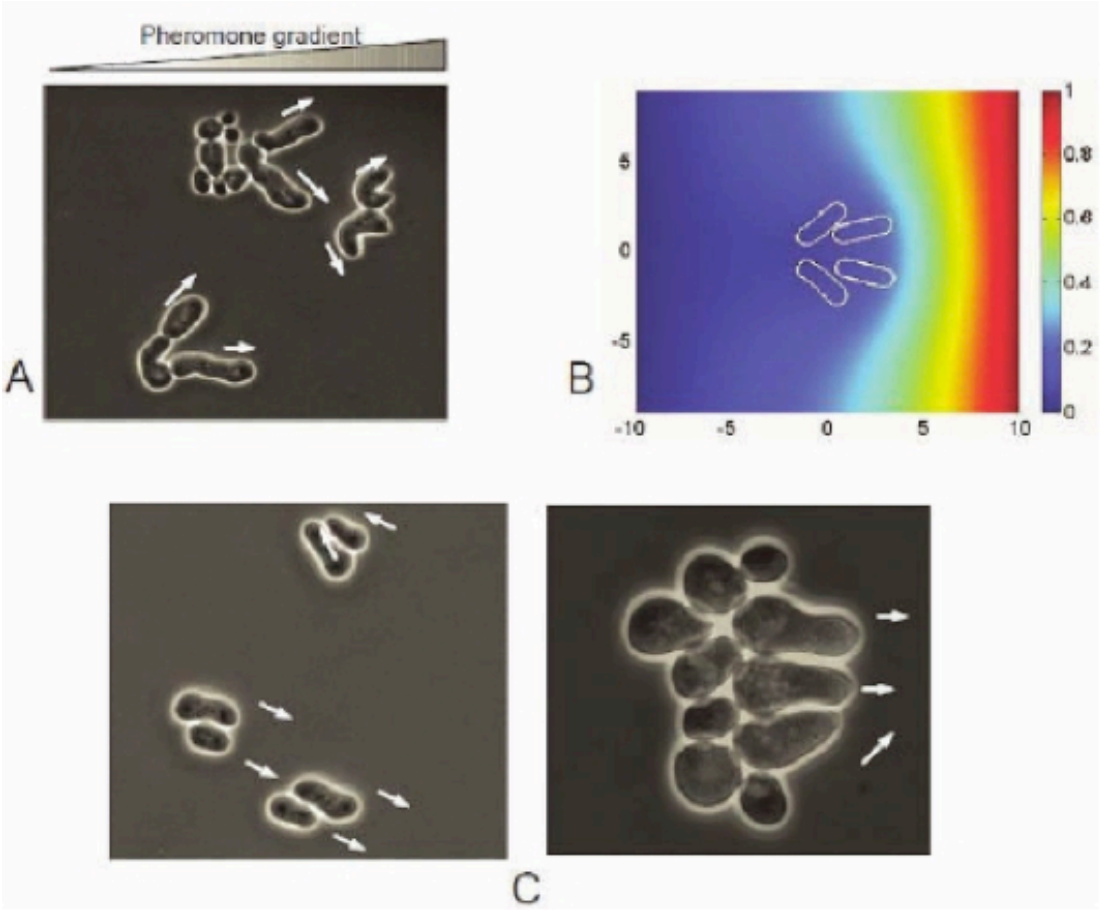

Figure 3.1: Bar1 causes the avoidance among a cells. A. a-cells tend to avoid each other during chemotropic growth in a gradient chamber. Pheromone gradient: right to left, 0-300nM. Arrow labels the front of the cell. B. Simulation shows that Bar1 decreases intercellular pheromone concentration between a-cells and the local gradient is no longer linear. Following the modified local gradient, a cells grow away from each other. C. a-cells without Bar1 grow close to each other and in one direction in a gradient chamber. Pheromone gradient: right to left, 0-10 nM.

3.3 Gradient chamber simulations

To simulate the self-avoiding behavior observed in the gradient chamber experiments, circular domains representing a-cells were placed in a larger square

domain. The concentration of pheromone on the left and right edges of the chamber domain is fixed at 0 and 1, respectively, which creates a linear gradient across the chamber domain. No flux boundary conditions are assumed along the top and bottom edges of the chamber. The boundary conditions for Bar1 are absorbing at four edges (i.e., the concentration is taken to be zero at these boundaries). The pheromone and Bar1 concentrations are computed from the following equations:

$$\frac{\partial[\text{Bar1}]}{\partial t} = D_{bar1} \quad [\text{Bar1}] + \sigma_b(x,y) - \delta_b[\text{Bar1}] \qquad (3.1)$$

$$\frac{\partial[\text{Ph}]}{\partial t} = D_{ph} \quad [\text{Ph}] - k_b[\text{Bar1}][\text{Ph}] - \delta_{ph}[\text{Ph}] \qquad (3.2)$$

where Dbar1 and Dph are the diffusion coefficients for Bar1 and pheromone, respectively, $\sigma b\,(x,y)$ is the flux of Bar1 from a cells, δb and δph are the rate constants for degradation of Bar1 and pheromone, respectively, and kb is the rate constant for Bar1 mediated degradation of pheromone. a-cells are assumed to emit Bar1 at constant rate uniformly across the entire cell. Because in these simulations the left and right boundaries of the chamber set up a background pheromone gradient and that this gradient is assumed to be sufficient to induce the gradient sensing, the a-cells do not need to compare the local gradient with threshold to determine the growth direction. The remaining parameters have the values of Dph = 10, Dbar1 = 2, $\sigma b(x,y) = 0.2$, $\delta b = 0.3$, $\delta ph = 0.002$.

3.3.1 Simulations with multiple cells

In this situation, multiple -and a cells are placed in different positions within the computational domain. α-cells emit α-factor (pheromone) uniformly across the cell surface. Again Bar1 is released from a-cells. The equations for the pheromone and Bar1 concentrations are the same as Eqs. (3.1) and (3.2) with the addition of a flux term $\sigma P\, h(x,y)$ for the release of α-factor. All boundary conditions at the edges of the computational domain are zero flux. The growth direction is determined using the relative gradient as described above.

3.3.2 Simulations with an internal gradient sensing mechanism

In these simulations, the a-cells grow in the direction of maximum Cdc42 activity. To reduce the computation time, we reduced the 7-variable model to 3 variables, Cdc42-GDP-GDI, Cdc42-GDP and Cdc42-GTP. The other 4 variables are eliminated using a quasi steady-state approximation. Notice that the quasi steady-state approximation changes the dynamics of the model. In particular, Cdc42-GTP is activated much faster. Because of this difference, the model parameters are adjusted slightly. The synthesis and degradation rates of Cdc42 are doubled and the GAP activity is half of that used in the full model (3.2). For the chamber simulations, the pheromone concentration on the left and right edges of the computational domain is fixed at 0 and 1, respectively. The boundary

conditions of Cdc42GDP-GDI, Cdc42GDP and Cdc42-GTP are zero flux at the cell edge.

3.3.3 Model assumptions and reactions for gradient sensing

The assumptions used to construct the model are as follows:

1. Synthesis and degradation of Cdc42, Bem1, Cdc24 and Ste20 are included in the model. These processes have the slowest kinetics among all reactions.

2. As most of Cdc42-GDP is bound with its GDI in cytosol, we do not consider a free pool of Cdc42 in the cytosol. When Cdc42 is synthesized or comes off the membrane it is assumed to immediately bind to a GDI protein.

3. The shuttling of Cdc42 on and off the membrane is assumed to have the fastest kinetics.

4. Far1 is involved in the translocation of Cdc24 out of the nucleus. Cdc24 is associated with Far1 in nucleus. Following stimulation with pheromone, Msn5p/Ste21p, a member of the exportin family, transports the Far1/Cdc24 complex to cytoplasm (Bradwell., 2005) In the cytoplasm, the Cdc24/Far1 complex can bind to Bem1 and Far1 binds to the Gβγ subunit of the heterotrimeric G-protein. We assume that Cdc24, Far1 and Bem1 are always in a complex. We assume Cdc24 becomes active when the complex interacts with the Gβγ subunit (Bradwell., 2005) When new Cdc24 is synthesized it is assumed to immediately complex with Far1 and Bem1.

5. Our model does not explicitly take into account the receptor and G protein. The effect of pheromone stimulation is modeled with a spatially dependent association rate for the binding of the Cdc24/Far1/Bem1 complex to the membrane. That is, the association rate is given by j2a + j2b S(r), where j2a models pheromone independent association with the membrane and j2b S(r) is pheromone dependent binding.

6. We assume that Cdc42-GTP binds the Cdc24/Far1/Bem1 complex first and then the PAK Ste20 interacts with this complex. It is possible that Cdc42-GTP binds Ste20 first, and then the heterodimer binds to Cdc24/Far1/Bem1. However, the order of these events does not qualitatively change the behavior of the model.

7. The positive feedback mediated by Ste20 is represented in the model in two ways: 1) when Ste20 is bound to the Cdc42-GTP/Cdc24/Bem1/Far1 complex, it increases the GEF activity of Cdc24 presumably through phosphorylation of Cdc24 or one of the other proteins in the complex and 2) Ste20 stabilizes the complex, increasing the amount of time Cdc24 spends on the membrane. Either mechanism alone is sufficient to generate Turing instability.

8. We assume that Cdc42-GTP, both in complex and free, is accessible for hydrolysis by its GAPs. When Cdc42-GTP is part of a protein complex, we assume that hydrolysis and dissociation from the complex occur in a one step.

9. Both Cdc42-GTP and Cdc42-GDP can be removed from the membrane through endocytosis.

3.3.4 Model equations and parameter values

The reactions listed above lead to the set of coupled reaction diffusion equations given by Eqs. (3.3)-(3.10). The abbreviations for the chemical species used in these equations are listed in 3.1. The values for the parameter values used in the simulations are given in 3.2.

Table 3.1: List of abbreviations for the chemical species considered

Reaction species	Notation
$(Cdc42GDP - GDI)_c$	$C42_c$
$Cdc42GDP$	$C42D$
$Cdc42GTP$	$C42T$
$(Bem1 - GEF)_c$	BG_c
$Bem1 - GEF$	BG
PAK_c	P_c
$Cdc42GTP - Bem1 - GEF$	$C42BG$
$Cdc42GTP - Bem1 - GEF - PAK$	$C42BGP$
$Pheromone$	Ph

Model equations:

$$\frac{\partial C42_c}{\partial t} = D_c \frac{\partial^2 C42_c}{\partial r^2} + s_0 - d_0 C42_c + \gamma(-j_1 C42_c + j_{1\gamma} C42D) \tag{3.3}$$

$$\frac{\partial C42D}{\partial t} = D_m \frac{\partial^2 C42D}{\partial r^2} + j_1 C42_c - j_{1\gamma} C42D - C42D(k_2(BG + C42BG) + K_{2p} C42BGP) + k_6 C42BGP + k_7 C42TBG - d_{0D} C42D \tag{3.4}$$

$$\frac{\partial C42T}{\partial t} = D_m \frac{\partial^2 C42T}{\partial r^2} + C42D(k_2(BG + C42TBG) - k_{2p} C42TBG) - k_3 C42T \cdot BG_c + k_{3r} C42TBG - k_4 C42T \cdot BG + k_{4r} C42TBG - D_{0T} C42T \tag{3.5}$$

$$\frac{\partial BG_c}{\partial t} = D_c \frac{\partial^2 BG_c}{\partial r^2} + s_1 - d_1 BG_c + \gamma(-j_2 BG_c + j_{2r} BG - k_3 C42T \cdot BG_c + k_{3r} C42TBG \tag{3.6}$$

$$\frac{\partial BG}{\partial t} = D_m \frac{\partial^2 BG}{\partial R^2} + j_2 \cdot Ph \cdot BG_c - j_{2r} BG - k_4 C42T \cdot BG + k_{4r} 42TBG + k_6 C42TBGP + K_7 C42TBG \tag{3.7}$$

$$\frac{\partial C42TBG}{\partial t} = D_m \frac{\partial^2 C42TBG}{\partial r^2} + k_3 C42T \cdot BG_c - k_{3r} C42TBG + k_4 C42T \cdot BG - k_{4r} C42TBG - k_5 C42TBG \cdot P - k_7 C42TBG \tag{3.8}$$

$$\frac{\partial P_c}{\partial t} = D_c \frac{\partial^2 P_c}{\partial r^2} + s_2 - d_2 P_c + \gamma(-k_5 C42TBG \cdot P + k_6 C42TBGP) \tag{3.9}$$

$$\frac{\partial C42TBGP}{\partial t} = D_m \frac{\partial^2 C42TBGP}{\partial r^2} + k_5 C42TBG \cdot P - k_6 C42TBGP \tag{3.10}$$

Table 3.2 :Model Parameters

Parameter	Biological meaning	Value	Unit
s_0	Synthesis of $(Cdc42GDP - GDI)_c$	0.0005	$\mu M s^{-1}$
d_0	Degradation of $(Cdc42GDP - GDI)_c$	0.00075	s^{-1}
j_1	Cdc42GDP binding to membrane, dissociating from $(Cdc42GDP - GDI)_c$	50	s^{-1}
j_{1r}	Dissociation of Cdc42GDP from membrane	25	s^{-1}
Γ	Volume of membrane reaction region/Volume of the whole cytosol	0.01	
k_2	Basal GEF activity of loading GTP to Cdc42GDP	0.2	$\mu M^{-1} s^{-1}$
k_{2p}	Enhanced GEF activity of loading GTP, after forming complex with PAK	0.6	$\mu M^{-1} s^{-1}$
k_{2r}	GTP hydrolysis rate by GAPs	0.1	s^{-1}
d_{0D}	Degradation/endocytosis of membrane bound Cdc42GDP	0.015	s^{-1}
d_{0T}	Degradation/endocytosis of membrane bound Cdc42GTP	0.015	s^{-1}
k_3	Cytosolic Bem1-GEF binding to membrane Cdc42GTP	0.8	$\mu M^{-1} s^{-1}$
k_{3r}	Cdc42GTP-Bem1-GEF dissociating to cytosolic Bem1-GEF and membrane Cdc42GTP	0.1	s^{-1}
k_4	Membrane bound Bem1-GEF binding to membrane Cdc42GTP	0.8	$\mu M^{-1} s^{-1}$
k_{4r}	Cdc42GTP-Bem1-GEF dissociating to membrane Bem1-GEF and Cdc42GTP	0.1	s^{-1}
k_5	Cytosolic PAK binding to membrane Cdc42GTP-Bem1-GEF	20	$\mu M^{-1} s^{-1}$
k_6	Break down of the complex Cdc42GTP-Bem1-GEF-PAK	0.5	s^{-1}
k_7	Break down of the complex Cdc42GTP-Bem1-GEF	0.5	s^{-1}
s_1	Synthesis of $(Bem1 - GEF)_c$	0.00001	$\mu M s^{-1}$
d_1	Degradation of $(Bem1 - GEF)_c$	0.0001	s^{-1}
s_2	Synthesis of PAK_c	0.00001	$\mu M s^{-1}$
d_2	Degradation of PAK_c	0.0002	s^{-1}
j_2	Membrane binding of $(Bem1 - GEF)_c$	2	s^{-1}
j_{2r}	Dissociation of Bem1-GEF from membrane	0.5	s^{-1}

3.3.5 Gradient sensing and self-avoidance mechanism

A microfluidic device (Hao et al., 2008) capable of exposing cells to a precisely controlled linear concentration gradient was used is used to verify the role of Bar1 in the self-avoidance of a cells (Lovejoy et al., 1998). The gradient in the device is achieved by passive diffusion between two parallel microchannels containing either no pheromone or a dose of pheromone sufficient to induce cell division arrest. Wild-type and bar1- a cells were grow in synthetic drop-out (SD)

medium containing 2% glucose supplemented with essential amino acids overnight. The appropriate yeast cultures were grown at 30 degrees centigrade until they grow to A600nm = 1.00.25 and then diluted with media to A600nm = 0.05 before loading them in to the microfluidic chamber. The pheromone concentration ranged from 0 to 300 nM for wild-type cells and 0- 10 nM for bar1- cells. Experiments followed the same procedure as in Hao et al., 2008.

3.4 Results

3.4.1 Bar1 allows a-cells to avoid one another

Previously we developed a microfluidics gradient chamber that allows a-cells to be exposed to precise gradients of α-factor (Hao et al., 2008). Experiments performed in the gradient chamber revealed that a-cells tend to avoid each other when undergoing chemotrophic growth (Fig. 1A and Supplemental Movie 1A). We reasoned that the mechanism underlying this self avoidance might involve the protease Bar1. Our hypothesis is that Bar1 depletes pheromone in the extra-cellular environment and alters the direction of the local pheromone concentration in such a way that the gradient is directed away from a-cells. To test this idea we developed a computational platform for simulating chemotrophic growth. The simulator simultaneously computes the external concentrations of pheromone and Bar1. Bar1 is synthesized and released from a-cells, diffuses

throughout the chamber and degrades pheromone. We performed gradient chamber simulations with various different initial geometries of a-cells (Fig. 1B and Supplemental Movies 1B). Consistent with our hypothesis, the simulations reveal that Bar1 tends to modify the pheromone concentration as cells elongated so that the local gradient always pointed away from a-cells. The simulations closely reproduced the qualitative behavior of real cells observed in the gradient chamber (Fig. 1A). To experimentally verify Bar1's role in self avoidance, experiments were performed in the gradient chamber with bar1 mutant cells. In striking contrast to the wild type strain, cells lacking Bar1, elongate parallel to one another and frequently collide (Fig. 1C and Supplemental Movie 1C). To quantify our results we measured the angle between the growth directions of two adjacent a-cells, once the cells have initiated chemotrophic growth. For wild-type cells, the average angle is about 90 , much larger than that of the bar1- cells (35). These results indicate that yeast not only passively sense their environment, but also actively modify it. We speculated that the ability to dynamically modify local pheromone concentrations should improve mating efficiency.

3.4.2 The Role of Bar1 in finding a mating partner

To determine the role of Bar1 in mating, we used our model to simulate mating between a-cells and alpha-cells arranged in various geometries. Based on measurements in the microfluidic chamber we set a relative gradient of 0.025 as

the threshold for detectable pheromone gradients (Hao et al., 2008). Before cell elongation, the gradient is measured across the entire a-cell. Once the cell has begun to grow, the gradient is measured across the leading growth segment (Figure 2). If the initial pheromone gradient is below threshold, then growth is initiated in a random direction. If the gradient drops below threshold during elongation, then growth continues in the current direction.

We investigated several different cell geometries. In the first case, a single a-cell is presented with two potential mating partners (Fig. 3A inset). The a-cell is slightly closer to the left α-cell. For this geometry, both BAR1 and bar1- cells are able to detect the initial pheromone gradient. However, in the presence of Bar1, the gradient significantly sharpens as the a-cell elongates (Fig. 3A, red curve), whereas without Bar1 the gradient falls below threshold during cell growth and starts to rise when the a-cell is very close to the α-cells (Fig. 3A, blue line). Therefore, the cell expressing Bar1 quickly finds the nearest mating partner (Fig. 3A, inset, red line), while the a-cell lacking Bar1 targets the α-cell later than the BAR1 cell (Fig. 3A, inset, blue line). Next we considered a geometry in which both the BAR1 and bar1- cell are initially unable to detect a pheromone gradient. In this case, both cell types are expected to polarize in a random direction. Figure 3B shows three initial angles of polarization. With the exception of the case in which polarization occurs in a direction perpendicular to the two α-cells, a super-threshold gradient quickly develops as the cell expressing Bar1 grows, enabling this cell to reorient its direction of growth and find a mating partner (Fig 3B, red lines). In contrast, the pheromone gradient across the bar1? cell

remains below the detectable limit, and cell growth remains in the original direction of polarization (Fig 3B, blue lines). Finally, we investigated a more complicated geometry in which an a-cell has three potential mating partners (Fig. 3C, inset).

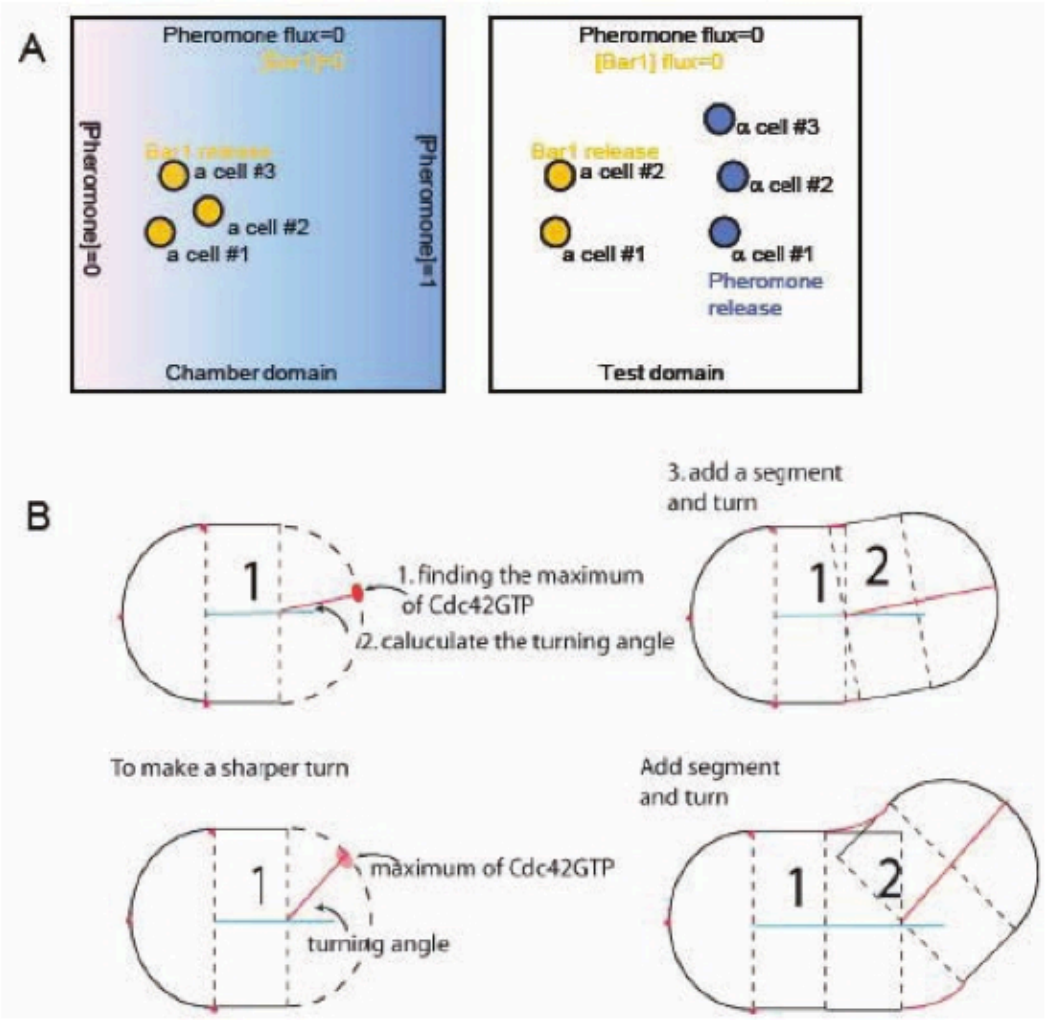

Figure 3.2: Schemes showing the layout of chemotropic growth simulator. A. Setup for simulating chemtropic growth in gradient chamber (left) and mating with multiple a cells (right). B. Schematic representation of cell elongation.

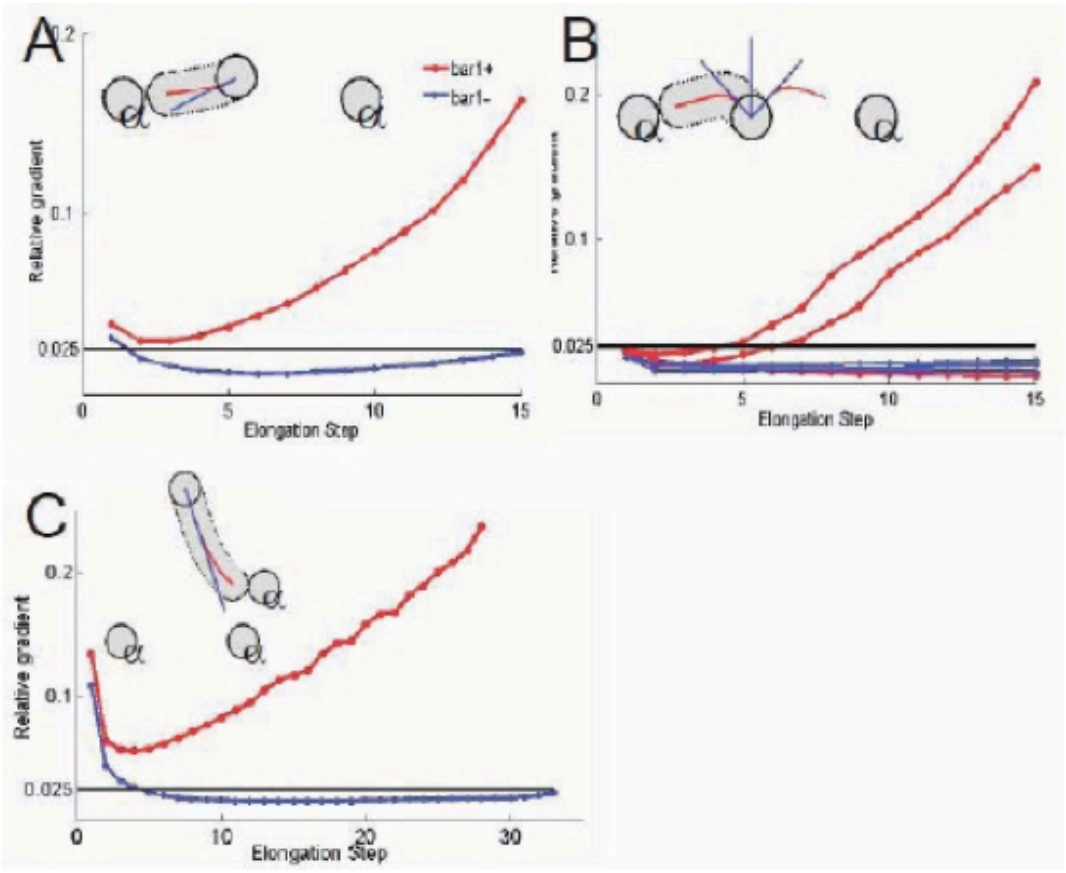

Figure 3.3: Bar1 improves mating efficiency by amplifying the relative difference of pheromone across an a cell. A. When the relative pheromone difference across the a-cell is larger than the turning threshold, bar1- a-cell finds the nearest a cell slower than bar1+ a-cell. With Bar1, the relative pheromone gradient increases much faster as a-cell approaches the a-cell. Black line: turning threshold. Inserted: the initial layout of a and a-cells (solid contour) and the growth of a-cell (dashed contour). Blue/red lines: growth trajectories with/without Bar1. B. With sub-threshold pheromone gradient for both bar1+ and bar1- cells, Bar1 increases the relative gradient as a-cell getting close to a-cell and redirects the a cell to the nearest a-cell. C. With three a-cells, a cell with Bar1 finds the nearest a-cell (insert, red line).

In this case, both a -BAR1 and -bar1 –α cells experience a large initial pheromone gradient across the cell. However, as the a-cells approach the α-cells, the bar1 cell loses the gradient and does not find the nearest mating partner. In

contrast, for the a-cell expressing Bar1 the gradient remains above threshold and the cell hones in on the closest mating partner.

Our results suggest that Bar1 improves mating efficiency by progressively amplifying the relative pheromone gradient across a-cells. This amplification occurs because the a-cell effectively acts like a pheromone sink. If we make the simplifying assumptions that (1) a-cells are perfect sinks (i.e., absorb all α- factor near them), (2) α-cells are constant source of α-factor and (3) the process takes place in one spatial dimension, then as a-cells elongate the relative pheromone gradient between an a- and an α- cell increases approximately as the inverse of the distance between the two cells. This prediction is in qualitative agreement with the results of our simulations (Fig. 3).

3.5 A Model of polarization and gradient sensing

The results presented above demonstrate the ability of yeast to modify their external environment to improve mating efficiency and do not consider an internal mechanism of gradient sensing. Our ultimate goal is to generate a self-consistent model of chemotrophic growth in which the direction of new growth is determined by intracellular signaling events. To this end, we developed a mathematical model for the spatiotemporal dynamics of the signaling proteins involved in gradient sensing. The model allows us to investigate the biochemical events that underlie pheromone-induced polarization and provides insight into regulatory role of key pathway components in gradient sensing. An important

feature of pheromone-induced polarization is that in the absence of an external pheromone gradient and internal polarity markers, yeast cells maintain their ability to polarize, but do so in a random direction (Irazoqui et al., 2003; Nern and Arkowitz, 2000). Therefore, we based the model on a diffusion-driven Turing mechanism that is capable of this symmetry breaking. The components of our model are the Rho-family GTPase Cdc42, its exchange factor, Cdc24, its guanine nucleotide dissociation inhibitor (GDI), the scaffold protein Bem1, Ste20, the p21 associated kinase (PAK), which is an effector of Cdc42, and G-protein activating proteins (GAPs) (Park and Bi, 2007) (Fig. 4) Key features of the model include different diffusion rates for cytosolic versus

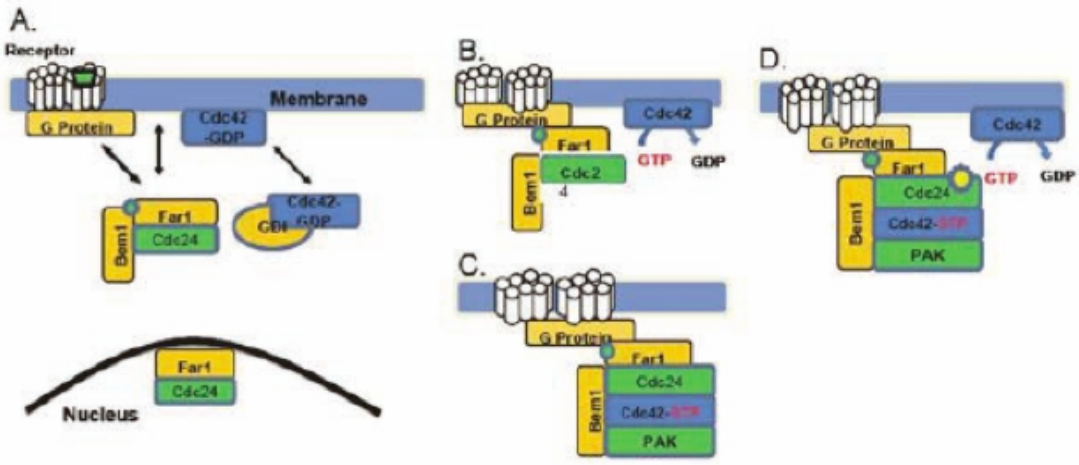

Figure 3.4: Scheme of the Cdc42 polarization model. A. Pheromone binds to G protein coupled receptor, activates G protein. Far1 exports Cdc24 out of nucleus and associates with the active G protein. Cdc42GDP attaches to membrane by dissociating from GDI. B. Cdc24 loads GTP to membrane bound Cdc42GDP. C. Active Cdc42 recruits its effector, PAK, forms Bem1/Cdc24/Cdc42GTP/PAK complex. D. PAK in the complex further stimulates the GEF activity of Cdc24, which in turn converts more Cdc42 to active state, establishing a positive feedback loop.

membrane bound proteins and a positive feedback loop in which the GTP-loading efficiency of the GEF, Cdc24, is increased when the PAK and Cdc24 are both associated with Cdc42GTP through the scaffold Bem1 (Kozubowski et al., 2008). These features are sufficient to generate a Turing instability through a substrate depletion mechanism. Our model includes synthesis and degradation of the pathway components. This feature is required in the growing cell simulations presented below to avoid the dilution of species due to increases in cell volume. Because our model does not take into account the full 3D volume of the cell, the ratio of the cell surface area to the volume is used to properly scale the fluxes of proteins that transition from the membrane to the cytosol.

3.5.1 Analysis of the Model

For simplicity we initially investigated the behavior of the model with one spatial variable, , describing the position along the circumference of a circle. We have verified that all qualitative features of the model carry over when two spatial coordinates are considered. With biologically reasonable parameter values, the model shows robust spontaneous polarization and gradient sensing behavior (Fig. 5A). Once the cell is polarized, the amount of active Cdc42 is around 5-20% of its total amount (Fig. 5B), which is consistent with experimental observations. In the model, the chemical species with the lowest molecular abundance is the Bem1/Cdc24 complex. However, it is not necessary for this complex to be the limiting species in the substrate-depletion mechanism, because simulations

performed with the cytosolic concentration of Bem1/Cdc24 held constant still produced polarization (data not shown). Figure 5C shows the Cdc42-GDI concentration before and after polarization. The small depletion of cytosolic Cdc42-GDI is sufficient to ensure that following pheromone stimulation Cdc42 remains localized and does not spread throughout the cell.

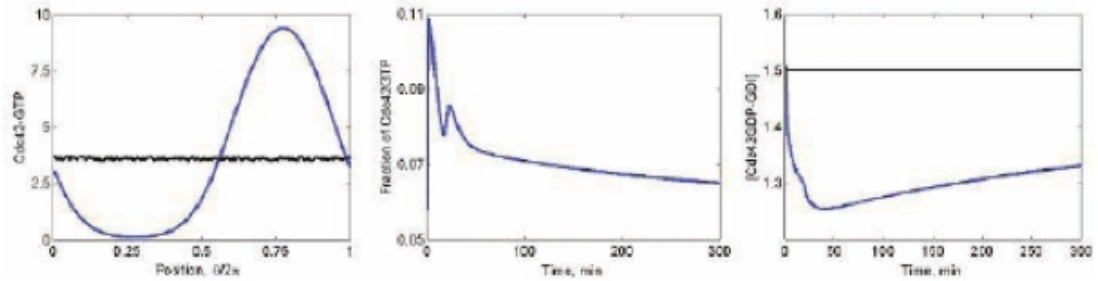

Figure 3.5: Spontaneous polarization. A. Spontaneous polarization from uniform initial condition with small fluctuations (initial: black; final: blue). B. Total Cdc42GTP is about 15% of the total amount of Cdc42 in the whole cell. C. Cdc42GDP-GDI in the cytosol is depleted during polarization (initial: black; final: blue).

In our model the GEF Cdc24 and GAP proteins are two major regulators of cell polarization. Therefore, we investigated how the qualitative behavior of the model depends on GEF and GAP activity. Figure 6A shows a two parameter bifurcation diagram for the model using the rate constants for GAP activity and basal GEF activity. Basal GEF activity refers to membrane bound Cdc24 molecules that are not in complex with the PAK. There exists a large range of values of GAP activity for which the system is Turing unstable (Fig. 6A, red region) indicating that the model is robust to this parameter. This behavior is

consistent with experimental results demonstrating that varying the abundance of the GAPs or their kinetics does not disrupt polarization (Irazoqui et al., 2004).

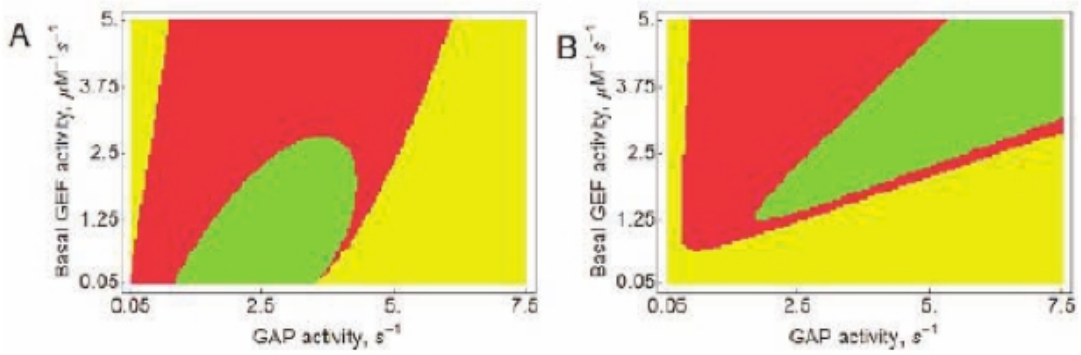

Figure 3.6: Bifurcation diagram of the model. Red: Turing instability; green: oscillation; yellow: uniformly stable. A. Turing instability is robust in the GEF-GAP parameter space. Notice that the area of Turing unstable exists where the basal GEF activity is larger than positive feedback induced GEF activity and the existence of oscillation. B. Similar pattern of Turing instability and oscillation appears if the positive feedback is through long membrane binding of Cdc24 in complex with Bem1, PAK and Cdc42GTP.

The results shown in Fig. 6A demonstrate the surprising result that a Turing instability can occur even if the basal GEF activity of Cdc24 is larger than its activity when in a complex with PAK (taken to be 0.6 M-1 s-1 in Fig. 6A). Superficially, this observation appears to contradict the necessity for a positive feedback loop to generate a Turing instability. However, in this situation, the positive feedback comes from the Bem1/Cdc42-GTP/PAK/Cdc24 complex increasing the life time of Cdc24 at the membrane, thereby allowing the GEF to activate more Cdc42 molecules. A bifurcation diagram for the case in which the intrinsic GEF activity of Cdc24 does not increase following the formation of the Bem1/Cdc42-GTP/PAK/Cdc24 complex is shown in Fig. 6B. We note that for this

mechanism alone to generate a Turing instability strong basal GEF activity is required (Fig. 6B). It is quite possible that both positive feedback mechanisms contribute to polarization, making the system more robust to inter- and intra-cellular fluctuations.

3.5.2 The role of G-protein activating proteins (GAPs)

The bifurcation diagrams in Figs. 6A and B indicate that GAP activity can vary in a large range without impairing the ability of the model to spontaneously polarize. Therefore, we sought to characterize the role of the GAPs in determining key characteristics of the system. In particular, we investigated how GAP activity influences the time required for polarization and the sharpness of the active Cdc42 distribution. We define the time to polarize as the time for the peak to reach 75% of its final height. The peak height is defined as [max(active Cdc42) - min(active Cdc42)] / min(active Cdc42) and the peak width is measured at the midpoint between the maximum and minimum levels of activity Cdc42. The sharpness is then calculated as the ratio: height/width. As shown in Fig. 7A, the time to polarize decreases and the sharpness of the active Cdc42 distribution increases with increasing GAP activity. If the GAP activity is too low, active Cdc42 accumulates almost everywhere on the membrane, making it difficult for symmetry breaking to occur (Fig. 7B top left). Modest to high GAP activity ensures low levels of active Cdc42, except in regions where the positive feedback is strong (Fig 7B top right). Note that the maximum value of Cdc42 significantly

increases with GAP activity, however, as expected the total amount of active Cdc42 (area under the curve) decreases (Fig. 7B). These results demonstrate that the GAP of Cdc42 are able to tune the dynamics of polarization. In particular, note that as the GAP activity is increased, the peak height overshoots its steady state value, giving rise to damped oscillations in the localized region of Cdc42 activity (Fig. 7B bottom right). A more detailed analysis of this unexpected behavior and its potential benefits to the cell are given next.

3.5.3 Tracking a changing gradient

Another desired property of gradient sensing is the ability to track temporal changes in the pheromone gradient. Therefore, we investigated how the model responds to a time-dependent pheromone gradient and which biochemical reactions regulate this response. Following polarization, the pheromone gradient is shifted by 60 . The response time is taken to be the time for the peak of active Cdc42 to move 40 . We tested how the response time depends on the following parameters: the rate constant for GAP activity, membrane binding and dissociation rates for Cdc42-GDP, and the endocytosis rates for both Cdc42-GTP and Cdc42-GDP. Interestingly, increasing the rate constant for GAP activity causes a non-monotonic change in the response time: it first increases and then slowly drops. During the increase stage of the response time, increasing the rate constants sharpens the polarization (Fig. 8). A comparison of the response time with peak sharpness reveals that there is a trade off between tracking changing gradients and the

sharpness of the peak, independent of the parameter that is varied (the rate constants for shuttling Cdc42-GDP on and off the membrane, the endocytosis rates for both Cdc42-GTP and Cdc42-GDP)(Fig. 8). That is, the sharper the peak takes longer time to track direction change. In the decline stage, high rate constants still keep the peak sharper, but the system is moving towards the state with both Turing and Hopf instability (Fig. 6). Now the change in the direction of gradient leads to a small collapse of the polarized peak, which makes the peak easier to move towards the new direction and reduces the response time. The declined stage is a transition from stable polarization to the oscillatory polarization in previous section. It suggests that although the sharp peak responses to direction change slowly, if the system is close to be both Turing and Hopf unstable, the polarization can achieve both sharpness and sensitivity to gradient change.

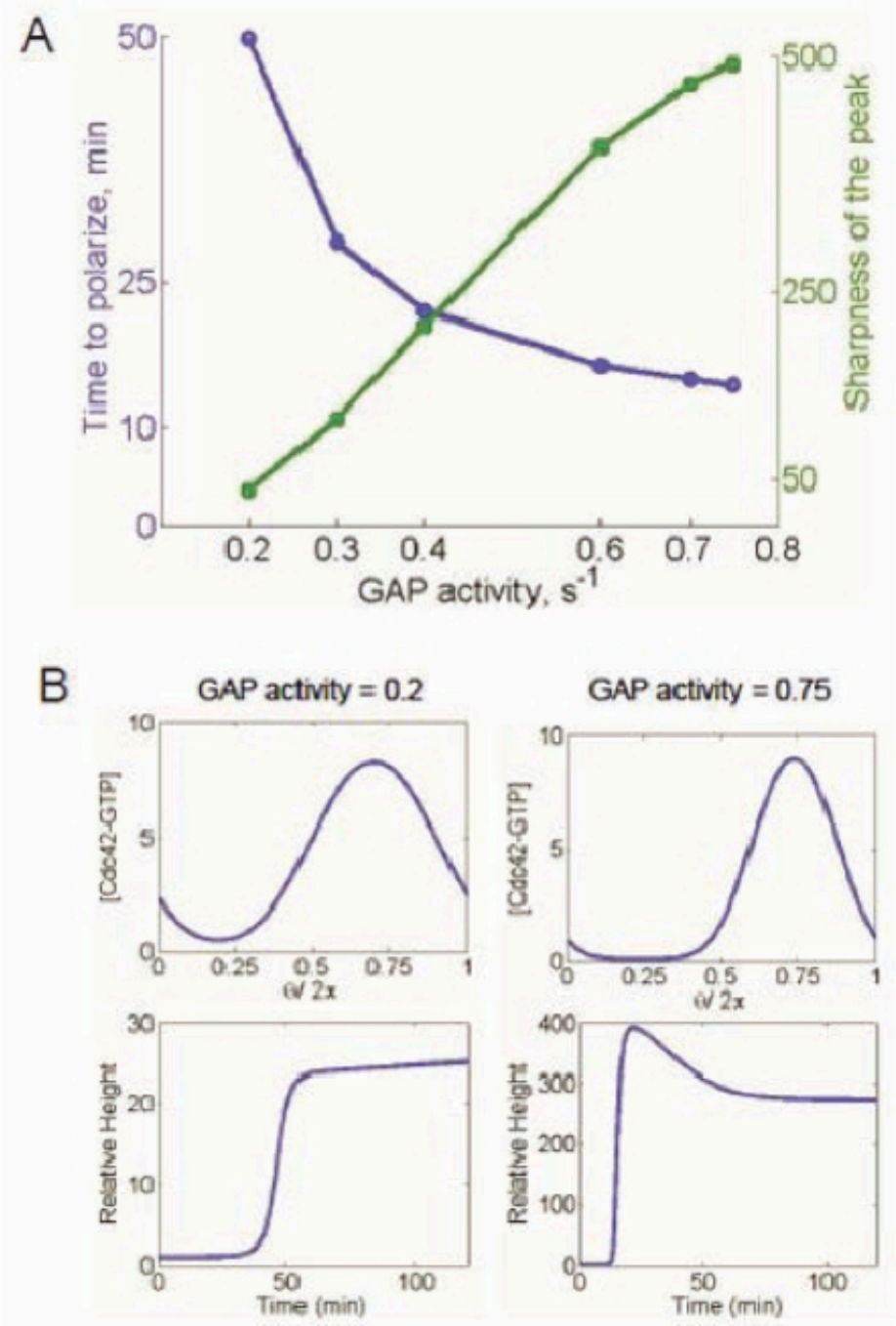

Figure 3.7: GAP fine tunes the kinetics of polarization. A. Time to polarize is reduced and the sharpness of the polarization is increased by raising GAP activity. B. The shape of the Cdc42GTP peak and the temporal profile of polarization at low and high GAP activity. Left column: GAP activity =0.2 s-1 right column: GAP activity = 0.75 s-1 .

3.5.4 Transient multiple Peaks

Our experiments have revealed that occasionally individual cells possess two peaks of localized Bem1. This situation arises either when a-cells are presented with multiple mating partners (Fig. 9A left panel) or within a cluster Bar1 expressing a-cell in the gradient chamber (data not shown). This behavior has also been observed in the context of polarization during budding (Howell et al., 2009). In each of these situations, the two peaks exist transiently with only a single peak remaining at later times (Fig. 9A, right panel). We tested the ability of the model to generate multiple peaks in two different ways. First we investigated the scenario in which cells are exposed to a spatially constant concentration of pheromone, but the initial concentration of active Cdc42 has two small peaks. Initially, the two peaks both grow. However, the two peak solution is not stable. The two peaks either merge to form a single peak or compete with each other with one peak eventually winning (Fig. 9B and C).

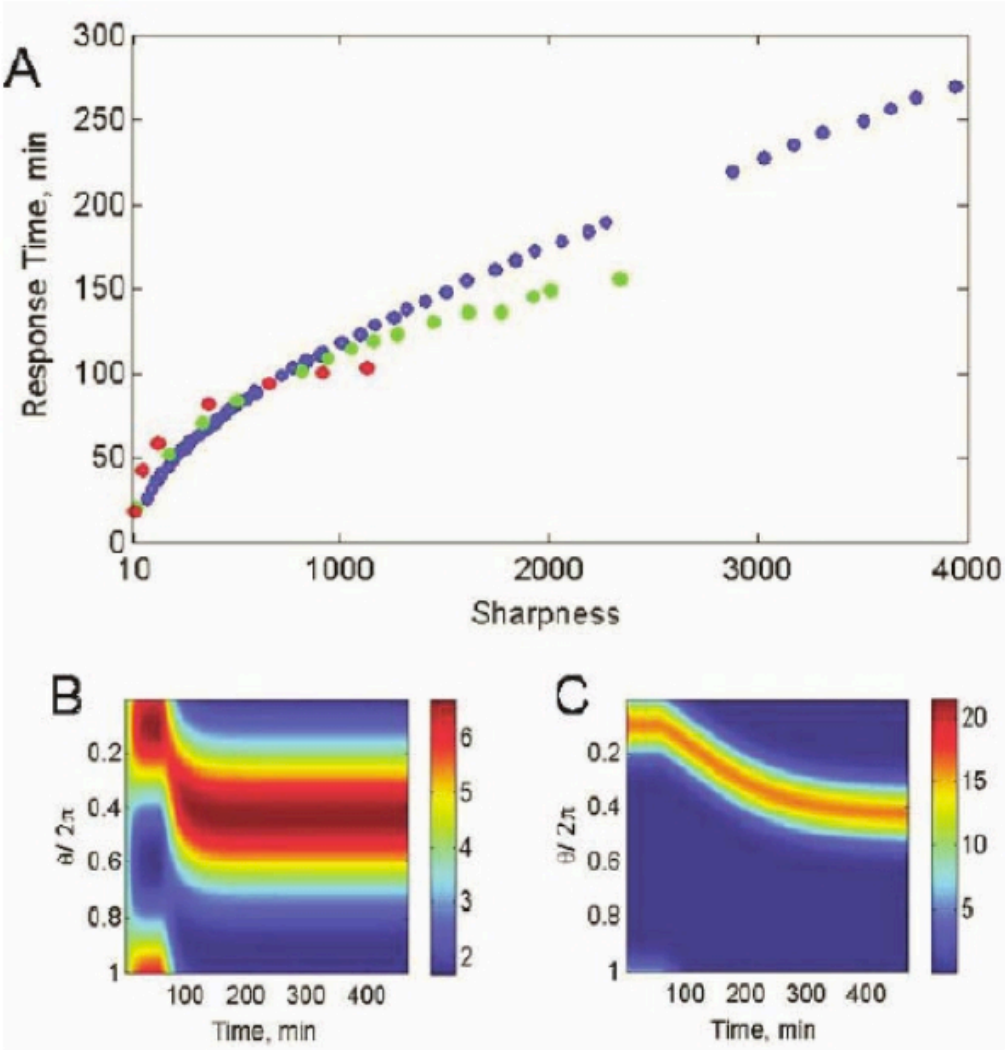

Figure 3.8: Tradeoff between tracking direction change and forming sharp polarization. A. As the polarity peak is sharper, it takes longer time to track the direction change. B-C. The shape of Cdc42GTP peak and the kinetics of tracking direction change at low (B) and high (C) GAP activity.

We also investigated the scenario in which the signal (pheromone concentration) has two local maxima. Similar results were found in this situation (data not shown). Howell et, al. have shown that the time for the two peaks to merge depends on the amount of Bem1 present in the cell (Howell et al., 2009).

Consistent with their results our model predicts that the competition time is longer if the synthesis rate of Bem1 is faster (Fig. 9D). Interestingly in two dimensions, a multi-peak solution becomes stable when the size of the cell is increased or shape of the cell is changed (Fig. 9E).

3.5.5 A model of chemotrophic growth

Finally, we combine our model for gradient sensing with the growing cell simulations to investigate the behavior of a-cells expressing Bar1 in the microfluidic gradient chamber and in the presence of multiple mating partners. In this case, the position of maximum Cdc42 activity determines the direction of growth. These simulations confirm that the proposed model for gradient sensing in combination with Bar1 degradation of pheromone is sufficient to explain the avoidance of similar mating types observed in the microfluidic chamber (Fig. 10A). We also investigated a scenario in which two a-cells compete for three α-cells. In the presence of Bar1, the two a-cells initially repel each other and therefore do not compete for the middle α-cell (Fig. 10B) and are each able to find a unique mating partner. However, without Bar1, the two a-cells tend grow toward the middle α-cell and collide during elongation (Fig. 10C).

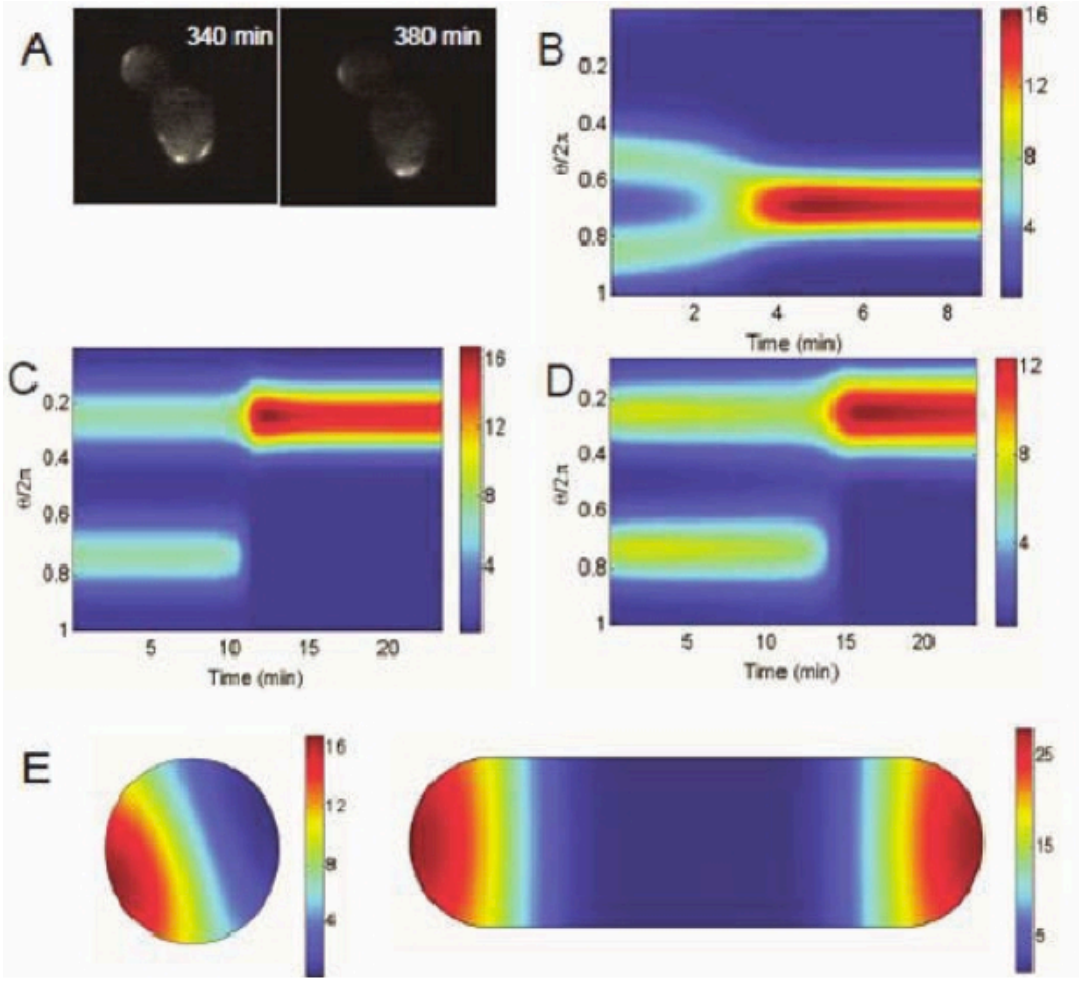

Figure 3.9: Two-peak solutions are transient. A. Transient two peaks of Bem1-GFP during pheromone induced polarization. B-C. Transient two peaks merge or compete to form only one stable peak. D. The duration of competition between two peaks are related with the amount of Bem1. (B-D)Simulations start with two-peak Cdc42GTP distribution. E. A multi-peak solution becomes stable when the size of the cell is increased.

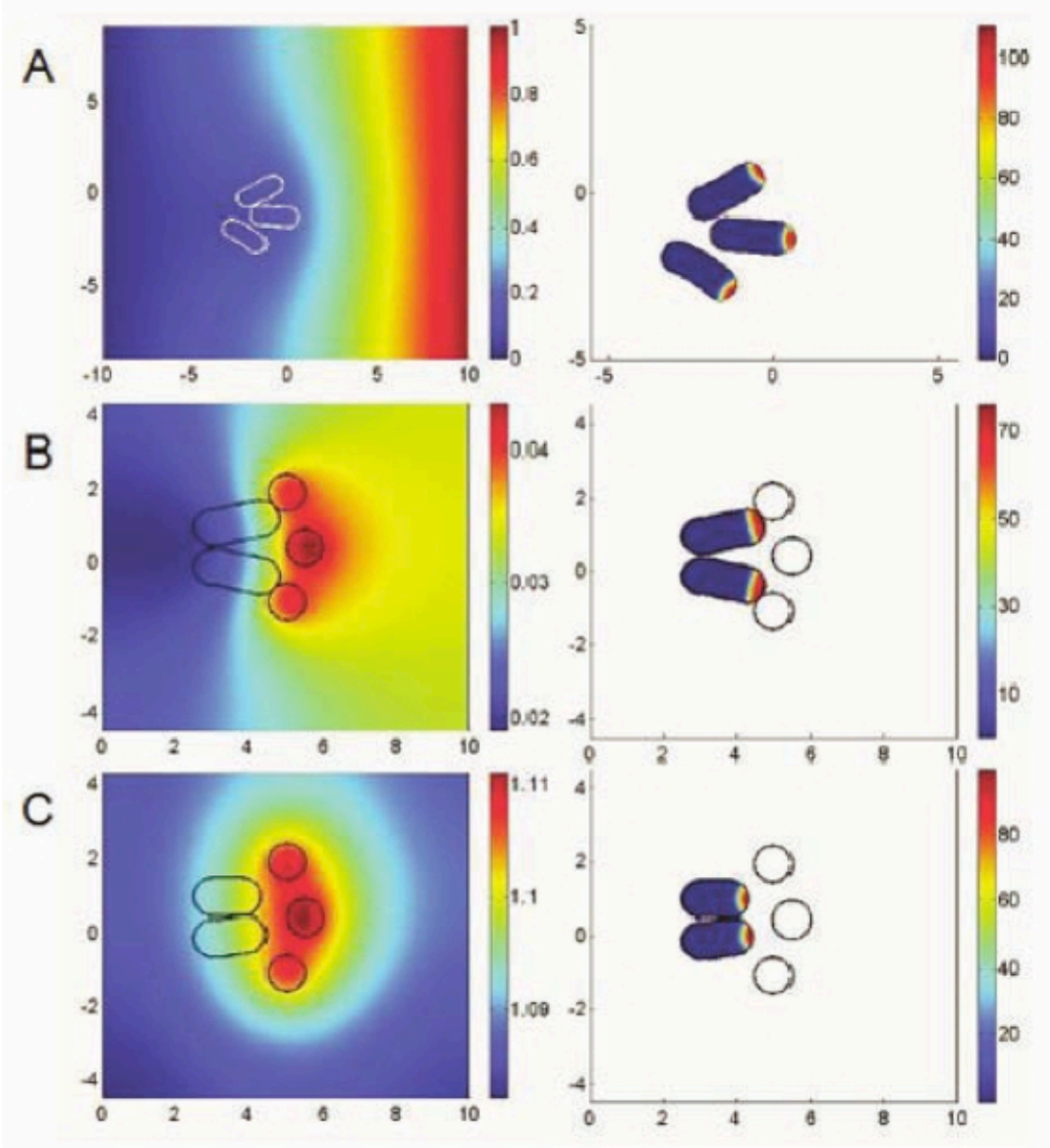

Figure 3.10: The Polarization of Cdc42 directs the chemotropic growth. Left column: pheromone distribution; right column: Cdc42GTP distribution. A. Inside a gradient chamber, Bar1 modifies local pheromone gradient, which changes the position of polarization and results in different growth direction. B. When mating with several a cells, Bar1 helps two a cells find different a cells. C. Without Bar1, two a cells grow in the same direction and compete for the same a cell.

3.6 Discussion

3.6.1 Bar1 in gradient sensing

Experiments have revealed that the protease Bar1 plays a role in yeast's ability to successfully find a mating partner. Jackson and Hartwell demonstrated that the protease Bar1 improves the ability of a-cells to discriminate between normal and pheromone less cells (Jackson and Hartwell, 1990). To explain this observation, Barkai et al. used an analogy to electrostatics to argue that Bar1 released from an a-cell reduces the diffusion range of ∝-factor and thereby sharpens the pheromone gradient in the direction of the nearest -cell (Barkai et al., 1998). More recently theoretical studies suggest that pheromone degradation by Bar1 also improves yeast's ability to detect a gradient by not allowing ∝-factor molecules to be resampled by pheromone receptors (Endres and Wingreen, 2009).

Our results demonstrate a novel role for Bar1 in which a-cells avoid each other. This self-avoidance mechanism occurs because Bar1 tends to accumulates between adjacent a-cells causing a depletion of -factor in the intercellular space, which in turn produces local pheromone gradients that point away from adjacent a-cells. It has recently been demonstrated that Bar1 has a role in ensuring heterothallic reproduction of C. albicans (Alby et al., 2009). Our finding suggests that Bar1 favors heterothallic over homothallic reproduction by preventing physical contact between cells of like mating type. The results of our simulations also

indicate that Bar1 dramatically sharpens the relative pheromone gradient as a-cells elongate toward ∝-cells. This reshaping of the pheromone gradient by Bar1 can be qualitatively understood by realizing that a-cells act as sinks for -factor. In this scenario, the relative pheromone gradient increases roughly as the inverse of the distance between an a- and an ∝-cell. In contrast, because in the absence of Bar1 the factor concentration does not change in time as the a-cell elongates the relative gradient is much less sensitive to the distance separating two potential mating partners. That is, it is the continuous reshaping of the local pheromone gradient that enables a-cells expressing Bar1 to efficiently locate a mating partner. In this sense, yeast cells not only passively sense the extracellular environment, but also modulate it to their benefit.

3.6.2 Model for yeast polarization

Several models for yeast polarization and gradient sensing have been proposed recently (Devreotes et al., 2003, Parent et al, 1999). Our model for gradient sensing is based on a substrate-depletion driven Turing instability and is similar to the model for yeast polarization proposed by Goryachev et al. with two key differences (Goryachev and Pokhilko, 2008). First, we do not assume mass conservation but allow for protein synthesis and degradation. One motivation for including protein turnover in the model was to avoid an artificial dilution of proteins during cell growth. Interestingly, however, including protein turnover introduced the possibility for localized oscillations Cdc42 activity (see discussion

below). Secondly, in our model the amount of active Cdc42GTP is not limited by the available amount of the Bem1-Cdc24 complex. In our simulations 90% of the Bem-Cdc24 complex remains in the cytosol following polarization even though its abundance is significantly less than that of the total available Cdc42, whereas in the Goryachev et al. model depletion of Bem1-Cdc24 limits the fraction of active Cdc42.

3.6.3 Positive feedback

How Bem1 mediates the positive feedback required for polarization is of particular interest. Butty et al. proposed that Bem1 interacts with the auto-inhibitory domain of Cdc24, opens the catalytic domain and activates the protein (Butty et al., 2002). However Kozubowski et al. demonstrated that the necessary requirement for Bem1 in polarization is to bring Cdc24 and the PAK-Ste20 (or -Cla4) together and that the kinase activity of the PAK is required for polarization (Kozubowski et al., 2008). The mechanism by which PAK activity promotes polarization remains unclear. One possibility is that the PAK phosphorylates and activates Cdc42. This scenario was the initial mechanism investigated in our model and the results demonstrate that it is sufficient to generate spontaneous symmetry breaking. Interestingly, our simulations demonstrated another positive feedback mechanism for spontaneous polarization that does not require the GEF activity of Cdc24 to be increased after PAK or Cdc42GTP binding. In this case,

binding with active Cdc42 or PAK increases the lifetime of the Bem1-Cdc24 complex on the membrane.

To be effective in generating a Turing instability, this positive feedback requires two assumptions: 1) membrane bound Cdc24 has GEF activity without binding to Cdc42GTP and 2) Cdc24 remains on the membrane longer in the Cdc42GTP/Bem1/Cdc24 and Cdc42GTP/PAK/Bem1/Cdc24 complexes than when only complexed with Bem1. The fact that Far1 and Bem1 attach Cdc24 to membrane and activate the GEF by opening its auto-inhibition domain provides support for the first assumption (Shimada et al., 2004); the high affinity between PAK and Cdc42GTP and the membrane association of Cdc42GTP makes the second assumption plausible (Sudhaharan et al., 2009). Of course it is quite possible that both mechanisms act cooperatively to make the process of polarization more robust to internal fluctuations.

3.6.4 The role of GAPs in gradient sensing

Proper polarization and gradient sensing require tight spatiotemporal regulation of the proteins involved in these processes. We used our model to investigate which interactions significantly affect the kinetics of polarization and the response of the system to changing pheromone gradients. Our analysis revealed several key functions for GAP activity in polarization. First, GAP activity is not only required to represses global activation of Cdc42, but significantly

reduces the time to establish polarity and sharpens the distribution of Cdc42 activity. Second, while increased GAP activity produced sharper peak of polarization (Fig. 6), it decreased the ability of cells to track a changing pheromone gradient (Fig. 10). Further simulations revealed that this tradeoff between peak sharpness and the mobility of the peak is a general property of the model and is not dependent on the parameter varied (Fig. 10). Third, if the GAP activity is high peak will be less stable when the gradient changes and retain the sensitivity of the direction change. If the system is operating in this regime, then it can achieve both sharpness and good tracking ability. We note that in our model we have not assumed any regulation of GAP activity. There is currently no conclusive evidence to suggest such a mechanism plays a role in polarization and gradient sensing in yeast. However, if GAP activity is positively regulated, this negative feedback loop would provide a potential mechanism for generating spontaneous symmetry braking through a Turing mechanism driven by the activation of a rapidly diffusing negative regulator.

In summary, our results show the mechanism to regulate the gradient sensing in budding yeast by positively modifying the external local gradient using protease degrades pheromone in the intercellular space. This strategy enables cells to reduce the probability of homothallic mating and competition for the same mating partner. Additionally, it sharpens the pheromone gradient towards potential mating partners similar to the establishment of morphogen gradient (Yu et al., 2009). Further fine-tuning of the temporal and spatial dynamics of gradient sensing can be achieved by regulations within the gradient sensing pathway, such

as hydrolysis of active proteins, complex formation, and protein synthesis and degradation. The model also predicts the potential of complicated spatiotemporal dynamics.

3.7 Acknowledgements

Chapter 3 contains material that is a preprint of, Jin,M., Behar, M., Nayak, S., Mather, W., Hasty,J., Errede, B., Dohlman, H.G., Elston, T.C., (2010): Computational modeling of yeast chemotrophic growth reveals the role of the protease Bar1 in gradient sensing., which is in preparation for submission by April 2010.

Chapter 4.

Metabolic gene regulation in a dynamically changing environment

4.1 Introduction

Natural selection dictates that cells constantly adapt to dynamically changing environments in a context-dependent manner. Gene-regulatory networks often mediate the cellular response to perturbation (Beadle and Tatum, 1941; Jacob and Monod, 1961; Douglas and Hawthorne, 1966), and an understanding of cellular adaptation will require experimental approaches aimed at subjecting cells to a dynamic environment that mimics their natural habitat (Thattai and Shraiman, 2003; Lipan and Wong, 2005; Kussell and Leibler, 2005; Kruse and Julicher, 2005; Ronen and Botstein, 2006; Thattai and van Oudenaarden, 2004). Here, we monitor the response of S. cerevisiae metabolic

gene regulation to periodic changes in the external carbon source by utilizing a microfluidic platform that allows precise, dynamic control over environmental conditions. We find that the metabolic system acts as a low-pass filter that reliably responds to a slowly changing environment, while effectively ignoring fluctuations that are too fast for the cell to mount an efficient response. We use computational modeling calibrated with experimental data to determine how frequency selection in the system is controlled by the interaction of coupled regulatory networks governing the signal transduction of alternative carbon sources.

Experimental verification of model predictions leads to the discovery of two novel properties of the regulatory network. First, we reveal a previously unknown mechanism for post-transcriptional control, by demonstrating that two key transcripts are degraded at a rate that depends on the carbon source. Second, we compare two *S. cerevisiae* strains and find that they exhibit the same frequency response despite having markedly different induction characteristics. Our results suggest that while certain characteristics of the complex networks may differ when probed in a static environment, the system has been optimized for a robust response to a dynamically changing environment. Importantly, the integration of a novel experimental platform with numerical simulations revealed previously masked network properties, and the approach establishes a framework for dynamically probing organisms in order to reveal mechanisms that have evolved to mediate cellular responses to unpredictable environments.

4.2 Results and Discussion

In order to probe the response of a metabolic gene network to a fluctuating environment, we developed a microfluidic platform which can subject a population of cells to a continuously varying media supply (Fig. 4.1). The device is designed to generate a fluctuating media signal by dynamically combining two media reservoirs according to a time-dependent function. Feeding channels deliver the media downstream to a customizable growth chamber, which for this study was constructed to constrain a population of yeast cells to grow in a monolayer, allowing for long-term data acquisition (Cookson et al., 2005). The composition of the media is dynamically controlled by a fluidic switch (Groisman et al., 2005b), such that changes in the upstream source may be detected almost immediately by the cells. The fluidic switch was optimized to generate a linear range of mixing ratios from the two media inputs, allowing a variety of periodic waveforms or random signals to be generated.

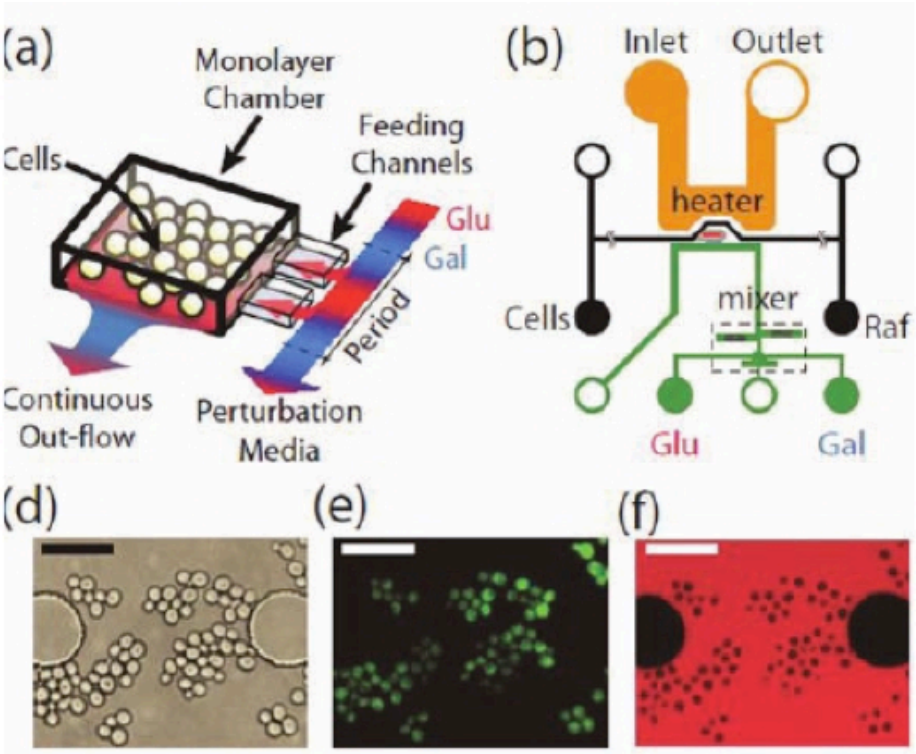

Figure 4.1: Design and implementation of the microfluidic platform developed for our study. (a) Conceptual design of the imaging chamber. The chamber is coupled to the switch output channel via multiple 1 μm tall "feeding" channels. The feeding channels are fed by a controllable wave-form generator that creates sinusoidal perturbations in the glucose concentration while maintaining constant background levels of galactose. (b) An overview of the design shows the layout of the device. The device makes use of three flow networks for (1) loading cells (middle, black), (2) generating microenvironmental waveforms (bottom, green), (3) and controlling on-chip temperature (top, orange). The imaging chamber (center, gray region) is designed to be about 4 microns tall in order to constrain a population of yeast cells to grow in a monolayer. (c) Representative brightfield image of cells growing in the imaging chamber. These images are used to measure the total size of the colony. Scale bar is 25 μm in length, and large circles are support posts in the chamber. (d) Green fluorescence image of the same cells as in (c). These images allow us to measure the amount of Gal1p in each cell. (e) Red fluorescence image of the chamber. The glucose media also contains a red fluorescent dye, and therefore the intensity of the red fluorescence is proportional to the amount of glucose in the chamber at any given time.

As a quantifiable reporter of the cellular response to environmental fluctuations, we fused the native Gal1p protein of S. cerevisiae to the yeast-optimized enhanced cyan fluorescent protein (yECFP) (Sheff and Thorn, 2004b; Raser and O'Shea, 2004). The enzymes for galactose utilization, including Gal1p, are among the most tightly regulated proteins in yeast. Because glucose requires much less energy to metabolize, cells will only consume galactose if glucose is not available. Therefore, S. cerevisiae has evolved a highly complex regulatory network to ensure that the galactose enzymes will be strongly activated when they are needed, but tightly repressed if glucose is present in the environment (Fig. 4.2(a)). Because the network is well studied and involves regulatory motifs common to many higher organisms, galactose utilization is a paradigm for gene regulation. In order to build on the current understanding of its robust regulatory mechanisms, we employed our microfluidic platform to monitor the dynamics of network activation and repression in response to sinusoidal perturbations of glucose over a galactose background.

A population of yeast cells was subjected to sinusoidal glucose waves over a 0.2% (w/v) galactose background, with varying glucose concen-tration from 0.0% (no repression of GAL1 transcription) to 0.25%. For each run we changed the frequency of the glucose signal, varying the period from 0.75 to 4.5 hr, and we imaged the population for a minimum of four full cycles. Time-lapse fluorescence imaging of the cell population in the growth chamber was used to calculate the amplitude ratio and phase shift of the cellular response relative to glucose signal. The results show a maximum response frequency of about 5.6 rads

hr-1 (1.125 hr period). At this frequency, the response trace was indistinguishable from a normal step function response, where as at the lower frequencies the temporal fluorescence trajectories clearly oscillated in response to the signal. In this sense, the galactose system appears to function as a low-pass filter that reliably responds to a slowly changing environment, while effectively ignoring fluctuations that are too fast for the cell to mount an efficient response. Since the sinusoidal driving of the galactose utilization network leads to complex cellular behavior, we used computational modeling to simulate the response and uncover key aspects of the network architecture that give rise to the observed behavior (Hasty et al., 2001b).

In particular, we were interested in how the interplay of the galactose and glucose utilization networks gives rise to the observed frequency response to carbon source fluctuations. By itself, the turnover of Gal1p-yECFP, either due to dilution or active degradation (or both), leads to low pass filtering of periodic signals. However, feedback loops inherent to gene regulatory networks can alter the response of proteins to stimuli (Savageau, 1974). Therefore, in order to simulate the effects of galactose activation and glucose repression on our experimental data, we adapted a comprehensive model of the galactose network originally described by deAtauri et al. (de Atauri et al., 2004) This model includes the transcription and translation of the GAL1, GAL2, GAL3, GAL4 and GAL80 genes as well as the interactions of their respective proteins with each other and galactose (such as dimerization, transport and metabolism). Whenever possible we used parameter values either at or close to the values reported by deAtauri et al.

In addition to this galactose network model, it was necessary to model the dynamics of the glucose network. The glucose network is much more complex than that of galactose (Demir and Kurnaz, 2006; Kaniak et al., 2004; Verma et al., 2005) and models for it are much less well established. Therefore, we chose to model the glucose network with a simplified module describing a basic transport regulatory system. In it, protein products of the glucose network are responsible for transporting external glucose into the cell while internalized glucose acts to induce transcription in the network, giving rise to a positive feedback loop (see Fig. 4.2(a)). Calibration of the computational model to the experimental data led to several important observations that would not have arisen from an analysis of steady-state batch culture data. The large amplitude ratios observed at low frequencies suggested that when glucose was added to the system the degradation rates of some galactose network components were greater than in the absence of glucose. Previous studies have suggested that components of the glucose network can actively degrade mRNA produced by genes involved in the galacose/glucose switch (Ronen and Botstein, 2006), and such a phenomenon has also been shown to exist for the mRNA of other genes (Scheffler et al., 1998; de la Cruz et al., 2002; Andrade et al., 2005). Therefore, we added enzymatic decay terms (governed by Michaelis-Menten dynamics) to the equations describing the dynamics of the GAL1 and GAL3 mRNA and found that it greatly increased the accuracy of the model. These two genes are among those in the galactose network that are targeted by the glucose induced Mig1p that represses transcription by binding to upstream regulatory sites (Verma et al., 2005).

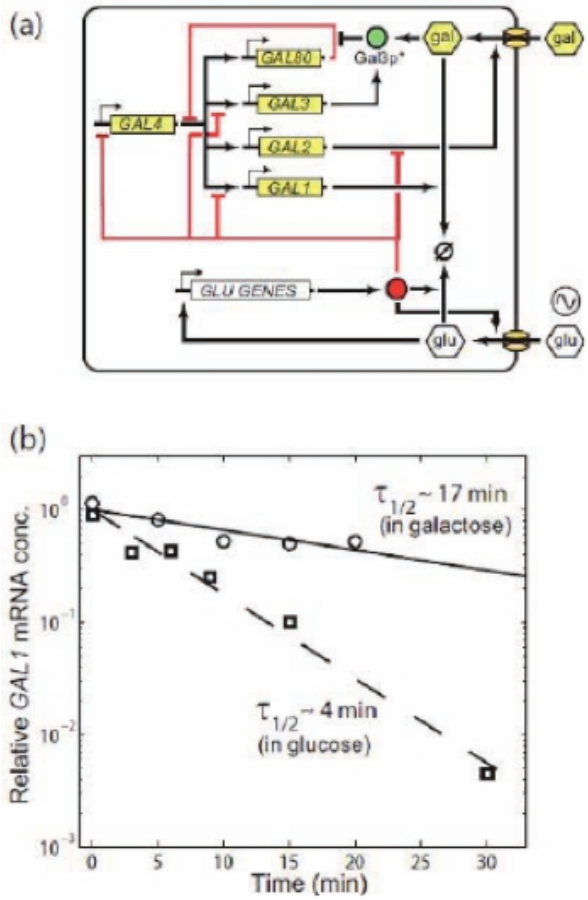

Figure 4.2: Regulation in the galactose utilization network (a) Schematic of the gene regulatory networks involved. The regulatory genes in the galactose network are activated by the Gal4p protein which binds to upstream activation sites. The GAL80 gene provides negative feedback in the system by prohibiting the inducing affects of Gal4p. Positive feedback is provided by both GAL2 and GAL3. Internalized galactose can bind to Gal3p and the resulting complex binds to Gal80p. Gal80p bound to the Gal3p-galactose complex is incapable of repressing Gal4p. Also, the transporter Gal2p increases the amount of internal galactose which stimulates the galactose network. The glucose network inhibits the transport of galactose and represses transcription of the galactose network in the presence of glucose through the action of Mig1p, which can bind to upstream regulatory sites of GAL1, GAL3 and GAL4 (Verma et al., 2005). The glucose network also regulates the hexose transporter genes (HXT) which are responsible for transporting glucose into the cell (Boles and Hollenberg, 1997), which then activates the glucose network. (b) Experimentally measured decay of GAL1 transcripts in galactose (circles) and glucose (squares). Also shown are the best-fit lines corresponding to half-lives of around 17 min in galactose (solid line) and 4 min in glucose (dashed line), similar to the values predicted by the numerical model.

Thus, if proteins from the glucose network do actively degrade galactose network transcripts, GAL1 and GAL3 are likely targets. To test this prediction, we measured the degradation rates of GAL1 and GAL3 in both galactose and glucose. Both transcripts showed a 2-8 fold increase in their decay rates when in the presence of glucose (see Fig. 4.2(b)), consistent with the values predicted by the computational model. This form of post-transcriptional regulation, in which glucose acts to down-regulate GAL protein synthesis, is a previously unknown source of regulation in the galactose utilization network.

Furthermore, the inclusion of glucose mediated mRNA decay results in a model that accurately reproduces the dynamic response of a population of cells to sinusoidal repression over a large range of frequencies (Fig. 4.3). Batch-culture induction characteristics for metabolic genes can vary from strain to strain or depend sensitively on the growth state of the culture. Therefore, we were also interested in using the model to determine how galactose induction differences would affect the response to the glucose fluctuations. The model demonstrated that significantly different galactose induction does not necessarily lead to significant differences in the response characteristics (data not shown). In other words, the model led to the hypothesis that deficiencies in network induction capabilities might not hinder a cell's ability to adapt and thrive in a changing environment. The yeast strain used to collect this data, K699, is sensitive to external galactose concentrations, with full induction of the galactose network occurring around 0.05% (w/v) galactose.

In order to test our hypothesis, we turned to a strain (YPH499) that is known to have a deficiency in the galactose utilization network, which causes it to require more galactose than “normal” to induce production of the galactose enzymes (Rohde et al., 2000). YPH499 is a derivative of a GAL2 mutant strain, and while the mutations were reportedly repaired, the GAL2 alleles in many of the derivative strains have been shown to cause significantly impaired galactose uptake (Rohde et al., 2000).

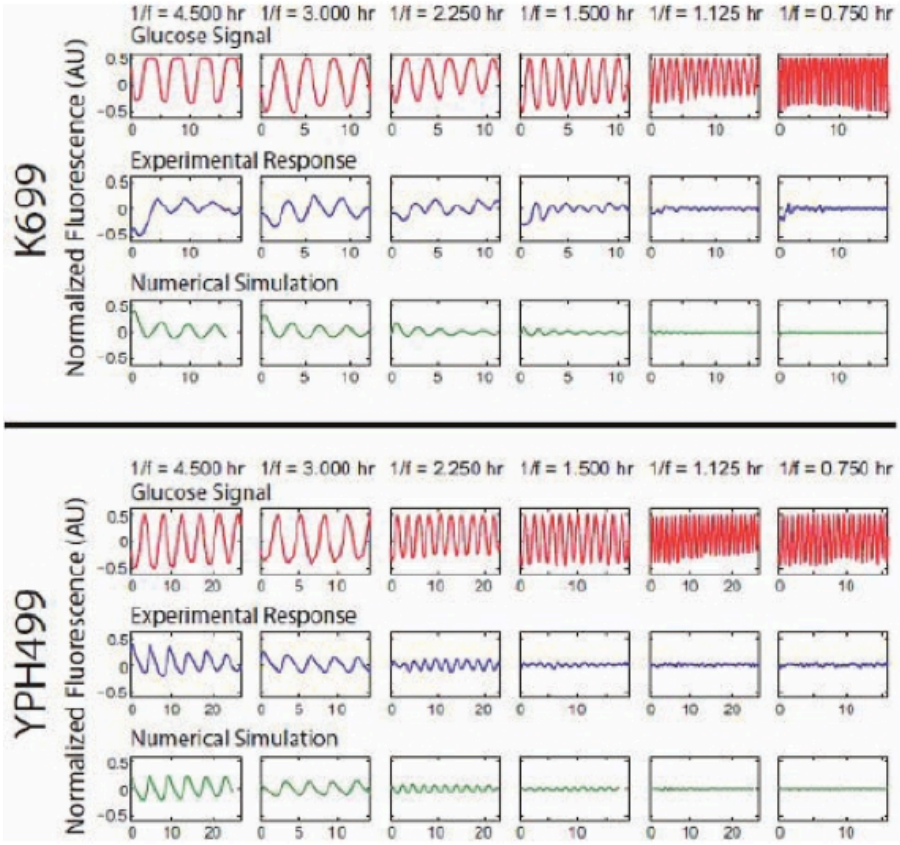

4.3: Experimental and computational results for cells expressing a GAL1-yECFP fusion gene in response to alternating glucose and galactose media for strains K699 and YPH499. The top row of each strain depicts the input glucose signal measured during each experimental run and also used to simulate the responses. The mean fluorescence of a red tracer dye, representing the glucose concentration in the media, is normalized and subtracted from 1 to represent the "induction" signal used in the experimental and computational runs above. The middle rows show normalized and detrended fluorescence trajectories for a population of cells as they respond to glucose waves of various frequencies over a galactose background. In the absence of glucose, galactose induces transcription of GAL1-yECFP causing an increase in cellular fluorescence. However, as glucose is introduced into the extracellular environment, transcription of the galactose enzymes is shut off, causing a decrease in fluorescence signal as the Gal1p-yECFP protein is degraded. Oscillation periods shown from left to right are 4.5, 3.0, 2.25, 1.5, 1.125, and 0.75 hr. For input waves with a period shorter than 1.125 hr, cells no longer respond to sinusoidal repression in a periodic fashion, demonstrating their ability to "filter" out high frequency environmental fluctuations. The bottom rows show simulation results for the same frequencies as above. The model, calibrated to experimental induction and repression data, accurately

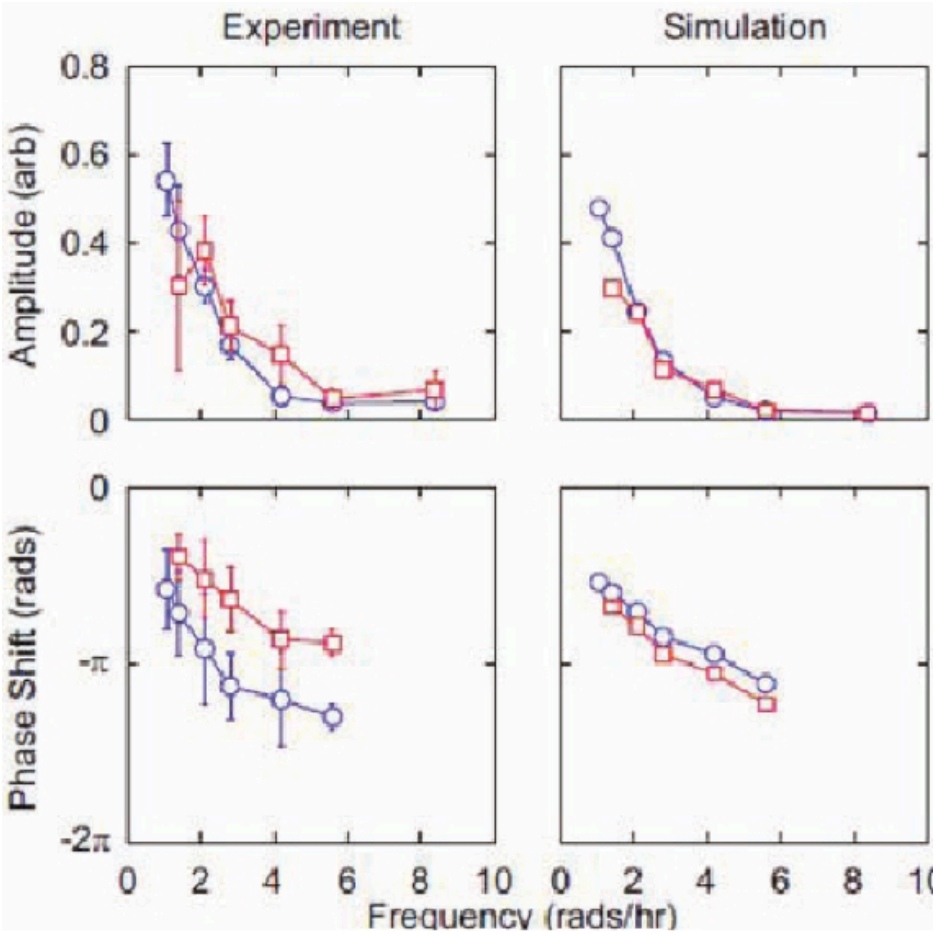

Figure 4.4: Experimental and computational comparison of two yeast strains, one of which (YPH499) is known to have a deficiency in the galactose utilization network. Amplitude (top row) and phase shift (bottom row) of the response of cells to sinusoidal repression at various frequencies are shown for both K699 (red) and YPH499 (blue) strains. For the highest frequency trial, reliable phases could not be calculated at all due to the noise, and have been omitted from the graphs. The experimental data (left column) demonstrate that the amplitude responses of the two strains are strikingly similar, especially considering their significantly different induction curves. This phenomenon was predicted by model simulations, as slight modifications to the model parameters that affected induction and repression curves did not affect the cell population's robust response to a dynamic environment. This suggests that the complex structure of the glucose and galactose networks may confer robustness to cells even if faced with seemingly detrimental network deficiencies. The phase responses (bottom row) of the two strains did show a marked difference, with YPH499 cells exhibiting a greater phase lag than K699.

It is known from the literature that the Gal2p protein is responsible for the transport of extracellular galactose into the cell and its activity is markedly different in YPH499 than in K699. Our flow cytometry population data demonstrated that YPH499 cells require about ten times more galactose to reach full induction than do K699 cells. Despite the difference in induction sensitivity between K699 and YPH499, our model predicted that inefficient Gal2p transport does not translate into a less robust response to a fluctuating environment. This suggests that the complex interplay of the glucose and galactose networks may confer robustness to cells even if faced with deficiencies in the induction characteristics. To validate this finding, we repeated the microfluidic runs at each frequency, this time using the YPH499 strain with a Gal1pyECFP fusion. As predicted, the amplitude responses of the two strains are strikingly similar (Fig. 4.4), especially considering the significant difference in their galactose sensitivity. We do not at present know the underlying mechanistic property of the regulatory network that leads to the robust response of the two strains. Future studies might endeavor to deduce this mechanism through the systematic deconstruction of the regulatory elements in a single strain. While the present study demonstrates how robustness can occur despite large differences in induction characteristics, one could further investigate the generality of this phenomenon by comparing the responses of many different strains to different types of temporal perturbation

4.3 Materials and Methods

4.3.1 Dynamic environment experiments

The PDMS (polydimethylsiloxane) microfluidic devices were designed to allow for monolayer growth of yeast cells in the imaging chamber and were fabricated using standard replica molding techniques (Whitesides et al., 2001, 2004; Xia and Whitesides, 1998). An upstream fluidic switch controlled the media input into the chamber by mixing the flows of the inducing and repressing media. The mixing ratio of the two media was governed by a software controlled, custom-designed pressurization system able to consistently produce time-varying waveforms. mRNA degradation experiments : The degradation rates of GAL1 and GAL3 transcripts were measured using standard rt-qPCR techniques. Knockout strains for both genes were first created, and then ectopic GAL1 and GAL3 were placed back into the cell under the control of a doxycycline repressible promoter. mRNA half-lives were measured from cells grown in the presence or absence of glucose.

4.4 Acknowledgements

Chapter 4 contains material originally published as Bennett, M.*, Pang, W.*, Ostroff, N., Baumgartner, B., Nayak, S., Tsimring, L., and Hasty, J., 2008:

Metabolic gene regulation in a dynamically changing environment. Nature, 454(7208):1119-22. (*equal contribution). Copyright permission to republish here was granted by Nature Publishing Group.

Chapter 5.

Developmental switching in temporally varying spatial gradient

5.1 Introduction

Chemical gradients play a central role in several biological processes, such as embryogenesis, wound healing, chemotaxis and cell migration. In particular, microbes must be able to sense and respond to spatiotemporal changes in environmental conditions. Here we present a novel microfluidic device that allows us to expose *Saccharomyces cerevisiae* (yeast) to a time-dependent gradient of pheromone concentration. Our investigations reveal three mechanisms by which yeast can reorient their direction of polarity and growth.

During the initial phase of chemotrophic growth, the polar cap is mobile and the direction of polarization can change without the need for noticeable cell

growth. At intermediate times, the polar cap is less mobile and new cell growth accompanies change in the direction of the polarization direction. At long times, highly elongated cells can form a second site of polarization distal to the leading edge. In this case, transient bipolar growth is observed until the initial site of polarization is lost. The ability to periodically modulate the direction of the pheromone gradient allows us to quantitatively characterize the time scales associated with these three mechanisms for responding to spatiotemporal changes in the environment. Recently a study in the Hasty lab combined theoretical and empirical approaches leading to new insight into the glucose/galactose regulatory networks in yeast. (Bennett et al., 2008). Here the usefulness of dynamic perturbation was verified in the context of mRNA degradation regulation in the GAL network. By exposing yeast to a dynamically changing environment in a microfluidic platform, it was discovered that the cells respond to long-term changes in nutrients but not to faster fluctuations. It was found that the metabolic system of yeast acts as a low-pass filter that reliably responds to a slowly changing environment, while effectively ignoring fluctuations that are too fast for the cell to mount an efficient response. This suggests that the way we choose to perturb biological systems leads us to investigate different aspects of the systems. And that a system probed in a dynamically changing environment, the system has been optimized for a robust response to a dynamically changing environment.

The pheromone signaling pathway has at least two components, and temporal. Varying the pheromone gradient both spatially and temporally can lead to the discovery of novel behavior as we show here. In this study, we monitored

the response of *S. cerevisiae* polarization pathway to periodic changes in the external pheromone concentration by utilizing a microfluidic platform that allows precise, dynamic control over environmental conditions. Yeast represents a unique and informative model system to investigate cell polarization and gradient sensing. Indeed, many of the mechanisms that direct cell polarity in yeast, e.g. regulation of the actin cytoskeleton, are conserved in higher eukaryotes (Moseley et al., 2006, Wedlich-Soldner et al., 2003). The yeast mating pathway provides one approach to understanding regulation of cell polarity. Haploid yeast cells can exist in one of two types. Different types will fuse (mate) into a diploid cell when in proximity to one another (Bardwell L., 2005, Segall J.E 1993). This mating response is directed by mutual pheromone signaling and, among other things, leads to the reorientation of cell growth along the complementary type's pheromone gradient. While much is known about the proteins that are required for polarization and gradient sensing, the precise mechanism by which these molecules interact to detect and respond to changing environments remains unclear. One reason for this lack of understanding has been our inability to accurately manipulate the spatiotemporal properties of the extracellular environment.

Recently many researchers have turned to microfluidic devices to overcome this deficiency. There have been microfluidic systems that generate stable chemical gradients (Hao et al., 2008; Paliwal et al., 2008). Although, these devices are very useful and have provided us with key insights, they are limited by the fact that the gradient remains constant in time. To date there has been no study on manipulating both temporal and spatial characteristics of the environment.

Here we report on a novel microfluidic device for studying yeast cell polarization that allows us to temporally modulate spatial gradients of an external stimulus. We seek to explore the response of yeast cells to dynamic perturbation, probing yeast's ability to cope with a fluctuating environment. Fabrication and operation of the device is straight-forward, as it requires only a single PDMS layer and has a relatively small number of ports. The gradient generation does not require high flow in the cell-trapping region, a critical factor for chemotropism studies in a concentration gradient for non adherent cells like yeast. Furthermore, cell clumping or flocculation is avoided by using a height-constrained cell chamber (Cookson et al., 2005). The mating and chemotrophic growth pathways employ the same cell surface receptor, G protein, and downstream effectors. While much work has been carried out to characterize the mating response that occurs at high pheromone concentrations less attention has been paid to chemotrophic growth. This behavior has been suggested to provide yeast with a mechanism for finding distant mating partners. However very little is known about the time scales involved with polarization and gradient sensing or how yeast responds to spatiotemporal changes in pheromone concentrations. Our gradient chamber allows us to begin to address both these issues.

5.2 Materials and Methods

Strain construction and experimental conditions: Strain BY4741 and BY4741-derived mutants were used through out the study unless otherwise mentioned. Strains of *Saccharomyces cerevisiae* with Fusions in Bem1 were obtained from Dohlman Lab in UNC.

The BAR1 protease helps yeast cells to find mating partners, since it cleaves and inactivates alpha factor, allowing cells to recover from alpha factor-induced cell cycle arrest. We chose to knock out the Bar1 protease to simplify the system so that there is no pheromone degradation in the cell chamber. And the cells see the amount of pheromone that we provide them with. We utililzed the widely used the yeast homologous recombination method (Ma et al., 1987) to knock Bar1 out of the genome G418 sequence was copied using PCR, the ends were tagged with approximately 40 base pairs of sequence homology to native yeast genome To aid in transformation efficiency, 400 bp homology extension sequences that flanked the insertion site and were anchored with the original 40 bp homologous sequence were cloned from genomic DNA. To replace the Bar1 gene with with a selective marker (G418 sequence), the resulting PCR product was used in the transformation reaction using heat shock, and the successful transformants were selected by growing the colonies on a media plate containing the drug G418. Isolates that were able to grow on G418 plates and hence had the Bar1 gene knocked out were stored as frozen stock for later use. For

subsequent experiments, frozen isolates were revived by streaking onto solid media plates. Plated cultures were grown at 30 degree C for 1-2 days and stored at 4 degree C for no longer than two weeks.

Experimental setup: The yeast cells were grown in synthetic complete media containing 2% glucose overnight and then the culture was diluted to an OD600 0.1 on the day of the experiment and grown to OD600 0.3-0.6 to ensure log phase growth. All the media consisted of synthetic complete media. For optimal yeast cell growth, the chip temperature was typically maintained at 30 degree C by the incubator attached to the microscope.

In preparation for cell imaging, the microfluidic devices were mounted on to the microscope stage and were primed with 0.2 mm-filtered water followed by media using a syringe. Each of the ports (see Fig. 2) was then connected to individual syringes (10 ml) filled with appropriate media using microbore Tygon tubing (Cole Parmer, ID 0.02”). Ports I1 , I2, I3 and I4 are the media input channels. C1 and C2 are the cell waste and cell loading channels respectively. Port S is the common shunt channel. All the ports have SC media during operation. Ports I1, I2, I3 and I4 have alpha factor added. In the ports I1 and I3 in addition to the SC media, and alpha factor (Sigma-Aldrich Corp. St. Louis, MO), a red fluorescent dye tracer (Sulphorhodamine 101, Sigma) was also added to visualize the gradient profile on the chip. All the flows were driven by gravity-based hydrostatic pressure (in H2O). The cell waste and the cell loading ports (C1 and C2) were maintained at equal heights. The syringe heights were set such

that in the beginning all the four media inputs (ports I1, I2, I3 and I4) were maintained at equal pressure.

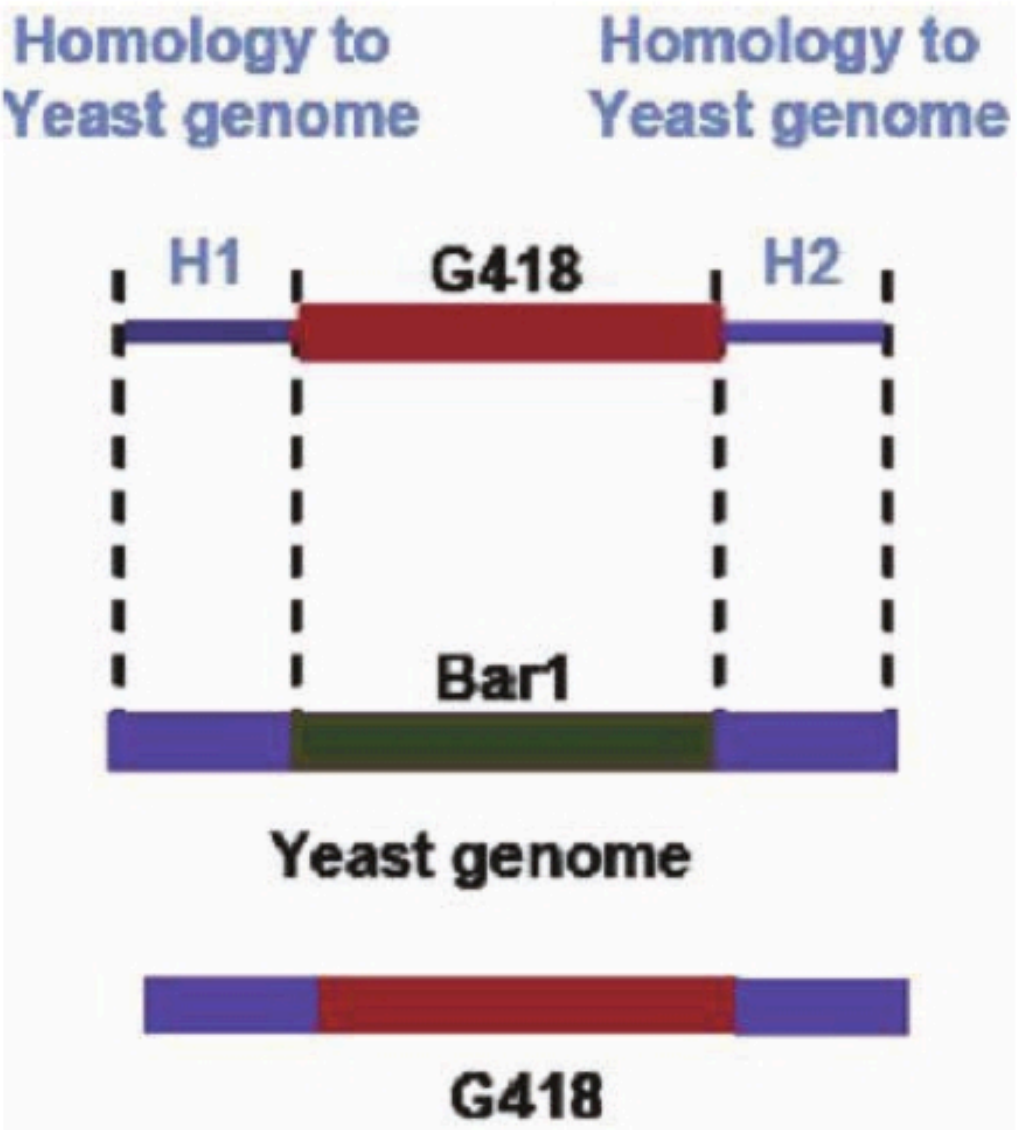

Figure 5.1: Yeast homologous recombination method to knock out Bar1.

The pressure differences at the various port pairs were carefully tuned such that during the operation there would be minimal active flow in the cell chamber.

And the concentration gradient in the cell chamber was established mostly due to molecular diffusion between the two input channels through the small diffusion channels.

The cells were introduced into the chamber using a syringe containing the cell suspension through the cell loading port C2. To facilitate cell loading, the cell port was pressurized by raising the height of the syringe. Once there was adequate number of cells in the chamber the syringe height was adjusted to the same height as that of the cell-waste port. The images were acquired using a 60x oil objective in the phase contrast and mCherry or GFP fluorescence every 5 minute over a period of around 24 hours. The pheromone concentration ranging from 0- 20nM was used for all of the gradient flipping runs, as the main interest of this study was to investigate the highly elongated morphology of the bar1 delete yeast cells.

As discussed before at intermediate pheromone concentration the cells tend to have the elongated morphology. The cells being Bar1 delete are far more sensitive to pheromone, at a concentration below 5 nM budding was observed and at a concentration higher than of 20 nM, shmoo morphology was observed (Taylor et al., PNAS 2008).

5.3 Microfluidic device Fabrication

The design of the microfluidic device used here was adapted from the original gradient device design that was developed in Hao et al. (2008). We modified the original device to create a novel system where we can create a linear gradient that can be precisely switched temporally. Fabrication and operation of the device is straightforward, as it requires only a single PDMS layer and has a relatively small number of ports. The gradient generation does not require strong media flow in the cell-trapping region, a critical factor for chemotropism studies of non-adherent cells. Furthermore, flocculation is avoided by using a height-constrained cell chamber (Cookson et al., 2005). Standard techniques of photolithography and replica molding (Duffy et al., 1999; Hansen and Quake, 2003) have become the ideal way of generating microfluidic devices. The very first step involves the concept development where the device design is drawn using a computer aided program such as AutoCAD 2005 (Autodesk Inc.).

As mentioned earlier the laws of fluid dynamics under the condition of low Reynolds number for micro-volume flow is analogous to that of Ohm's law and hence it is very easy to calculate the fluidic resistance in the microchannels and if need be can be altered to get desired flow rates and driving pressures. The device design is separated into multiple layers, where all features of a particular height are positioned on a single layer for photolithographic purposes based on the device in question. Once finalized, the designs for different layers are printed as patterns of clear and opaque regions at 20,000 DPI onto phototransparancy film (Output City, Bandon OR) to be used as photomasks in the photolithographic process. Patterned features are printed as clear regions on a black opaque

background that are ideal for negative-photo resists such as SU-8, (Microchem Corp), a photocurable epoxy that crosslink's when exposed to UV light. Printed transparencies are trimmed into individual masks and mounted onto clean 3"3"1/8" borosilicate glass plates (McMaster-Carr) by gluing using Loctite formula 495 super-bonder. The glass serves as a rigid support for the mask so that it could be mounted to alignment equipment easily.

The next step involves the creation of the master mold for which, a clean silicon wafer is spin coated with SU-8 2000 (MicroChem Corp., Newton, MA) to appropriate depths using a Headway PWM32 programmable spinner (Headway Research Inc., Garland, TX) and patterned by UV light through the Photomask that selectively crosslinks the features represented by the mask. Multiple layers can be integrated by repeated the process of spin-coating, exposing to UV, and removing unexposed photoresist in SU-8 developer (Microchem Corp.). Finally we get a positive relief of photoresist on the silicon wafer, or the "master mold," whose topology precisely reflects the desired device channel and geometry. This master mold can be used repeatedly to generate several batches of microfluidic device. The final step is called replica molding where, the silicon/SU-8 master mold is treated with chlorotrimethylsilane vapors (Sigma) for 2 minutes to facilitate the release the PDMS monolith. Poly-dimethylsiloxane (PDMS, Sylgard 184, Dow Corning, Midland, MI) is mixed 10:1 (resin:crosslinking agent), degassed in a vacuum dessicater and poured onto the silicon/SU-8 master mold and baked at 80C for 1.5 h in a dry gravity oven (Fisher Scientific). Cured PDMS monolith was then peeled off the master mold and fluidic ports (for

media/cell loading etc.) were punched with a 20 gauge Luer stub (McMaster-Carr). The punched holes are then flushed with a 0.2- mm syringe and filtered dH2O to remove debris. Chips are individually cut out from the PDMS monolith and the surfaces cleaned using office grade Scotch Tape (Type 810, 3M). These clean individual chips are then plasma bonded to glass cover slips to be used in the experiment.

Briefly, the PDMS chips and the cover slips (24-40 mm, Corning Inc., Corning, NY) were cleaned sequentially with acetone, isopropanol, and methanol and then air dried using a high velocity stream of filtered air, followed by exposure to oxygen plasma for 3 minutes in UVO cleaner (Jelight 342/BLW200 - UV ozone cleaner). Next, the chip was laid on top of the cover slip and baked at 80C overnight to develop bonding (Wu et al., 2002). This creates an irreversibly bonded interface capable of withstanding up to 25 psi of pressure. The fluidic channels (blue in Fig. 2) were 10 microns high. The cell trapping region was fabricated to a height of 4 microns. The small diffusion channels were fabricated to a height of 0.6 microns so as to restrict the cells in the chamber and to allow for diffusion to occur between the two input channels. The gradient can be switched in direction within about 1 min timescale, and this is sufficiently rapid relative to the phenomena presently under study.

The principle of generating a fluctuating gradient direction is by dynamically combining two media reservoirs in a time-dependent manner via a fluidic switch (Figure 3). The cell chamber is about 4 micron tall, comparable to the size of yeast cells. Hence, the colony of yeast cells is distributed in a planar

fashion, and it is easier and hence colony of yeast cells are distributed in a planar fashion and it is easier to extract single-cell fluorescence data. The cell-trapping region receives a continuous supply of fresh media through a series of "feeding" channels (10 microns tall) downstream of the fluidic switch (Groisman et al. 2005), such that changes in the upstream source are detected by the cells within few minutes. This lag in time is due to the fact that the establishment of gradient is done mostly through diffusion. Gradient within the chamber is established by diffusion between input L and input R via the feeding channels that connect the media channels to the cell

Image acquisition and Data Analysis:

The phase-contrast setup comprised a TI2000-U epifluorescent inverted micro-scope (Nikon Instruments Inc., Tokyo, Japan) equipped with fluorescence excitation and emission filter wheels (?lter set #89006 for CFP/YFP/mCherry, Chroma Technology Corp., Rockingham, VT) and a GFP ?lter cube (#GFP-3035B-NTE, Semrock Inc., Rochester, NY). Automation was achieved by NIS-Elements Advanced Research software (Nikon Instruments Inc., Tokyo, Japan). The set up has a ProScan II XY motorized stage and fine focus motor with a hardware-based auto focus controller (Prior Scientific, Rockland, MA) and an Uniblitz VS35 high-speed shutters (Vincent Associates, Rochester, NY), Images were acquired using a Hamamatsu ORCA-ERG cooled CCD camera (Hamamatsu Photonics, Hamamatsu,

Japan), and an X-Cite Series 120 fluorescent lamp (EXFO, Quebec, Canada). The focus was maintained during image collection by the contrast-based autofocus algorithms.

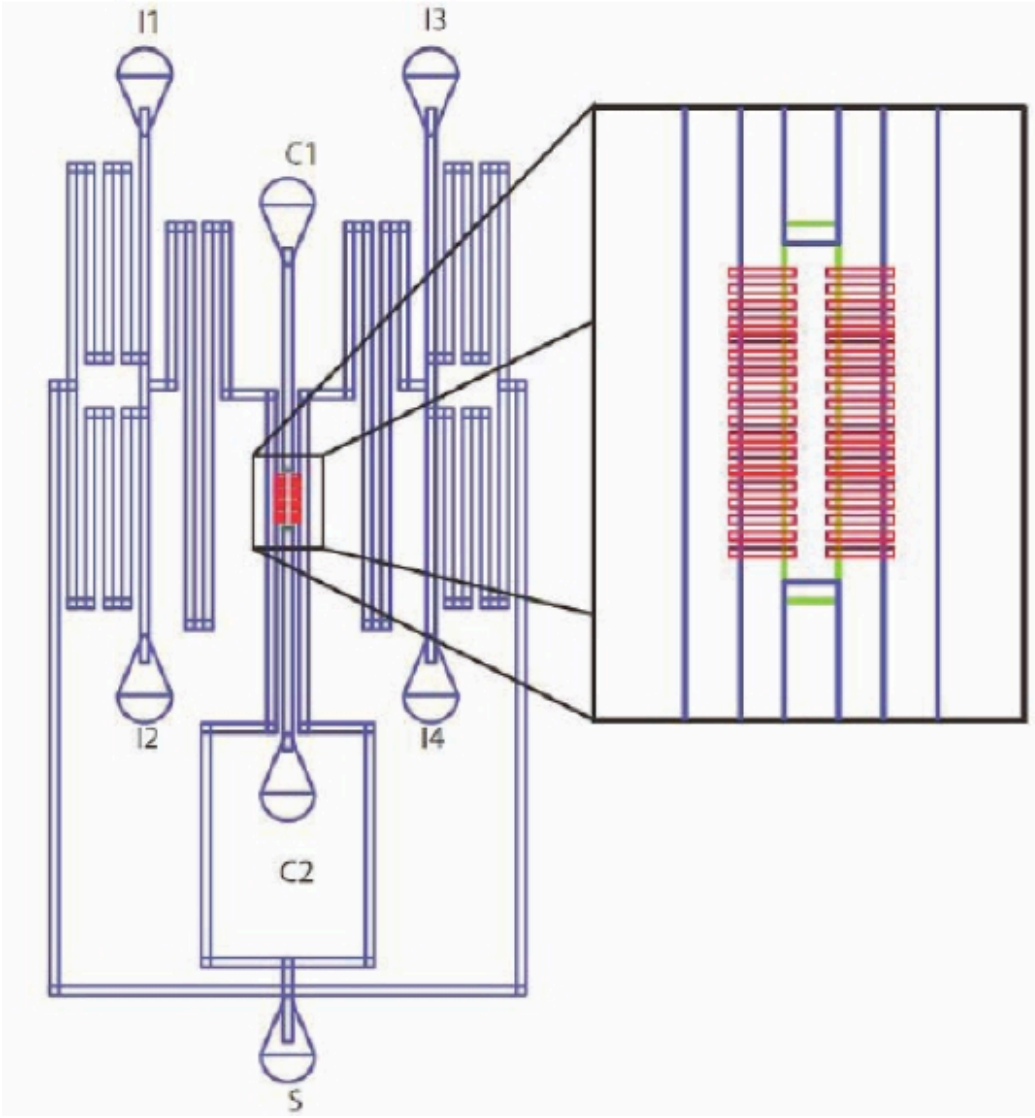

Figure 5.2: Schematic of the microfluidic dynamic gradient device with a magnified view of the cell chamber (green). The cell chamber is coupled to input channels (blue) by 0.6 micron feeding channels (red). Concentrations in each of the input channels are controlled by a microfluidic switch. Mixing of the two input channels leads to a gradient within the cell chamber. Cells are loaded through the port C2.

5.4 Single cell tracking

Images obtained from fluorescence microscopy allowed us to construct single cell trajectories for polarization direction with the assistance of WCIF ImageJ image analysis software (Wayne Rasband, Research Services Branch, National Institute of Mental Health, Bethesda, MD with plug-in collation and organization by the Wright Cell Imaging Facility, Toronto, ON). Trajectories were constructed by manual tracking, described in the following. The ends of an elongated yeast cell are approximately circular, such that each end has an approximate center of curvature. The center of the end with brightest Bem1-GFP signal was determined by eye, and a ray was drawn from this center towards localized Bem1-GFP fluorescence signal. In the cases where Bem1-GFP was not highly localized, the approximate center of Bem1-GFP signal was used. The angle of this ray measured from the image horizontal was recorded as the polarization direction. Polarization direction was not recorded when Bem1-GFP was sufficiently dim (potentially due to delocalization), when Bem1-GFP was delocalized by more than 180 degrees, or when a cell had initiated apparent budding.

5.5 Results and Discussion

5.5.1 Temporal Gradient generation and device characterization

A microfluidic device capable of creating create temporal gradient (Irimia et al., 2006) has been reported, but it suffers from the fact that the principle of gradient generation is based on active flow and the device is very complex and cumbersome to fabricate and operate. As the gradient generation relies on flow, it this approach cannot be used for experiments with non-adherent cells such as yeast.

To monitor the behavior of the yeast cells, in a dynamically changing environment of pheromone concentration there is a need to develop experimental techniques that enable the acquisition of temporal cell dynamics data. In this paper we have developed a novel micro fluidic device where we can create a linear spatial gradient that can be precisely switched temporally. The principle of gradient generation is based on diffusion and the direction of the gradient is switched based of an on chip fluidic switch. All device flows were driven by gravity-based hydrostatic pressure. Tracking of on-chip pheromone concentration was done using a red fluorescent tracer dye (0.01 mg/mL, sulforhodamine 101) in the media containing alpha factor. The fluidic switch in our device was designed such that it can generate intermediate mixing ratios between the two inputs, but for all our experiments, we used all or none pheromone concentration. Based on the pressure differences, one of the media sources (I1 or I2) from either side was sent to the cell chamber, and a gradient was established. The direction of the gradient was switched successfully and faithfully each time based on the state of the on chip media switch.

The fluidic switch actuation was automated and was controlled using custom LabVIEW software (National Instruments). The device was characterized using a red fluorescent tracer dye (0.01 mg/mL, sulforhodamine 101) in the media. Experimental data was acquired by imaging fluorescent dye entering the trapping region as the direction of the gradient was switched. For each run the frequency of the gradient switching was changed varying the period from mere 5 minutes to 30 minutes to ensure that the gradient switching was accurate and faithful. Figure 4 shows the gradient profile before and after the direction of the gradient is flipped.

Fluorescence imaging of Bem1-GFP was used to detect polarization in the yeast cells, and sulforhodamine dye was used to monitor the gradient. The concentration of sulforhodamine is sufficiently dilute such that division rates in batch culture are unperturbed. Cells are exposed to filtered excitation lamp light corresponding to GFP and sulforhodamine dye wavelengths for 0.5 s and 20 ms, respectively.

Figure 4 shows how yeast cells track the gradient and change direction as a result of gradient switching. For most of our experiments, we apply a gradient of 0 to 20 nM pheromone, such that cells centered in the gradient tend to be exposed to 10 nM mean pheromone. Cell polarization was measured in live cells expressing a fluorescent protein fusion of an essential scaffold protein, Bem1-GFP. Bem1 is thought to be associated with a key positive feedback in yeast polarization machinery (Wedlich-Soldner, R et al 2004). We used cells lacking the

protease Bar1 for our studies to prevent cells from interacting via degradation of pheromone (Moore, et al., 2008, Barkai et al., 1998).

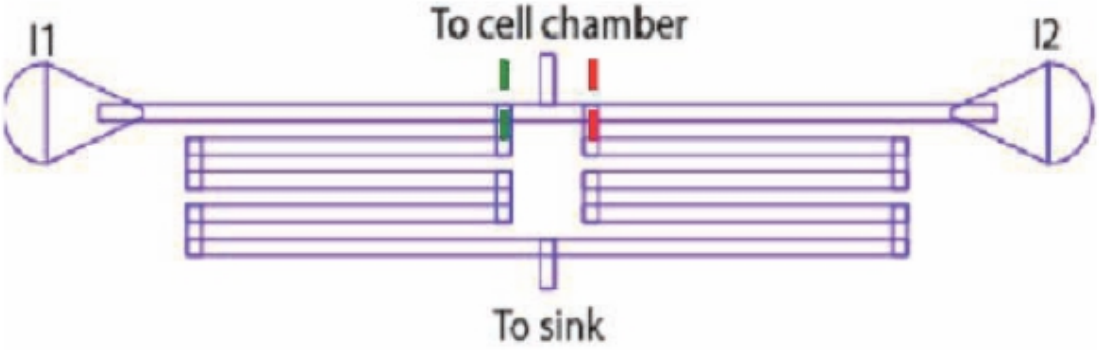

Figure 5.3: Diagram for the microfluidic switch. When inputs I1 and I2 are at the same pressure, the boundary that splits the laminar flows of input I1 and I2 is at the dashed black line. And by shifting this (boundary that splits the laminar flows of input I1 and input I2) to the center of the channel at the left (dashed green line), media input I2 is send to the cell chamber. While in the reverse configuration, when the boundary is in the center of the channel at the right (dashed red line), input media I1 is send to the cell chamber. In both cases the flow from both the input is sent to sink via the shunt channel, this helps in preventing the cross-contamination of the media reservoirs.

In the Gradient chamber, polarization direction and new cell growth are seen to continuously adapt to the direction of pheromone gradient, leading to a "snaking" morphology in a switching gradient (see Figure 6a). These typical cells responded to a switching gradient by continuous adaptation of polarization direction. There are some interesting observations that we note in the switching gradient runs. We see that Bem1 tends to accumulate in the areas of high curvature. (See Figure 7).

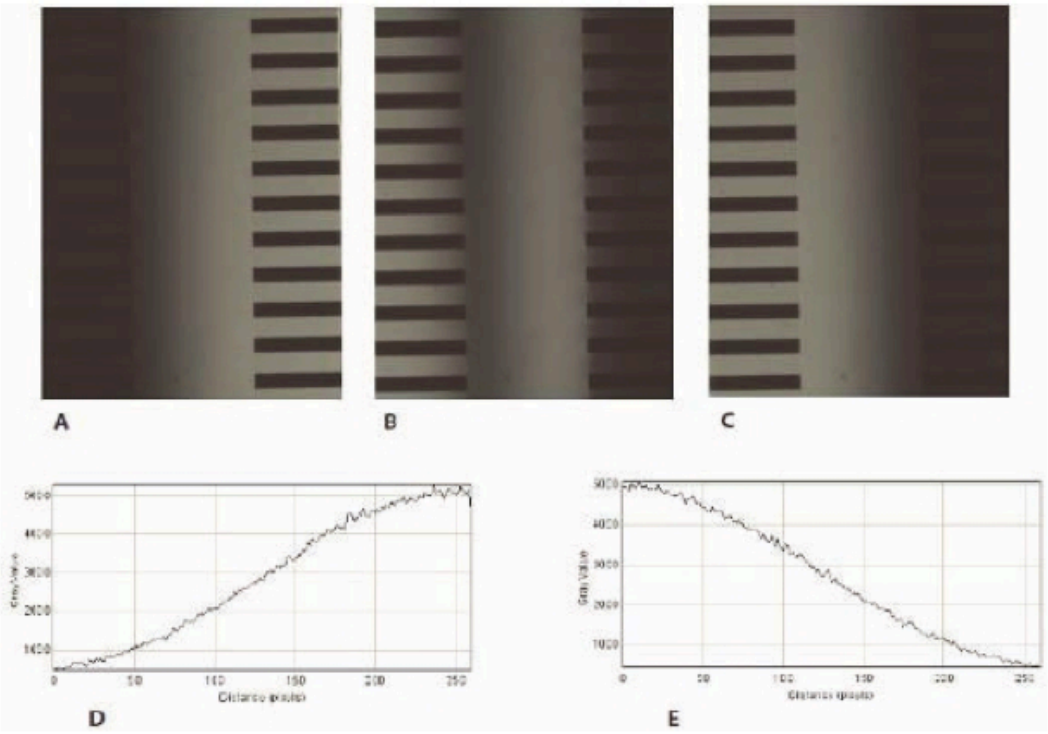

Figure 5.4: The time-dependent gradient. A) Gradient of dye in the chamber before the switch. Light regions indicate regions of high dye concentration. The horizontal stripes on the left are the input channels. B) The gradient of the dye in the chamber halfway through the switching. C) Gradient after the direction has been switched (after 10 minutes). D) Plot of the gradient profile shown in A E) Plot of the gradient profile shown in C.

Another interesting observation that we note is the existence of multinucleated cells. As the cells get very long in the chamber we hypothesized that is a possibility of the cells developing more than one nucleus. To check for the multi nucleated cell in the chamber, we used the Ste12-GFP strain. Ste12 is a transcription factor that is an excellent nuclear marker. (See figure 8). Though the results are preliminary and more experiments need to be done it is quite amazing to be able to see that yeast cells can be made to make multiple nucleus.

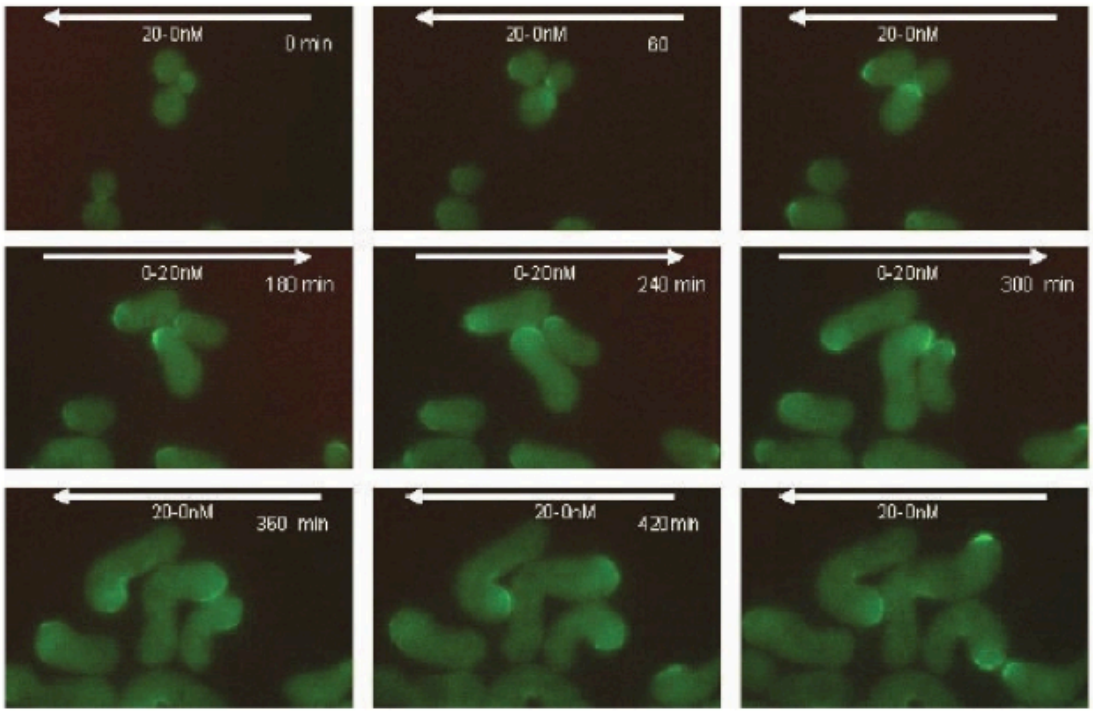

Figure 5.5: Fluorescence images of cells expressing a leading edge marker for polarization, Bem1-GFP (shown in green), to show cells tracking the gradient. The white arrows indicate the direction of the gradient.

5.5.2 Mechanisms for Tracking Gradient

We use the microfluidic device discussed above to quantify the different mechanisms for changing directions response in yeast to periodically switching gradients. Our investigations reveal three distinct mechanisms by which yeast can reorient their direction of polarization and growth: movement of the polar cap, directed growth and bipolar growth. The ability to vary the frequency with which the gradient direction is switched allows us to probe the time scales associated with all three processes. During the initial phase of chemotrophic growth (0-20

min), the polar cap is highly mobile and the direction of polarization can change without the need for cell growth. If the gradient is switched after the cells have polarized, but before they commit to elongation, we find that the polar cap changes directions by moving around

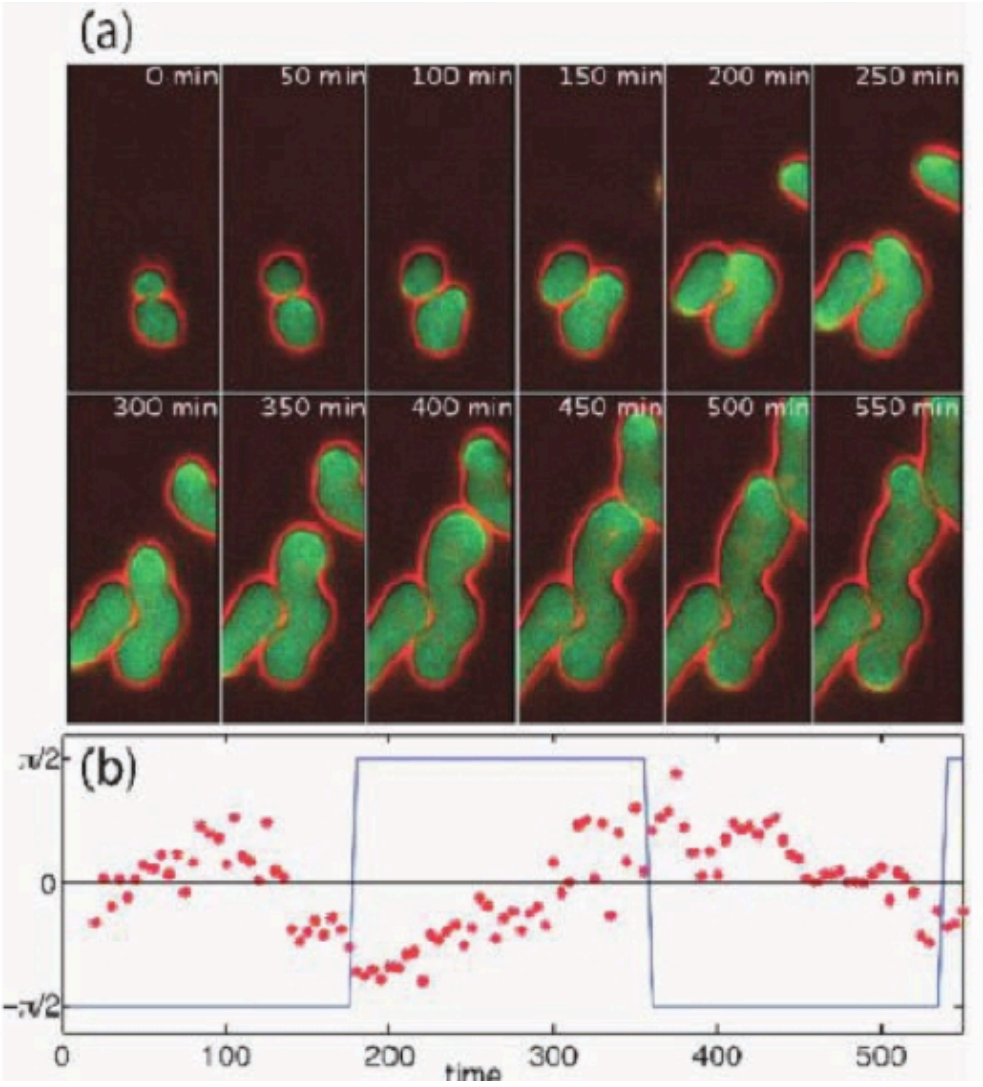

Figure 5.6: Tracking individual cells. a) Fluorescence measurements of Bem1-GFP for a cell snaking under the exposure to a switching gradient with a 3 hour period. The gradient switches horizontally from left to right. b) A time series for the angle of polarization. An angle of $\pi/2$ corresponds to a gradient pointing to the left.

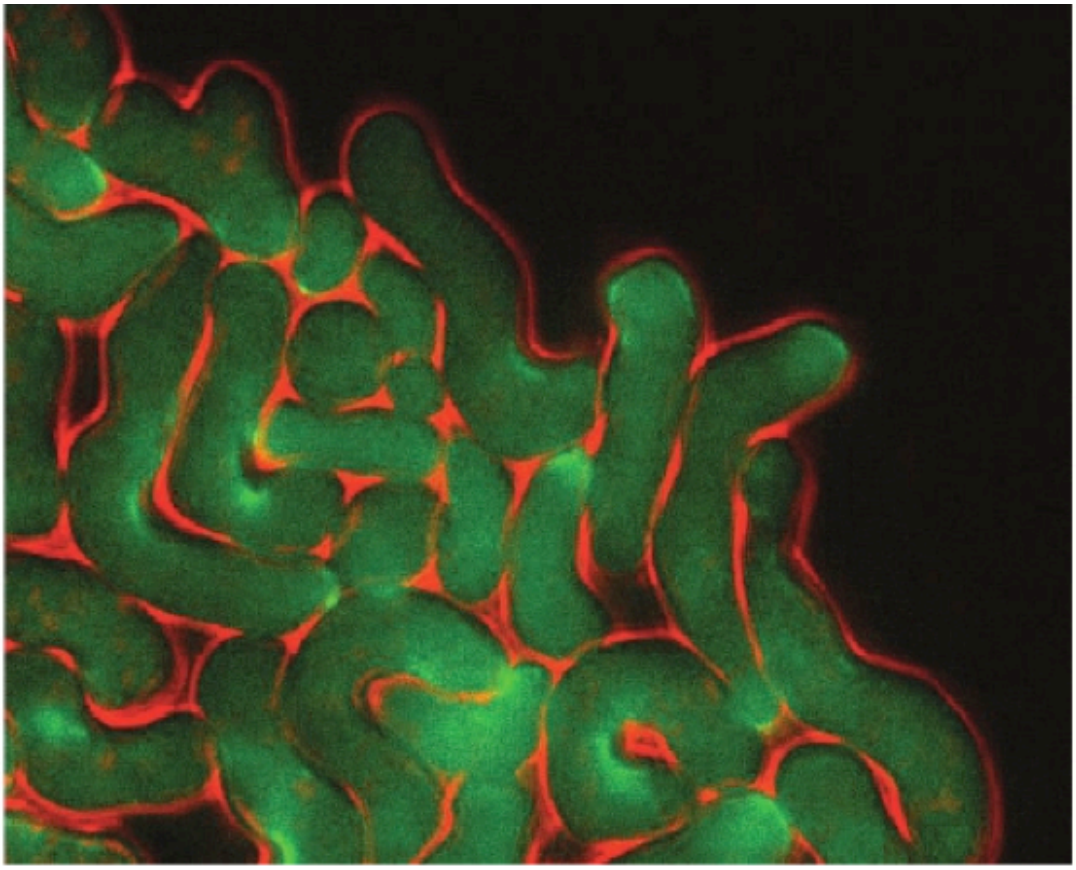

Figure 5.7: Curvature Effect Bem1 fluorescence in green accumulates at the region of high curvature.

the cell membrane (see Figure 9). This highly mobile state appears to be similar to that seen in earlier works (Ozbudak et al., 2005). At intermediate times (2 hrs), the polar cap is less mobile and new cell growth is required to change the direction of the leading edge (see Figure 10). At long times, highly elongated cells can form a second site of polarization distal to the leading edge. In this case, transient bipolar growth is observed until the initial site of polarization is lost.

A minority of highly elongated cells exhibit this form of polarization switching. These cells nucleate a second site of polarization distal to the growing end. Transient bimodal growth is then observed until the initial site of polarization is traded for the newer site (see Figure10). We hypothesize polarization switching is related to the tendency for long yeast cells in homogenous pheromone to spontaneously switch from unimodal to bimodal growth via a reduction in interaction between distal ends

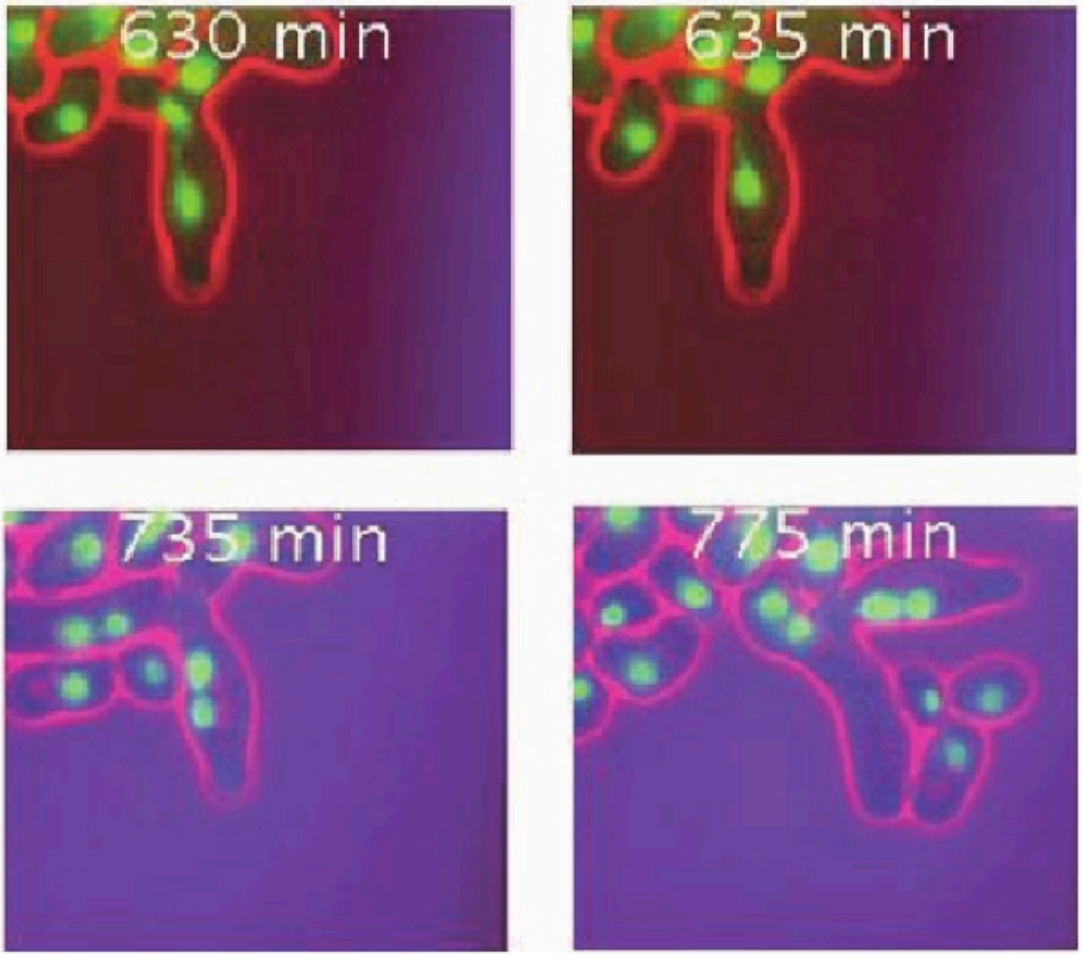

Figure 5.8: Multi nucleated yeast cells in the gradient chamber. Ste12-GFP fluorescence is shown in green.

of a long cell. These results suggest the different mechanisms that yeast use to navigate a changing environment.

5.5.3 Characterization of the frequency response of yeast to periodically switching gradients

Our ability to precisely modulate the spatiotemporal properties of the external pheromone gradient provides us with an important tool for investigating the mechanisms that underlie yeast's navigation system.

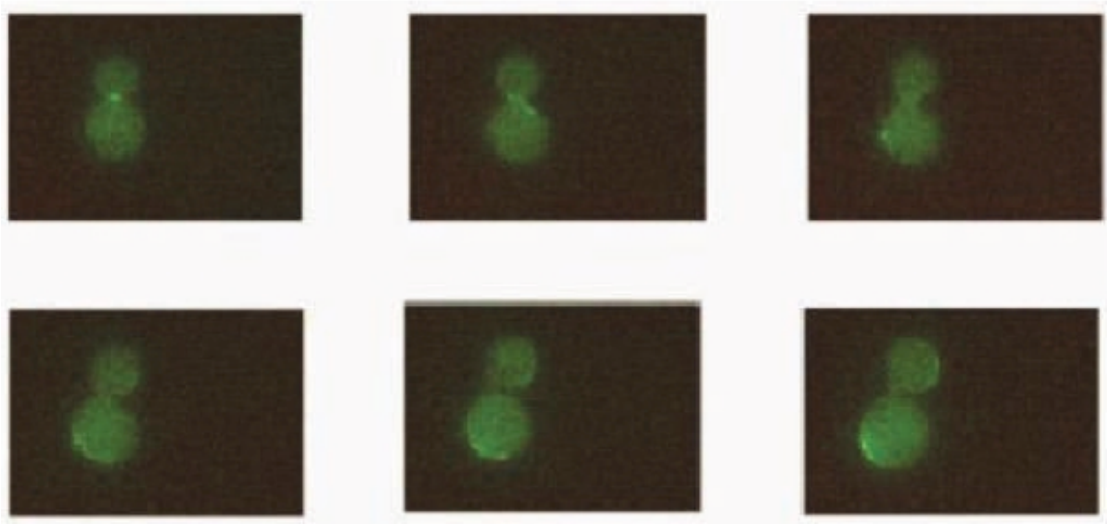

Figure 5.9: Continuous patch movement exhibited by cells as a mode of polarization switching at early time scales. (The time between frames is 5 minutes).

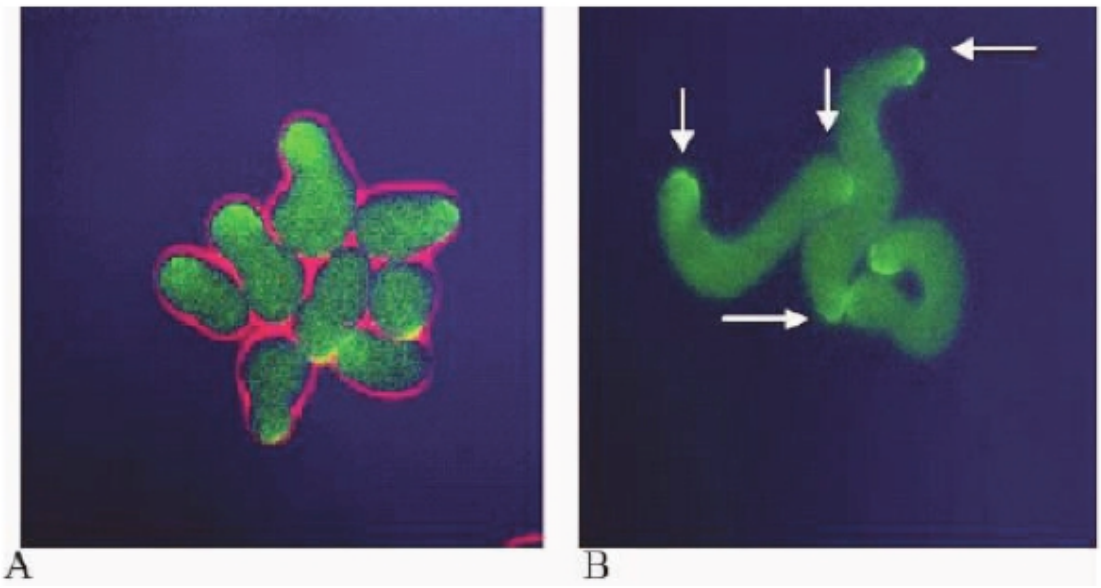

Figure 5.10: Illustrates the mechanisms of reorientation (2 hour switching frequency) A) reorientation by new cell growth at intermediate time scales B) At longer time scales transient bipolar growth is observed until the initial site of polarization is lost.

By switching the direction of the gradient at varying frequencies, we probed the time scales associated with polarization and gradient sensing. We repeated the experiments in periodically modulated gradients. We measured the direction of the angle of polarization as a function of time for various switching frequencies. These time series were used to compute the frequency response of the gradient sensing system. In Figures 11, 12 and 13, we plot the average cell polarization direction for a maximum of about 20 cells for the switching times (half the drive period) 60 minutes, 120 minutes and 180 minutes, respectively. These time series data were generated by manually tracking the cells and giving them a direction of either left right, up or down as discussed above in the method section.

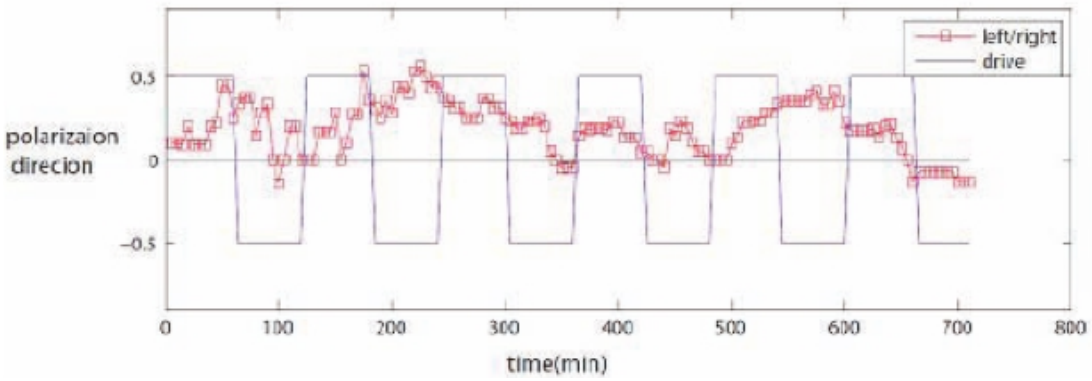

Figure 5.11: Quantification of the frequency response for multiple cells at a switching frequency of 1hour. The red squares are the average direction of polarization and the blue lines are the direction of the gradient. An angle of $\pi/2$ corresponds to gradient from left to right. The x axis has a.u.

An interesting feature in our results is that cells continue in a given direction for some time after a switch of the gradient, sometimes suddenly changing their polarization direction. We also observe from the plots that the population response noticeably lags behind the direction of applied pheromone gradient (red). The sample trajectories of individual cells (see figure 6 and 14) are also seen to respond in a delayed fashion to external signal. We do not at present attempt to explain this delay. Though it is clear that cell response is heterogeneous across the population, significant polarization adjustment is observed at both the single cell and population level.

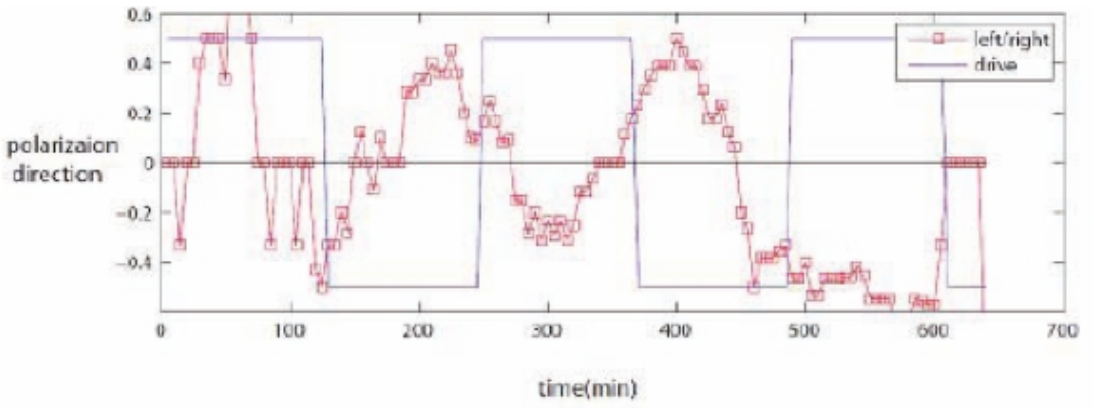

Figure 5.12: Quantification of the frequency response for multiple cells at a switching frequency of 2 hour. The red squares are the average direction of polarization and the blue lines are the direction of the gradient. An angle of π/2 corresponds to gradient from left to right.

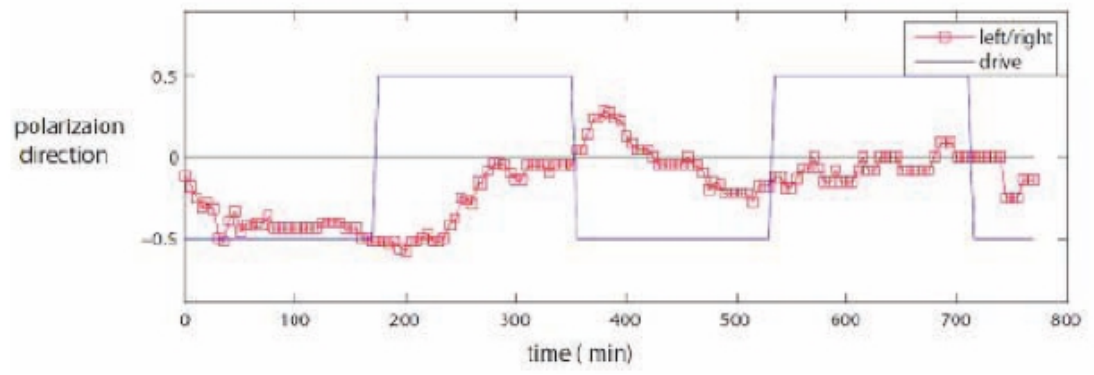

Figure 5.13: Quantification of the frequency response for multiple cells at a switching frequency of 3 hour. The red squares are the average direction of polarization and the blue lines are the direction of the gradient. An angle of π/2 corresponds to gradient from left to right.

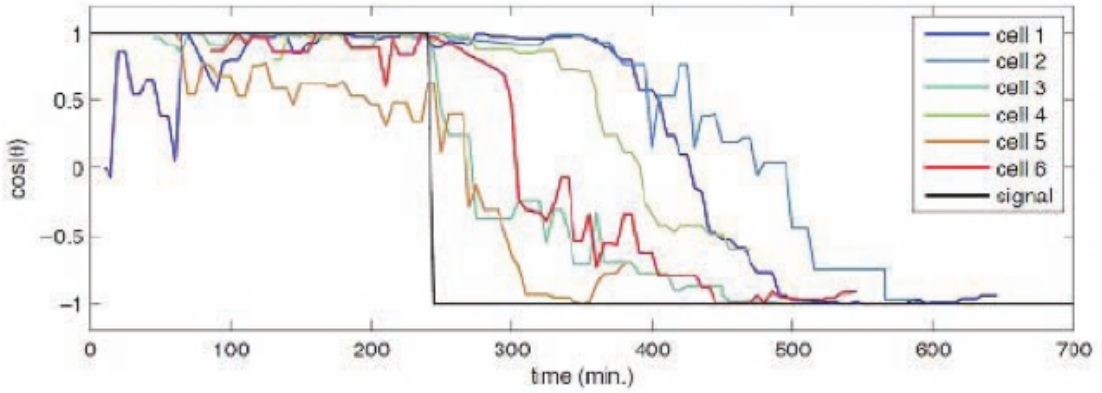

Figure 5.14: Individual trajectories of the cells subjected to a single switch frequency of 240 minutes. The vertical axis is the cosine of the angle of polarization.

5.6 Summary

Our novel microfluidic device enables us to precisely modulate the direction of the pheromone gradient. This technology provides us with an avenue to investigate important characteristics of cell polarization dynamics. Our investigation of polarization adaptation in yeast has revealed mechanisms that may be important for increasing mating efficiency in a dynamic environment.

Fluctuating ambient fluid flow and motion of cells can fool cells to polarize in an initially incorrect direction. Reorientation of the cell polarization can correct for such mistakes. Understanding such modes of cell adaptation could place important constraints on the systems-level mechanisms responsible for yeast polarization. This knowledge is critical for progress toward an ultimate understanding of the fundamental molecular mechanisms that cells use to respond to changing environmental conditions.

5.7 Acknowledgements

The text of this chapter is a preprint of Mather, W*., Nayak, S*., Henrik Dohlman., Beverly Errede., Jeff Hasty., Tim Elston. (2010): Developmental switching in a spatially changing environment.

Chapter 6.

Summary

Powerful tools like microfluidics persist to display immense potential in mimicking in vivo-like microenvironments for investigating various cellular processes. Through their capabilities to dynamically control the cellular growth environment and provide the cells with dynamic external stimuli microfluidic technology supports real-time and long-term measurements. Here, we have presented several studies intended to probe the dynamic behavior of the model organism *Saccharomyces cerevisiae.* Together, these studies highlight the importance of studying the dynamics of biological systems using methods that allow the tracking of long-term behavior in single cells. The ability to take high-resolution data over long time periods for comparison with computational modeling allows us to elucidate novel properties of biological systems.

In chapter 2, we demonstrated the use of our gradient device to study the differentiation switch induced by spatial gradients of the concentration of a single stimulus. (Hao, N., Nayak, S., Behar, M., Shanks, R.H., Nagiec, M.J., Errede, B., Hasty, J., Elston, T.C., and Dohlman, H.G., 2008). Yeast cells exposed to a high dose of pheromone undergo cell division arrest, but continue to expand in a polarized manner (shmoo morphology). Cells exposed to an intermediate dose become elongated, grow slowly, and divide in the direction of a pheromone gradient (chemotropic-growth). Either of the pheromone-responsive MAP kinases, Kss1 and Fus3, promotes cell elongation. However Fus3 alone promotes cell elongation towards a gradient. Whereas Kss1 is activated rapidly and with a graded dose-response profile, Fus3 is activated slowly and exhibits a steeper dose-response relationship (ultra sensitivity). Fus3 activity requires the scaffold protein Ste5; when binding to Ste5 is abrogated Fus3 behaves like Kss1 and the cells no longer respond to a gradient. We conclude that Ste5 slows the rate of Fus3 MAP kinase activation, increases pathway ultra sensitivity, and promotes chemotropic growth. These events may ensure that cells undergo growth arrest only when sufficiently close to a potential mating partner.

In chapter 3, we studied the chemotropic growth using our gradient chamber using the Bar1 delete strain. (Jin,M., Behar, M., Nayak, S., Mather, W., Hasty,J., Errede, B., Dohlman, H.G., Elston, T.C., (2010)). Experiments performed in our gradient chamber revealed that a-cells tend to avoid each other when performing chemotropic growth. We reasoned that the mechanism underlying this self avoidance might involve the protease Bar1. Our hypothesis is that Bar1

depletes pheromone in the extra-cellular environment and alters the direction of the local pheromone concentration in such a way that the gradient is directed away from a-cells. We used our model for chemotropic growth to test this idea. Consistent with our hypothesis, simulations revealed that Bar1 tended to modify the pheromone concentration as cells elongated so that the local gradient was always pointed away from a-cells. The computer simulations reproduced the qualitative behavior of real cells observed in the gradient chamber.

In Chapter 4, we monitored the response of *S. cerevisiae* metabolic gene regulation to periodic changes in the external carbon source by utilizing a microfluidic platform that allows precise, dynamic control over environmental conditions (Bennett*, Pang*, Ostroff, Baumgartner, Nayak, Tsimring, and Hasty, 2008, *equal contribution). We found that the metabolic system acts as a low-pass filter that reliably responds to a slowly changing environment, while effectively ignoring fluctuations that are too fast for the cell to mount an efficient response. We used computational modeling along with experimental data to determine how frequency selection in the system is controlled by the interaction of coupled regulatory networks governing the signal transduction of alternative carbon sources. Experimental verification of model predictions led to the discovery of two novel properties of the regulatory network. First, we revealed a pre- viously unknown mechanism for post-transcriptional control by demonstrating that two key transcripts are degraded at a rate that depends on the carbon source. Our results suggest that while certain characteristics of the complex networks may differ when

probed in a static environment, the system has been optimized for a robust response to a dynamically changing environment.

In chapter 5 we analyze yeast's ability to cope with dynamic pheromone gradients. We developed a novel microfluidic device that allows us to temporally modulate spatial gradients of an external stimulus. (Mather, W*, Nayak, S*, Henrik Dohlman, Beverly Errede, Jeff Hasty, Tim Elston., 2010 *equal contribution). We use the device to probe the mechanisms of polarization and gradient sensing that underlie yeast chemotrophic growth. Our investigations reveal three distinct mechanisms by which yeast can reorient their direction of polarization and growth: movement of the polar cap, directed growth and bipolar growth. The ability to vary the frequency with which the gradient direction is switched allows us here to investigate all the time scales associated with all three processes.

Referances

D. M. Thompson, K. R. King, K. J. Wieder, M. Toner, M. L. Yarmush, and A. Jayaraman. Dynamic gene expression profiling using a microfabricated living cell array. Analytical Chemistry, 76(14):4098-4103, (2004).

F. K. Balagadde, L. You, C. L. Hansen, F. H. Arnold, and S. R. Quake. Long- term monitoring of bacteria undergoing programmed population control in a microchemo-stat. Science, 309(5731):137-40, (2005).

F. K. Balagadde, L. C. You, F. H. Arnold, and S. R. Quake. Programmed population control by cell-cell communication in microfluidic chemostats. Biophysical Journal, 88(1):519a-519a, (2005).

B. Banerjee, S. Balasubramanian, G. Ananthakrishna, T. V. Ramakrishnan, and G. V. Shivashankar. Tracking operator state fluctuations in gene expression in single cells. Biophysical Journal, 86(5):3052-3059, (2004).

Cookson, S.*, Ostroff, N.*, Pang, W. L.*, Volfson, D., and Hasty, J., Monitoringdynamics of single-cell gene expression over multiple cell cycles. Mol. Syst. Biol., 1, msb4100032-E1-6.(*equal contribution). (2005).

Dertinger, S. K. W., Chiu, D. T., Jeon, N. L., and Whitesides, G. M., 2001: Generation of gradients having complex shapes using microfluidic networks. Anal. Chem., 73(6),1240 6

Duffy, D. C., Schueller, O. J. A., Brittain, S. T., and Whitesides, G. M., 1999: Rapid prototyping of microfluidic switches in poly(dimethyl siloxane) and their actuation by electro-osmotic flow. J. Micromech. Microeng., 9(3), 211-7.

Frazoqui, J.E., A.S. Gladfelter, andD.J. Lew. 2003. Scaffold-mediated symmetry breaking by Cdc42p. Nat Cell Biol 5(12):1062-1070

Groisman, A., Enzelberger, M., and Quake, S. R., 2003: Microfluidic memory and control devices. Science, 300(5621), 955-8.

Groisman, A., Lobo, C., Cho, H., Campbell, J. K., Dufour, Y. S., Stevens, A. M., and Levchenko, A., 2005: A microfluidic chemostat for experiments with bacterial and yeast cells. Nat. Methods, 2(9), 685-9.

Hansen, C., and Quake, S. R., 2003: Microfluidics in structural biology: smaller, faster. . . better. Curr. Opin. Struct. Biol.,13(5), 538-44.

Huh, D., Gu, W., Kamotani, Y., Grotberg, J. B., and Takayama, S., 2005: Microfluidicsfor flow cytometric analysis of cells and particles. Physiol. Meas., 26(3), R73-98.

Wu, Z. Y., Xanthopoulos, N., Reymond, F., Rossier, J. S., and Girault, H. H., 2002: Polymer microchips bonded by O2-plasma activation. Electrophoresis, 23(5), 782-90.

M. Y. Ye, Q. Fang, X. F. Yin, and Z. L. Fang. Studies on bonding techniques for poly (dimethylsiloxane) microfluidic chips. Chemical Journal of Chinese Universities-Chinese, 23(12):2243-2246, (2002).

Jackson, C.L., and L.H. Hartwell. 1990. Courtship in S. cerevisiae: both cell types choose mating partners by responding to the strongest pheromone signal. Cell 63(5):1039-1051.

Otsuji, M., S. Ishihara, C. Co, K. Kaibuchi, A. Mochizuki, and S. Kuroda. 2007. A mass conserved reaction-diffusion system captures properties of cell polarity. PLoS Comput Biol 3(6):e108.

Chiu, D. T., Jeon, N. L., Huang, S., Kane, R. S., Wargo, C. J., Choi, I. S., Ingber, D. E., and Whitesides, G. M., 2000: Patterned deposition of cells and proteins onto surfaces by using three-dimensional microfluidic systems. Proc. Natl. Acad. Sci. U. S. A., 97(6), 2408-13.

Yang, L., A.M. Zhabotinsky, andI.R. Epstein. 2004. Stable squares and other oscillatory turing patterns in a reaction-diffusion model. Phys Rev Lett 92(19):198303.

Segall, J.E. 1993. Polarization of yeast cells in spatial gradients of alpha mating factor. Proc Natl Acad Sci U S A 90(18):8332-8336.

Poritz et al., 2001 M.A. Poritz, S. Malmstrom, M.K. Kim, P.J. Rossmeissl and A. Kamb, Graded mode of transcriptional induction in yeast pheromone signalling revealed by single-cell analysis, Yeast 18 (2001), pp. 1331-1338.

J.E.J. Ferrell and E.M. Machleder, The biochemical basis of an all-or-none cell fate switch in Xenopus oocytes, Science 280 (1998), pp. 895-898.

Dohlman HG, Thorner JW: Regulation of G protein-initiated signal transduction in yeast: paradigms and principles. Annu Rev Biochem 2001, 70:703-754.

Erdman S, Snyder M: A filamentous growth response mediated by the yeast mating pathway. Genetics 2001, 159:919-928.

Devreotes PN, Zigmond SH: Chemotaxis in eukaryotic cells: a focus on leukocytes and Dictyostelium. Annu Rev Cell Biol 1988, 4:649-686.

Servant G, Weiner OD, Herzmark P, Balla T, Sedat JW, Bourne HR: Polarization of chemoattractant receptor signaling during neutrophil chemotaxis. Science 2000, 287:1037-1040.

Srinivasan S, Wang F, Glavas S, Ott A, Hofmann F, Aktories K, Kalman D, Bourne HR: Rac and Cdc42 play distinct roles in regulating PI(3,4,5)P3 and polarity during neutrophil chemotaxis. J Cell Biol 2003, 160:375-385.

Weiner OD, Neilsen PO, Prestwich GD, Kirschner MW, Cantley LC, Bourne HR: A PtdInsP(3)- and Rho GTPase-mediated positive feedback loop regulates neutrophil polarity. Nat Cell Biol , 4:509-513. (2002).

Hao N, Nayak S, Behar M, Shanks RH, Nagiec MJ, Errede B, Hasty J, Elston TC, Dohlman HG: Regulation of cell signaling dynamics by the protein kinase-scaffold Ste5. Mol Cell , 30:649-656. (2008).

Ciejek E, Thorner J: Recovery of *S. cerevisiae* a cells from G1 arrest by alpha factor pheromone requires endopeptidase action. Cell , 18:623-635. (1979).

MacKay VL, Armstrong J, Yip C, Welch S, Walker K, Osborn S, Sheppard P, Forstrom J: Characterization of the Bar proteinase, an extracellular enzyme from the yeast *Saccharomyces cerevisiae.* Adv Exp Med Biol , 306:161-172, (1991).

Schneider IC, Haugh JM: Quantitative elucidation of a distinct spatial gradient-sensing mechanism in fibroblasts. J Cell Biol , 171:883-892. (2005).

Shimada Y, Gulli MP, Peter M: Nuclear sequestration of the exchange factor Cdc24 by Far1 regulates cell polarity during yeast mating. Nat Cell Biol , 2:117- 124. (2000).

Nern A, Arkowitz RA: G proteins mediate changes in cell shape by stabilizing the axis of polarity. Mol Cell, 5:853-864, (2000).

Alby, K., D. Schaefer, andR.J. Bennett. Homothallic and heterothallic mating in the opportunistic pathogen Candida albicans. Nature 460 (7257):890-893. (2009).

Wedlich-Soldner R, Altschuler S, Wu L, Li R: Spontaneous cell polarization through actomyosin-based delivery of the Cdc42 GTPase. Science , 299:1231-1235. (2003).

Sohrmann M, Peter M: Polarizing without a clue. Trends in Cell Biol , 13:526-533. (2003).

Andersson, D.M. Simpson, M. Qi, Y. Wang and E.A. Elion, Differential input by Ste5 scaffold and Msg5 phosphatase route a MAPK cascade to multiple outcomes, EMBO J. 23, pp. 2564-2576. (2004).

Howell, A.S., N.S. Savage, S.A. Johnson, I. Bose, A.W. Wagner, T.R. Zyla, H.F. Nijhout, M.C. Reed, A.B. Goryachev, andD.J. Lew. Singularity in polarization: rewiring yeast cells to make two buds. Cell 139(4):731-743. (2009).

A. Gartner, K. Nasmyth and G. Ammerer, Signal transduction in *Saccharomyces cerevisiae* requires tyrosine and threonine phosphorylation of FUS3 and KSS1, Genes Dev. 6, pp. 1280-1292. (1992)

A. Goldbeter and D.E. Koshland Jr., An amplified sensitivity arising from covalent modification in biological systems, Proc. Natl. Acad. Sci. USA 78 , pp. 6840-6844. (1981).

D.E. Koshland Jr., A. Goldbeter and J.B. Stock, Amplification and adaptation in regulatory and sensory systems, Science 217 (1982),pp. 220-225.

A.B. Kusari, D.M. Molina, W. Sabbagh Jr., C.S. Lau and L. Bardwell, A conserved protein interaction network involving the yeast MAP kinases Fus3 and Kss1, J. Cell Biol. 164, pp. 267-277. (2004).

H. Liu, C.A. Styles and G.R. Fink, Elements of the yeast pheromone response pathway required for filamentous growth of diploids, Science 262, pp. 1741-1744. (1993).

K. Madden and M. Snyder, Specification of sites for polarized growth in *Saccharomyces cerevisiae* and the influence of external factors on site selection, Mol. Biol. Cell 3, pp. 1025-1035. (1992).

Frazoqui, J.E., A.S. Gladfelter, andD.J. Lew. Scaffold-mediated symmetry breaking by Cdc42p. Nat Cell Biol 5(12):1062-1070. (2003).

R.P. Bhattacharyya, A. Remenyi, M.C. Good, C.J. Bashor, A.M. Falick and W.A. Lim, The Ste5 scaffold allosterically modulates signaling output of the yeast mating pathway, Science 311, pp. 822-826. (2006).

S. Erdman and M. Snyder, A filamentous growth response mediated by the yeast mating pathway, Genetics 159, pp. 919-928. (2001).

A. Breitkreutz, L. Boucher and M. Tyers, MAPK specificity in yeast pheromone response independent of transcriptional activation, Curr. Biol. 11, pp. 1266- 1271. (2001).

K.Y. Choi, B. Satterberg, D.M. Lyons and E.A. Elion, Ste5 tethers multiple protein kinases in the MAP kinase cascade required for mating in S. cerevisiae, Cell 78, pp. 499-512. (1994).

J.G. Cook, L. Bardwell and J. Thorner, Inhibitory and activating functions for MAPK Kss1 in the *S. cerevisiae* filamentous-growth signalling pathway, Nature 390 pp. 85-88. (1997).

R. Dorer, P.M. Pryciak and L.H. Hartwell, *Saccharomyces cerevisiae* cells execute a default pathway to select a mate in the absence of pheromone gradients, J. Cell Biol. 131, pp. 845-861. (1995).

J.E.J. Ferrell and E.M. Machleder, The biochemical basis of an all-or-none cell fate switch in Xenopus oocytes, Science 280, pp. 895-898. (1998).

L.J. Flatauer, S.F. Zadeh and L. Bardwell, Mitogen-activated protein kinases with distinct requirements for Ste5 scaffolding influence signaling specificity in *Saccharomyces cerevisiae*, Mol. Cell. Biol. 25, pp. 1793-1803, (2005).

H.D. Madhani and G.R. Fink, Combinatorial control required for the specificity of yeast MAPK signaling, Science 275, pp. 1314-1317 (1997).

C.I. Maeder, M.A. Hink, A. Kinkhabwala, R. Mayr, P.I. Bastiaens and M. Knop, Spatial regulation of Fus3 MAP kinase activity through a reaction-diffusion mechanism in yeast pheromone signalling, Nat. Cell Biol. 9 ,pp. 1319-1326 (2007).

Wedlich-Soldner, R., S. Altschuler, L. Wu, andR. Li. Spontaneous cell polarization through actomyosin-based delivery of the Cdc42 GTPase. Science 299 (5610), (2003).

C.J. Marshall, Specificity of receptor tyrosine kinase signaling: transient versus sustained extracellular signal-regulated kinase activation, Cell 80, pp. 179-185 (1995).

A. Nern and R.A. Arkowitz, A GTP-exchange factor required for cell orientation, Nature 391, pp. 195-198. (1998).

S. Paliwal, P.A. Iglesias, K. Campbell, Z. Hilioti, A. Groisman and A. Levchenko, MAPK-mediated bimodal gene expression and adaptive gradient sensing in yeast, Na-
ture 446, pp. 46-51 (2007).

J.A. Printen and G.F. Sprague Jr., Protein-protein interactions in yeast pheromone response pathway: Ste5p interacts with all members of the MAP kinase cascade, Genetics 138, pp. 609-619. (1994).

M.A. Poritz, S. Malmstrom, M.K. Kim, P.J. Rossmeissl and A. Kamb, Gradedmode of transcriptional induction in yeast pheromone signalling revealed by single-cell analysis, Yeast 18 , pp.1331-1338. (2001).

R.L. Roberts and G.R. Fink, Elements of a single MAP kinase cascade in *Saccharomyces cerevisiae* mediate two developmental programs in the same cell type: mating and invasive growth, Genes Dev. 8 pp. 2974-2985 (1994).

C.J. Roberts, B. Nelson, M.J. Marton, R. Stoughton, M.R. Meyer, H.A. Bennett, Y.D. He, H. Dai, W.L. Walker and T.R. Hughes et al., Signaling and circuitry of multiple MAPK pathways revealed by a matrix of global gene expression profiles, Science 287 pp. 873-880, (2000).

W. Sabbagh Jr., L.J. Flatauer, A.J. Bardwell and L. Bardwell, Specificity of MAP kinase signaling in yeast differentiation involves transient versus sustained MAPK activation, Mol. Cell 8 (2001), pp. 683-691

Beadle, G. W. & Tatum, E. L. Genetic control of biochemical reactions in Neurospora. Proc. Natl Acad. Sci. USA 27, 499-506 (1941).

Jacob, F. & Monod, J. Genetic regulatory mechanisms in the synthesis of proteins. J. Mol. Biol. 3, 318-356, (1961).

S.C. Strickfaden and P.M. Pryciak, Distinct roles for two Galpha-Gbeta interfaces in cell polarity control by a yeast heterotrimeric G protein, Mol. Biol. Cell 19, pp. 181-197 (2007).

N. Valtz, M. Peter and I. Herskowitz, FAR1 is required for oriented polarization of yeast cells in response to mating pheromones, J. Cell Biol. 131 pp. 863-873. (1995).

Y. Wang and H.G. Dohlman, Pheromone signaling mechanisms in yeast: a prototypical sex machine, Science 306 pp. 1508-1509. (2004).

Burchett, S., Scott, A., Errede, B., and Dohlman, H. G. Identification of novel pheromone-response regulators through systematic overexpression of 120 protein kinases in yeast. J Biol Chem 276, 26472-26478. (2001).

Paliwal, S., Iglesias, P. A., Campbell, K., Hilioti, Z., Groisman, A., and Levchenko, A. MAPK-mediated bimodal gene expression and adaptive gradient sensing in yeast. Nature 446, 46-51. (2007).

Shimada, Y., P. Wiget, M.P. Gulli, E. Bi, andM. Peter. The nucleotide exchange factor Cdc24p may be regulated by auto-inhibition. Embo J 23(5):1051-1062. (2004).

Sudhaharan, T., P. Liu, Y.H. Foo, W. Bu, K.B. Lim, T. Wohland, andS. Ahmed. Determination of in vivo dissociation constant, KD, of Cdc42-effector complexes in live mammalian cells using single wavelength fluorescence cross-correlation spectroscopy. J Biol Chem 284(20):13602-13609. (2009).

Turing, A.M. 1952. The chemical basis of morphogenesis. Philosophical Transactions of the Royal Society of London. B 237:37-72.

Tyson, J.J., K.C. Chen, andB. Novak. Sniffers, buzzers, toggles and blinkers: dynamics of regulatory and signaling pathways in the cell. Curr Opinion Cell Biol 15(2):221-231 (2003).

Vanag, V.K., L. Yang, M. Dolnik, A.M. Zhabotinsky, andI.R. Epstein. Oscillatory cluster patterns in a homogeneous chemical system with global feedback. Nature 406(6794):389-391. (2000).

Yu, S.R., M. Burkhardt, M. Nowak, J. Ries, Z. Petrasek, S. Scholpp, P. Schwille, and M. Brand. Fgf8 morphogen gradient forms by a source-sink mechanism with freely diffusing molecules. Nature 461(7263):533-536 (2009).

Douglas, H. C. & Hawthorne, D. C. Regulation of genes controlling synthesis of the galactose pathway enzymes in yeast. Genetics 54, 911-916 (1966).

Thattai, M. & Shraiman, B. I. Metabolic switching in the sugar phosphotrans ferase system of Escherichia coli. Biophys. J. 85, 744-754 (2003).

Lipan, O. & Wong, W. H. The use of oscillatory signals in the study of genetic networks. Proc. Natl Acad. Sci. USA 102, 7063-7068 (2005).

Kussell, E.& Leibler, S. Phenotypic diversity, population growth, and information in fluctuating environments. Science 309, 2075-2078 (2005).

Kruse, K. & Julicher, F. Oscillations in cell biology. Curr. Opin. Cell Biol. 17, 20-26 (2005).

Ronen, M. & Botstein, D. Transcriptional response of steady-state yeast cultures to transient perturbations in carbon source. Proc. Natl Acad. Sci. USA 103, 389-394 (2006).

Thattai, M. & van Oudenaarden, A. Stochastic gene expression in fluctuating environments. Genetics 167, 523-530 (2004).

Sheff, M. A. & Thorn, K. S. Optimized cassettes for fluorescent protein tagging in *Saccharomyces cerevisiae.* Yeast 21, 661-670 (2004).

Raser, J. M. & O'Shea, E. K. Control of stochasticity in eukaryotic gene expresion.Science 304, 1811-1814 (2004).

Kussell, E.& Leibler, S. Phenotypic diversity, population growth, and information in fluctuating environments. Science 309, 2075-2078 (2005).

Kruse, K. & Julicher, F. Oscillations in cell biology. Curr. Opin. Cell Biol. 17, 20-26 (2005).

Ronen, M. & Botstein, D. Transcriptional response of steady-state yeast cultures to transient perturbations in carbon source. Proc. Natl Acad. Sci. USA 103, 389-394 (2006).

Thattai, M. & van Oudenaarden, A. Stochastic gene expression in fluctuating environments. Genetics 167, 523-530 (2004).

Hasty, J., McMillen, D., Isaacs, F. & Collins, J. J. Computational studies of gene regulatory networks: in numero molecular biology. Nature Rev. Genet. 2, 268-279 (2001).

Savageau, M. A. Comparison of classical and autogenous systems of regulation in inducible operons. Nature 252, 546-549 (1974).

Atauri, P., Orrell, D., Ramsey, S. & Bolouri, H. Evolution of 'design' principles in biochemical networks. Syst. Biol. 1, 28-40 (2004).

Demir, O. & Kurnaz, I. A. An integrated model of glucose / galactose metabolism regulated by the GAL genetic switch. Comput. Biol. Chem. 30, 179-192 (2006).

Kaniak, A., Xue, Z., Macool, D., Kim, J. & Johnston, M. Regulatory network connecting two glucose signal transduction pathways *in Saccharomyces cerevisiae.* Eukaryotic Cell 3, 221-231 (2004).

Whitesides, G. M., Ostuni, E., Takayama, S., Jiang, X. Y. & Ingber, D. E. Soft lithography in biology and biochemistry. Annu. Rev. Biomed. Eng. 3, 335-373 (2001).

Whitesides, G. M. et al. Soft lithography and bioanalysis. Abstr. Pap. Am. Chem. Soc. 227, U113-U113 (2004).

Xia, Y. & Whitesides, G. M. Soft lithography. Angew. Chem. Int. Edn Engl. 7, 550-575

Sheff, M. A. & Thorn, K. S. Optimized cassettes for fluorescent protein tagging in *Saccharomyces cerevisiae*. Yeast 21, 661-670 (2004).

Raser, J. M. & O'Shea, E. K. Control of stochasticity in eukaryotic gene expression.Science 304, 1811-1814 (2004).

Jackson, C.L., and L.H. Hartwell. Courtship in *S. cerevisiae*: both cell types choose mating partners by responding to the strongest pheromone signal. Cell (1990).

Howell, A.S., N.S. Savage, S.A. Johnson, I. Bose, A.W. Wagner, T.R. Zyla, H.F. Nijhout, M.C. Reed, A.B. Goryachev, andD.J. Lew. Singularity in polarization: rewiring yeast cells to make two buds. Cell 139(4):731-743 (2009)

Verma, M., Bhat, O. J. & Venkatesh, K. V. Steady-state analysis of glucose repression reveals hierarchical expression of proteins under Mig1p control in *Saccharomyces cerevisiae.* Biochem. J. 388, 843-849 (2005).

Scheffler, I. E., de la Cruz, B. J. & Preito, S. Control of mRNA turnover as a mechanism of glucose repression in *Saccharomyces cerevisiae.* Biochem. Cell Biol. 30, 1175-1193 (1998).

De la Cruz, B. J., Prieto, S. & Scheffler, I. E. The role of the 59 untranslated region (UTR) in glucose-dependent mRNA decay. Yeast 19, 887-902 (2002).

Andrade, R. P., Kotter, P., Entian, K. D. & Casal, M. Multiple transcripts regulate glucose-triggered mRNA decay of the lactate transporter JEN1 from *Saccharomyces cerevisiae.* Biochem. Biophys. Res. Commun. 332, 254-262 (2005).

Rohde, J. R., Trinh, J. & Sadowski, I. Multiple signals regulate GAL transcription in yeast. Mol. Cell. Biol. 20, 38803886 (2000).

Boles, E. & Hollenberg, C. P. The molecular genetics of hexose transport in yeasts. FEMS Microbiol. Rev. 21, 85-111 (1997).

Mark A She and Kurt S Thorn. Optimized cassettes for fluorescent protein tagging in *Saccharomyces cerevisiae*. Yeast, 21(8):661670, Jun (2004).

David Ross, Michael Gaitan, and Laurie E Locascio. Temperature measurement in microfluidic systems using a temperature-dependent fuorescent dye. Anal. Chem., 73(17):4117-4123, (2001).

S. K. W. Dertinger, D. T. Chiu, N. L. Jeon, and G. M. Whitesides. Generation of gradients having complex shapes using microfluidic networks. Anal. Chem., 73(6):12406, Mar (2001).

N. L. Jeon, S. K. W. Dertinger, D. T. Chiu, I. S. Choi, A. D. Stroock, and G. M. White- sides. Generation of solution and surface gradients using microfuidic systems. Langmuir, 16(22):83116, (2000).

A. D. Stroock, S. K. Dertinger, G. M. Whitesides, and A. Ajdari. Patterning flows using grooved surfaces. Analytical Chemistry, 74(20):53065312, (2002).

G. M. Whitesides, E. Ostuni, S. Takayama, X. Y. Jiang, and D. E. Ingber. Soft lithography in biology and biochemistry. Ann. Rev. Biomed. Eng., 3:335373, (2001).

G. M. Whitesides, J. Jiang, S. Sia, V. Linder, B. Parviz, A. Sigel, and J. Lee. Soft lithography and bioanalysis. Abstr. Paper Am. Chem. Soc., 227:U113U113, (2004).

Y. N. Xia and G. M. Whitesides. Soft lithography. Angew. Chem. Int. Edit., 37(5):55075, Mar (1998).

Endres, R.G., and N.S. Wingreen. Accuracy of direct gradient sensing by cell-surface receptors. Prog Biophys Mol Biol 100 (1-3):33-39. (2009).

Irazoqui, J.E., A.S. Gladfelter, and D.J. Lew. Cdc42p, GTP hydrolysis, and the cell's sense of direction. Cell Cycle 3(7):861-864. (2004).

Alby, K., D. Schaefer, and R.J. Bennett. Homothallic and heterothallic mating in the opportunistic pathogen Candida albicans. Nature 460(7257):890-893. (2009)

Barkai, N., M.D. Rose, and N.S. Wingreen. Protease helps yeast find mating partners. Nature 396(6710):422-423. (1998)

Goryachev, A.B., and A.V. Pokhilko. Dynamics of Cdc42 network embodies a Turing-type mechanism of yeast cell polarity. FEBS Lett 582(10):1437-1443. (2008).

Faty M., Fink, M. & Barral, Y. Curr. Genet. 41 , 123-131.pmid:12111093 (2002) .

Jackson, C.L., and L.H. Hartwell. Courtship in S. cerevisiae: both cell types choose mating partners by responding to the strongest pheromone signal. Cell 63(5):1039-1051. (1990).

Kozubowski, L., K. Saito, J.M. Johnson, A.S. Howell, T.R. Zyla, and D.J. Lew.. Symmetry-breaking polarization driven by a Cdc42p GEF-PAK complex. Curr Biol 18(22):1719-1726. (2008).

Meinhardt, H. Orientation of chemotactic cells and growth cones: models and mechanisms. J Cell Sci 112 (Pt 17):2867-2874. (1999).

Meinhardt, H., and A. Gierer. Applications of a theory of biological pattern formation based on lateral inhibition. J Cell Sci 15(2):321-346. (1974).

Otsuji, M., S. Ishihara, C. Co, K. Kaibuchi, A. Mochizuki, and S. Kuroda. A massconserved reaction-diffusion system captures properties of cell polarity. PLoS Comput Biol 3(6):e108. (2007).

Park, H.O., and E. Bi. Central roles of small GTPases in the development of cell polarity in yeast and beyond. Microbiol Mol Biol Rev 71(1):48-96. (2007).

Abraham D. Stroock, Stephan K. W. Dertinger, Armand Ajdari, Igor Mezic, Howard A. Stone, and George M. Whitesides. Chaotic mixer for microchannels. Science, 295(5555):647651, (2002).

Bennett MR, Pang WL, Ostroff NA, Baumgartner BL, Nayak S, Tsimring LS, Hasty J. Metabolic gene regulation in a dynamically changing environment.Nature. Aug 28; 454(7208):1119-22. (2008).

A. Breitkreutz, L. Boucher and M. Tyers, MAPK specificity in the yeast pheromone response independent of transcriptional activation, Curr. Biol. 11 (2001).

K.Y. Choi, B. Satterberg, D.M. Lyons and E.A. Elion, Ste5 tethers multiple protein kinases in the MAP kinase cascade required for mating in *S. cerevisiae,* Cell 78 (1994).

J.G. Cook, L. Bardwell and J. Thorner, Inhibitory and activating functions for MAPK Kss1 in the *S. cerevisiae* filamentous-growth signaling pathway, Nature 390 (1997).

R. Dorer, P.M. Pryciak and L.H. Hartwell, *Saccharomyces cerevisiae* cells execute a default pathway to select a mate in the absence of pheromone gradients, J. Cell Biol. 131 (1995).

S. Erdman and M. Snyder, A filamentous growth response mediated by the yeast mating pathway, Genetics 159 (2001).

Ferrell and Machleder, 1998 J.E.J. Ferrell and E.M. Machleder, The biochemical basis of an all-or-none cell fate switch in Xenopus oocytes, Science 280 (1998).

Ciejek, E., and J. Thorner. Recovery of *S. cerevisiae* a cells from G1 arrest by alpha factor pheromone requires endopeptidase action. Cell 18(3):623-635. (1979).

De Wit, A., D. Lima, G. Dewel, and P. Borckmans. Spatiotemporal dynamics near a codimension-two point. Phys Rev E Stat Phys Plasmas Fluids Relat Interdiscip Topics 54(1):261-271. (1996).

Hicks, J.B., andI. Herskowitz. 1976. Evidence for a new diffusible element of
mating pheromones in yeast. Nature 260(5548):246-248.

S. Maleri, Q. Ge, E.A. Hackett, Y. Wang, H.G. Dohlman and B. Errede, Persistent activation by constitutive Ste7 promotes Kss1-mediated invasive growth but fails to support Fus3-dependent mating in yeast, Mol. Cell. Biol. 24 (2004),

K. Madden and M. Snyder, Specification of sites for polarized growth in *Saccharomyces cerevisiae* and the influence of external factors on

site selection, Mol. Biol. Cell 3 (1992).

M.A. Poritz, S. Malmstrom, M.K. Kim, P.J. Rossmeissl and A. Kamb, Graded mode of transcriptional induction in yeast pheromone signalling revealed by single-cell analysis, Yeast 18 (2001).

J.A. Printen and G.F. Sprague Jr., Protein-protein interactions in the yeast pheromone response pathway: Ste5p interacts with all members of the MAP kinase cascade, Genetics 138 (1994).

Moseley J.B., Goode B.L., The Yeast Actin Cytoskeleton: from Cellular Function to Biochemical Mechanism. Microbiol. Mol. Biol. Rev. (2006).

Wedlich-Soldner R., Li R. Spontaneous cell polarization: undermining determinism. Nature Cell Biol. 5, 267-270. (2003).

Segall J.E Polarization of yeast cells in spatial gradients of alpha mating factor. PNAS 90, 8332-8336. (1993) .

Squires, T.M., Quake S.R. Microfluidics: fluid physics at the nanoliter scale. Rev. Mod. Phys. 77, 977-1026. (2005).

Iglesias P.A., Levchenko A. Modeling the cell's guidance system. Sci. STKE (2002)

Gierer, A., andH. Meinhardt. A theory of biological pattern formation. Kybernetik 12(1):30-39. (1972).

De Wit, A., D. Lima, G. Dewel, andP. Borckmans. Spatiotemporal dynamics near a codimension-two point. Phys Rev E Stat Phys Plasmas Fluids Relat Interdiscip Topics 54(1):261-271. (1996).

Alby, K., D. Schaefer, andR.J. Bennett. Homothallic and heterothallic mating in the opportunistic pathogen Candida albicans. Nature 460(7257):890-893. (2009).

Endres, R.G., andN.S. Wingreen. Accuracy of direct gradient sensing by cell-surface receptors. Prog Biophys Mol Biol 100(1-3):33-39. (2009).

Goryachev, A.B., andA.V. Pokhilko. Dynamics of Cdc42 network embodies a Turing-type mechanism of yeast cell polarity. FEBS Lett 582(10):1437-1443 (2008).

Gierer, A., andH. Meinhardt. A theory of biological pattern formation. Kybernetik 12(1):30-39. (1972).

Turing, A.M. The chemical basis of morphogenesis. Philosophical Transactions of the Royal Society of London. B 237:37-72. (1952).

Tyson, J.J., K.C. Chen, andB. Novak. Sniffers, buzzers, toggles and blinkers: dynamics of regulatory and signaling pathways in the cell. Curr Opin Cell Biol 15(2):221-231. (2003).

R.L. Roberts and G.R. Fink, Elements of a single MAP kinase cascade in *Saccharomyces cerevisiae* mediate two developmental programs in the same cell type: mating and invasive growth, Genes Dev. 8 (1994).

C.J. Roberts, B. Nelson, M.J. Marton, R. Stoughton, M.R. Meyer, H.A. Bennett, Y.D. He, H. Dai, W.L. Walker and T.R. Hughes et al., Signaling and circuitry of multiple MAPK pathways revealed by a matrix of global gene expression profiles, Science 287 (2000).

W. Sabbagh Jr., L.J. Flatauer, A.J. Bardwell and L. Bardwell, Specificity of MAP kinase signaling in yeast differentiation involves transient versus sustained MAPK activation, Mol. Cell 8 (2001).

C. Sette, C.J. Inouye, S.L. Stroschein, P.J. Iaquinta and J. Thorner, Mutational analysis suggests that activation of the yeast pheromone response mitogen-activated protein kinase pathway involves conformational changes in the ste5 scaffold protein, Mol. Biol. Cell 11 (2000).

N. Valtz, M. Peter and I. Herskowitz, FAR1 is required for oriented polarization of yeast cells in response to mating pheromones, J. Cell Biol. 131 (1995).

Altschuler SJ, Angenent SB, Wang Y, Wu LF: On the spontaneous emergence of cell polarity. Nature (2008).

Takizawa P. A., DeRisi, J. L., Wilhelm, J. E. & Vale, R. D. Science 290 , 341-344.pmid:11030653. (2000).

Narang A: Spontaneous polarization in eukaryotic gradient sensing: a mathematical model based on mutual inhibition of frontness and backness pathways. J Theor Biol (2006) .

Butty, A. C., N. Perrinjaquet, A. Petit, M. Jaquenoud, J.E. Segall, K. Hofmann, C. Zwahlen, and M. Peter. A positive feedback loop stabilizes the guanine-nucleotide exchange factor Cdc24 at sites of polarization. Embo J 21(7):1565-1576. (2002).

Ciejek, E., and J. Thorner. Recovery of *S. cerevisiae* a cells from G1 arrest by alpha factor pheromone requires endopeptidase action. Cell 18(3):623-635. (1979).

Ma H, Kunes S, Schatz PJ, Botstein D. Plasmid construction by homologous recombination in yeast. Gene. 58:201-216 (1987).

Ozbudak EM, Becskei A, van Oudenaarden A: A system of counteracting feedback loops regulates Cdc42p activity during spontaneous cell polarization. Dev Cell 9:565-571 (2005).

Alby, K., D. Schaefer, and R.J. Bennett. Homothallic and heterothallic mating in the opportunistic pathogen Candida albicans. Nature 460 (7257):890-893. (2009).

Barkai, N., M.D. Rose, and N.S. Wingreen. Protease helps yeast find mating partners. Nature 396 (6710):422-423. (1998).